NASA/CR-2002-211628
ICASE Report No. 2002-10

The Virtual Crack Closure Technique: History, Approach and Applications

Ronald Krueger
ICASE, Hampton, Virginia

April 2002

REPORT DOCUMENTATION PAGE

Form Approved
OMB No. 0704-0188

1. AGENCY USE ONLY *(Leave blank)*

2. REPORT DATE
April 2002

3. REPORT TYPE AND DATES COVERED
Contractor Report

4. TITLE AND SUBTITLE
The virtual crack closure technique: History, approach and applications

5. FUNDING NUMBERS
C NAS1-97046
WU 505-90-52-01

6. AUTHOR(S)
Ronald Krueger

7. PERFORMING ORGANIZATION NAME(S) AND ADDRESS(ES)
ICASE
Mail Stop 132C
NASA Langley Research Center
Hampton, VA 23681-2199

8. PERFORMING ORGANIZATION REPORT NUMBER
ICASE Report No. 2002-10

9. SPONSORING/MONITORING AGENCY NAME(S) AND ADDRESS(ES)
National Aeronautics and Space Administration
Langley Research Center
Hampton, VA 23681-2199

10. SPONSORING/MONITORING AGENCY REPORT NUMBER
NASA/CR-2002-211628
ICASE Report No. 2002-10

11. SUPPLEMENTARY NOTES
Langley Technical Monitor: Dennis M. Bushnell
Final Report
To be presented at Composite Materials Handbook, Next General Session.

12a. DISTRIBUTION/AVAILABILITY STATEMENT
Unclassified–Unlimited
Subject Category 34
Distribution: Nonstandard
Availability: NASA-CASI (301) 621-0390

12b. DISTRIBUTION CODE

13. ABSTRACT *(Maximum 200 words)*

An overview of the virtual crack closure technique is presented. The approach used is discussed, the history summarized, and insight into its applications provided. Equations for two-dimensional quadrilateral elements with linear and quadratic shape functions are given. Formulae for applying the technique in conjuction with three-dimensional solid elements as well as plate/shell elements are also provided. Necessary modifications for the use of the method with geometrically nonlinear finite element analysis and corrections required for elements at the crack tip with different lengths and widths are discussed. The problems associated with cracks or delaminations propagating between different materials are mentioned briefly, as well as a strategy to minimize these problems. Due to an increased interest in using a fracture mechanics based approach to assess the damage tolerance of composite structures in the design phase and during certification, the engineering problems selected as examples and given as references focus on the application of the technique to components made of composite materials.

14. SUBJECT TERMS
finite element analysis, fracture mechanics, crack closure integral, composite structures, delamination, interlaminar fracture

15. NUMBER OF PAGES
64

16. PRICE CODE
A04

17. SECURITY CLASSIFICATION OF REPORT	18. SECURITY CLASSIFICATION OF THIS PAGE	19. SECURITY CLASSIFICATION OF ABSTRACT	20. LIMITATION OF ABSTRACT
Unclassified	Unclassified		

The NASA STI Program Office . . . in Profile

Since its founding, NASA has been dedicated to the advancement of aeronautics and space science. The NASA Scientific and Technical Information (STI) Program Office plays a key part in helping NASA maintain this important role.

The NASA STI Program Office is operated by Langley Research Center, the lead center for NASA's scientific and technical information. The NASA STI Program Office provides access to the NASA STI Database, the largest collection of aeronautical and space science STI in the world. The Program Office is also NASA's institutional mechanism for disseminating the results of its research and development activities. These results are published by NASA in the NASA STI Report Series, which includes the following report types:

- TECHNICAL PUBLICATION. Reports of completed research or a major significant phase of research that present the results of NASA programs and include extensive data or theoretical analysis. Includes compilations of significant scientific and technical data and information deemed to be of continuing reference value. NASA's counterpart of peer-reviewed formal professional papers, but having less stringent limitations on manuscript length and extent of graphic presentations.

- TECHNICAL MEMORANDUM. Scientific and technical findings that are preliminary or of specialized interest, e.g., quick release reports, working papers, and bibliographies that contain minimal annotation. Does not contain extensive analysis.

- CONTRACTOR REPORT. Scientific and technical findings by NASA-sponsored contractors and grantees.

- CONFERENCE PUBLICATIONS. Collected papers from scientific and technical conferences, symposia, seminars, or other meetings sponsored or cosponsored by NASA.

- SPECIAL PUBLICATION. Scientific, technical, or historical information from NASA programs, projects, and missions, often concerned with subjects having substantial public interest.

- TECHNICAL TRANSLATION. English-language translations of foreign scientific and technical material pertinent to NASA's mission.

Specialized services that complement the STI Program Office's diverse offerings include creating custom thesauri, building customized data bases, organizing and publishing research results . . . even providing videos.

For more information about the NASA STI Program Office, see the following:

- Access the NASA STI Program Home Page at ***http://www.sti.nasa.gov***

- Email your question via the Internet to help@sti.nasa.gov

- Fax your question to the NASA STI Help Desk at (301) 621-0134

- Telephone the NASA STI Help Desk at (301) 621-0390

- Write to:
  NASA STI Help Desk
  NASA Center for AeroSpace Information
  7121 Standard Drive
  Hanover, MD 21076-1320

NASA/CR-2002-211628
ICASE Report No. 2002-10

The Virtual Crack Closure Technique: History, Approach and Applications

Ronald Krueger
ICASE, Hampton, Virginia

ICASE
NASA Langley Research Center
Hampton, Virginia

Operated by Universities Space Research Association

Prepared for Langley Research Center
under Contract NAS1-97046

April 2002

Available from the following:

NASA Center for AeroSpace Information (CASI)
7121 Standard Drive
Hanover, MD 21076-1320
(301) 621-0390

National Technical Information Service (NTIS)
5285 Port Royal Road
Springfield, VA 22161-2171
(703) 487-4650

THE VIRTUAL CRACK CLOSURE TECHNIQUE: HISTORY, APPROACH AND APPLICATIONS

RONALD KRUEGER*

Abstract. An overview of the virtual crack closure technique is presented. The approach used is discussed, the history summarized, and insight into its applications provided. Equations for two-dimensional quadrilateral elements with linear and quadratic shape functions are given. Formulae for applying the technique in conjuction with three-dimensional solid elements as well as plate/shell elements are also provided. Necessary modifications for the use of the method with geometrically nonlinear finite element analysis and corrections required for elements at the crack tip with different lengths and widths are discussed. The problems associated with cracks or delaminations propagating between different materials are mentioned briefly, as well as a strategy to minimize these problems. Due to an increased interest in using a fracture mechanics based approach to assess the damage tolerance of composite structures in the design phase and during certification, the engineering problems selected as examples and given as references focus on the application of the technique to components made of composite materials.

Key words. finite element analysis, fracture mechanics, crack closure integral, composite structures, delamination, interlaminar fracture

Subject classification. Structures and Materials

1. Introduction. One of the most common failure modes for composite structures is delamination [1-3]. The remote loadings applied to composite components are typically resolved into interlaminar tension and shear stresses at discontinuities that create mixed-mode I, II and III delaminations. To characterize the onset and growth of these delaminations the use of fracture mechanics has become common practice over the past two decades [4-6]. The total strain energy release rate, G_T, the mode I component due to interlaminar tension, G_I, the mode II component due to interlaminar sliding shear, G_{II}, and the mode III component, G_{III}, due to interlaminar scissoring shear, as shown in Figure 1, need to be calculated. In order to predict delamination onset or growth for two-dimensional problems, these calculated G components are compared to interlaminar fracture toughness properties measured over a range from pure mode I loading to pure mode II loading [7-11]. A quasi static mixed-mode fracture criterion is determined by plotting the interlaminar fracture toughness, G_c , versus the mixed-mode ratio, G_{II}/G_T, determined from data generated using pure Mode I DCB (G_{II}/G_T=0), pure Mode II 4ENF (G_{II}/G_T=1), and mixed-mode MMB tests of varying ratios, as shown in Figure 2 for IM7/8552 [12]. A curve fit of these data is performed to determine a mathematical relationship between G_c and G_{II}/G_T. [5]. Failure is expected when, for a given mixed mode ratio G_{II}/G_T, the calculated total energy release rate, G_T, exceeds the interlaminar fracture toughness, G_c. Although several specimens have also been suggested for the measurement of the mode III interlaminar fracture toughness property [13-16], an interaction criterion incorporating the scissoring shear, however, has not yet been established. The virtual crack closure technique (VCCT) [17-19] is widely used for computing energy release rates based on results

* ICASE Staff Scientist, Mail Stop 132C, NASA Langley Research Center, Hampton, VA, 23681-2199, (email: rkrueger@icase.edu). This research was supported by the National Aeronautics and Space Administration under NASA Contract No. NAS1-97046 while the author was in residence at ICASE, NASA Langley Research Center, Hampton, VA 23681-2199.

from continuum (2D) and solid (3D) finite element analyses to supply the mode separation required when using the mixed-mode fracture criterion.

Although the original publication on VCCT dates back a quarter century [17], the virtual crack closure technique has not yet been implemented into any of the large commercial general purpose finite element codes such as MSC NASTRAN, ABAQUS, ANSYS, ASKA, PERMAS or SAMCEF. Currently FRANC2D, developed by the Cornell Fracture Group (CFG) at Cornell University, appears to be the only publically available, highly specialized finite element code that uses the virtual crack closure technique [20, 21]. The virtual crack closure technique has been used mainly by scientists in universities, research institutions and government laboratories and is usually implemented in their own specialized codes or used in post-processing routines in conjunction with general purpose finite element codes. Lately, an increased interest in using a fracture mechanics based approach to assess the damage tolerance of composite structures in the design phase and during certification has also renewed the interest in the virtual crack closure technique. Efforts are underway to incorporate these approaches in the *Composites Material MIL-17 Handbook*[1] .

The goal of the current paper is to give an overview of the virtual crack closure technique, discuss the approach used, summarize the history, and provide insight into its application. Equations for two-dimensional quadrilateral elements with linear and quadratic shape functions will be provided. Formulae for applying the technique in conjuction with three-dimensional solid elements as well as plate/shell elements will also be given. Necessary modifications for the use of the method with geometrically nonlinear finite element analysis and corrections required for elements at the crack tip with different lengths and widths will be discussed. The problems associated with cracks or delaminations propagating between different materials (the so-called bi-material interface) will be mentioned briefly, as well as a strategy to minimize these problems. The selected engineering problems shown as examples and given as references will focus on the application of the technique related to composite materials as mentioned above.

2. Background. A variety of methods are used to compute the strain energy release rate based on results obtained from finite element analysis. The *finite crack extension method* [22, 23] requires two complete analyses. In the model the crack gets extended for a finite length prior to the second analysis. The method provides one global total energy release rate as global forces on a structural level are multiplied with global deformations to calculate the energy available to advance the crack. The *virtual crack extension method* [24-33] requires only one complete analysis of the structure to obtain the deformations. The total energy release rate or *J-integral* is computed locally at the crack front and the calculation only involves an additional computation of the stiffness matrix of the elements affected by the virtual crack extension. The method yields the total energy release rate as a function of the direction in which the crack was extended virtually, yielding information on the most likely growth direction. Modifications of the method have been suggested in the literature to allow the mode separation for two-dimensional analysis [34, 35]. An *equivalent domain integral method* which can be applied to both linear and nonlinear problems and additionally allows for mode separation was proposed in [36, 37]. The methods above have been mentioned here

[1] http://www.mil17.org/

briefly to complement the background information. A comprehensive overview of different methods used to compute energy release rates is given in [38]. Alternate approaches to compute the strain energy release rate based on results obtained from finite element analysis have also been published recently [39-41].

For delaminations in laminated composite materials where the failure criterion is highly dependend on the mixed-mode ratio and propagation occurs in the laminate plane, the virtual crack closure technique [17-19, 42] has been most widely used for computing energy release rates because fracture mode separation is determined explicitely. Recently new methods to compute mixed-mode energy release rates suitable for the application with the p-version of the finite element method have also been developed [43]. Some modified and newly developed formulations allow applications independent of the finite element analysis and suitable for boundary element analysis [21, 44].

2.1. Crack Closure Method Using Two Analysis Steps. Even though the virtual crack closure technique is the focus of this paper and is generally mentioned in the literature it appears appropriate to include a related method: The *crack closure method* or *two-step virtual crack closure technique.* The terminology in the literature is often inexact and this two-step method is sometimes referred to as VCCT. It may be more appropriate to call the method the *crack closure method* because the crack is physically extended, or closed, during two complete finite element analyses as shown in Figure 3. The crack closure method is based on Irwin's crack closure integral [45, 46]. The method is based on the assumption that the energy ΔE released when the crack is extended by Δa from a (Figure 3a) to $a+\Delta a$ (Figure 3b) is identical to the energy required to close the crack between location ℓ and i (Figure 3a). Index "1" denotes the first step depicted in Figure 3a and index "2" the second step as shown in Figure 3b. For a crack modeled with two-dimensional four noded elements as shown in Figure 3 the work ΔE required to close the crack along one element side can be calculated as

$$\Delta E = \frac{1}{2}\left[X_{1\ell} \quad \Delta u_{2\ell} + Z_{1\ell} \quad \Delta w_{2\ell}\right]$$

where $X_{1\ell}$ and $Z_{1\ell}$ are the shear and opening forces at nodal point ℓ to be closed (Figure 3a) and $\Delta u_{2\ell}$ and $\Delta w_{2\ell}$ are the differences in shear and opening nodal displacements at node ℓ as shown in Figure 3b. The crack closure method establishes the original condition before the crack was extended. Therefore the forces required to close the crack are identical to the forces acting on the upper and lower surfaces of the closed crack. The forces $X_{1\ell}$ and $Z_{1\ell}$ may be obtained from a first finite element analysis where the crack is closed as shown in (Figure 3a). The displacements $\Delta u_{2\ell}$ and $\Delta w_{2\ell}$ are obtained from a second finite element analysis where the crack has been extended to its full length $a+\Delta a$ as shown in Figure 3b.

2.2. The Modified Crack Closure Method. The modified, or virtual, crack closure method is based on the same assumptions as the crack closure method described above. Additionally, however, it is assumed that a crack extension of Δa from $a+\Delta a$ (node i) to $a+2\Delta a$ (node k) does not significantly alter the state at the crack tip (Figure 4). Therefore the displacements behind the crack tip at node i are approximately equal to the displacements behind the original crack tip at node l. Further, the energy ΔE released when the crack is extended by Δa from $a+\Delta a$

to $a+2\Delta a$ is identical to the energy required to close the crack between location i and k. For a crack modeled with two-dimensional, four-noded elements, as shown in Figure 4, the work ΔE required to close the crack along one element side therefore can be calculated as

$$\Delta E = \frac{1}{2}\left[X_i \quad \Delta u_\ell + Z_i \quad \Delta w_\ell\right]$$

where X_i and Z_i are the shear and opening forces at nodal point i and Δu_ℓ and Δw_ℓ are the shear and opening displacements at node ℓ as shown in Figure 4. Thus, forces and displacements required to calculate the energy ΔE to close the crack may be obtained from one single finite element analysis. The details of calculating the energy release rate $G=\Delta E/\Delta A$, where ΔA is the crack surface created, and the separation into the individual mode components will be discussed in the following section.

3. Equations for Using the Virtual Crack Closure Technique. In the following paragraphs equations are presented to calculate mixed-mode strain energy release rates using two-dimensional finite element models such as plane stress or plane strain. Different approaches are also discussed for the cases where the crack or delamination is modeled with plate/shell elements or with three-dimensional solids.

3.1. Formulae for Two-Dimensional Analysis. In a two-dimensional finite element plane stress, or plane strain model, the crack of length a is represented as a one-dimensional discontinuity by a line of nodes as shown in Figure 5. Nodes at the top surface and the bottom surface of the discontinuity have identical coordinates, however, are not connected with each other as shown in Figure 5a. This lets the elements connected to the top surface of the crack deform independently form those connected to the bottom surface and allows the crack to open as shown in Figure 5b. The crack tip and the undamaged section, or the section where the crack is closed and the structure is still intact, is modeled using single nodes, or two nodes with identical coordinates coupled through multi-point constraints if a crack propagation analysis is desired. This is discussed in detail in Appendix A, which explains specific modeling issues.

For a crack propagation analysis, it is important to advance the crack in a kinematically compatible way. Node-wise opening/closing, where node after node is sequentially released along the crack, is possible for the four-noded element as shown in Figure 6a. It is identical to element-wise opening in this case as the crack is opened over the entire length of the element. Node-wise opening/closing, however, results in kinematically incompatible interpenetration for the eight-noded elements with quadratic shape functions as shown in Figure 6b, which caused initial problems when eight noded elements were used in connection with the virtual crack closure technique. Element-wise opening – where edge and mid-side nodes are released - provides a kinematically compatible condition and yields reliable results, which was demonstrated in references [4, 47, 48] and later generalized expressions to achieve this were derived by Raju in [18].

The mode I, and mode II components of the strain energy release rate, G_I and G_{II} are calculated for four-noded elements as shown in Figure 7a

$$G_I = -\frac{1}{2\Delta a} Z_i \left(w_\ell - w_{\ell^*}\right)$$

$$G_{II} = -\frac{1}{2\Delta a} X_i \left(u_\ell - u_{\ell^*}\right)$$

where Δa is the length of the elements at the crack front and X_i and Z_i are the forces at the crack tip (nodal point i). The relative displacements behind the crack tip are calculated from the nodal displacements at the upper crack face u_ℓ and w_ℓ (nodal point ℓ) and the nodal displacements u_{ℓ^*} and w_{ℓ^*} at the lower crack face (nodal point ℓ^*) respecively. The crack surface ΔA created is calculated as $\Delta A=\Delta a \cdot 1$, where it is assumed that the two-dimensional model is of unit thickness "1". While the original paper by Rybicki and Kanninen is based on heurisitic arguments [17], Raju proved the validity of the equation [18]. He also showed that the equations are applicable if triangular elements, obtained by collapsing the rectangular elements, are used at the crack tip.

The mode I, and mode II components of the strain energy release rate, G_I, G_{II} are calculated for eight-noded elements as shown in Figure 7b

$$G_I = -\frac{1}{2\Delta a} \left[Z_i \left(w_\ell - w_{\ell^*}\right) + Z_j \left(w_m - w_{m^*}\right)\right]$$

$$G_{II} = -\frac{1}{2\Delta a} \left[X_i \left(u_\ell - u_{\ell^*}\right) + X_j \left(u_m - u_{m^*}\right)\right]$$

where Δa is the length of the elements at the crack front as above. In addition to the forces X_i and Z_i at the crack tip (nodal point i) the forces X_j and Z_j at the mid-side node in front of the crack (nodal point j) are required. The relative sliding and opening behind the crack tip are calculated at nodal points ℓ and ℓ^* from displacements at the upper crack face u_ℓ and w_ℓ and the displacements u_{ℓ^*} and w_{ℓ^*} at the lower crack face. In addition to the relative displacements at nodal points ℓ and ℓ^* the relative displacements at nodal points m and m^* are required, which are calculated from displacements at the upper crack face u_m and w_m and the displacements u_{m^*} and w_{m^*} at the lower crack face [18]. The crack surface ΔA created is calculated as $\Delta A=\Delta a \cdot 1$, where it is assumed that the two-dimensional model is of unit thickness "1". The equations are also applicable if triangular parabolic elements, obtained by collapsing the parabolic rectangular elements, are used at the crack tip [18].

The total energy release rate G_T is calculated from the individual mode components as

$$G_T = G_I + G_{II} + G_{III}$$

where $G_{III} \equiv 0$ for the two-dimensional case discussed.

The VCCT proposed by Rybicki and Kanninen did not make any assumptions of the form of the stresses and displacements. Therefore, singularity elements are not required at the crack tip. However, others have proposed special two-dimensional crack tip elements with quarter-point nodes as shown in Figure 8. Based on the location of the nodal points at ξ =0.0, 0.25 and 1.0, these quarter point elements accurately simulate in $1/\sqrt{r}$ singularity of the stress field at the crack tip. Triangular quarter-point elements are obtained by collapsing one side of the rectangular

elements, as shown in Figure 8b. Due to the fact that these elements are not readily available in most of the commonly used finite element codes, quarter-point elements are not discussed further and the interested reader is refered to the literature [18, 49-52]

3.2. Formulae for Three-Dimensional Solids and Plate/Shell Elements. In a finite element model made of three-dimensional solid elements (Figure 9a) or plate or shell type elements (Figure 9b) the delamination of length a is represented as a two-dimensional discontinuity by two surfaces. The additional dimension allows to calculate the distribution of the energy release rates along the delamination front and makes it possible to obtain G_{III}, which is idential to zero for two-dimensional models. Nodes at the top surface and the bottom surface have identical coordinates and are not connected with each other as explained in the previous section. The delamination front is represented by either a row of single nodes or two rows of nodes with identical coordinates, coupled through multi-point constraints. The undamaged section where the delamination is closed and the structure is intact is modeled using single nodes or two nodes with identical coordinates coupled through multi-point constraints if a delamination propagation analysis is desired. This is discussed in detail in Appendix A, which explains specific modeling issues.

3.2.1. Formulae for Three-Dimensional Solids. For convenience, only a section of the delaminated area which is modeled with eight-noded three-dimensional solid elements is illustrated in Figure 10. The mode I, mode II, and mode III components of the strain energy release rate, G_I, G_{II}, and G_{III} are calculated as

$$G_I = -\frac{1}{2\Delta A} Z_{Li} \left(w_{L\ell} - w_{L\ell^*} \right)$$

$$G_{II} = -\frac{1}{2\Delta A} X_{Li} \left(u_{L\ell} - u_{L\ell^*} \right)$$

$$G_{III} = -\frac{1}{2\Delta A} Y_{Li} \left(v_{L\ell} - v_{L\ell^*} \right)$$

with $\Delta A = \Delta a \cdot b$ as shown in Figure 10 [53]. Here ΔA is the area virtually closed, Δa is the length of the elements at the delamination front, and b is the width of the elements. For better identification in this and the following figures, columns are identified by capital letters and rows by small letters as illustrated in the top view of the upper surface shown in Figure 10b. Hence, X_{Li}, Y_{Li} and Z_{Li} denote the forces at the delamination front in column L, row i. The corresponding displacements behind the delamination at the top face node row ℓ are denoted $u_{K\ell}$, $v_{K\ell}$ and $w_{K\ell}$ and at the lower face node row ℓ^* are denoted $u_{K\ell^*}$, $v_{K\ell^*}$ and $w_{K\ell^*}$ as shown in Figure 10. All forces and displacements are obtained from the finite element analysis with respect to the global system. A local crack tip coordinate system (x', y', z'), that defines the normal and tangential coordinate directions at the delamination front in the deformed configuration, has been added to the illustration. Its use with respect to geometrically nonlinear analyses will be discussed later.

For twenty noded solid elements, the equations to calculate the strain energy release rate components at the element corner nodes (location Li) as shown in Figure 11 are

$$G_I = -\frac{1}{2\Delta A_L}\left[\frac{1}{2} Z_{Ki}\left(w_{K\ell} - w_{K\ell^*}\right) + Z_{Li}\left(w_{L\ell} - w_{L\ell^*}\right) + Z_{Lj}\left(w_{Lm} - w_{Lm^*}\right) + \frac{1}{2} Z_{Mi}\left(w_{M\ell} - w_{M\ell^*}\right)\right]$$

$$G_{II} = -\frac{1}{2\Delta A_L}\left[\frac{1}{2} X_{Ki}\left(u_{K\ell} - u_{K\ell^*}\right) + X_{Li}\left(u_{L\ell} - u_{L\ell^*}\right) + X_{Lj}\left(u_{Lm} - u_{Lm^*}\right) + \frac{1}{2} X_{Mi}\left(u_{M\ell} - u_{M\ell^*}\right)\right]$$

$$G_{III} = -\frac{1}{2\Delta A_L}\left[\frac{1}{2} Y_{Ki}\left(v_{K\ell} - v_{K\ell^*}\right) + Y_{Li}\left(v_{L\ell} - v_{L\ell^*}\right) + Y_{Lj}\left(v_{Lm} - v_{Lm^*}\right) + \frac{1}{2} Y_{Mi}\left(v_{M\ell} - v_{M\ell^*}\right)\right]$$

where $\Delta A_L = \Delta a \cdot b$ as shown in Figure 11 [54]. Here X_{Ki}, Y_{Ki} and Z_{Ki} denote the forces at the delamination front in column K, row i. The relative displacements at the corresponding column K are calculated from the displacements behind the delamination at the lower face node row ℓ^* as $u_{K\ell^*}$, $v_{K\ell^*}$ and $w_{K\ell^*}$ and at the top face node row ℓ, as $u_{K\ell}$, $v_{K\ell}$ and $w_{K\ell}$ (Figure 11b). Similar definitions are applicable in column M for the forces at node row i and displacements at node row ℓ and in column L for the forces at node row i and j and displacements at node row ℓ and m respectively. Only one half of the forces at locations Ki and Mi contribute to the energy required to virtually close the area ΔA_L. Half of the forces at location Ki contribute to the closure of the adjacent area ΔA_J and half of the forces at location Mi contribute to the closure of the adjacent area ΔA_N.

The equations to calculate the strain energy release rate components at the mid-side node (location Mi) as shown in Figure 12 are as follows [54, 55].

$$G_I = -\frac{1}{2\Delta A_M}\left[\frac{1}{2} Z_{Li}\left(w_{L\ell} - w_{L\ell^*}\right) + \frac{1}{2} Z_{Lj}\left(w_{Lm} - w_{Lm^*}\right) + Z_{Mi}\left(w_{M\ell} - w_{M\ell^*}\right) + \frac{1}{2} Z_{Ni}\left(w_{N\ell} - w_{N\ell^*}\right) + \frac{1}{2} Z_{Nj}\left(w_{Nm} - w_{Nm^*}\right)\right]$$

$$G_{II} = -\frac{1}{2\Delta A_M}\left[\frac{1}{2} X_{Li}\left(u_{L\ell} - u_{L\ell^*}\right) + \frac{1}{2} X_{Lj}\left(u_{Lm} - u_{Lm^*}\right) + X_{Mi}\left(u_{M\ell} - u_{M\ell^*}\right) + \frac{1}{2} X_{Ni}\left(u_{N\ell} - u_{N\ell^*}\right) + \frac{1}{2} X_{Nj}\left(u_{Nm} - u_{Nm^*}\right)\right]$$

$$G_{III} = -\frac{1}{2\Delta A_M}\left[\frac{1}{2} Y_{Li}\left(v_{L\ell} - v_{L\ell^*}\right) + \frac{1}{2} Y_{Lj}\left(v_{Lm} - v_{Lm^*}\right) + Y_{Mi}\left(v_{M\ell} - v_{M\ell^*}\right) + \frac{1}{2} Y_{Ni}\left(v_{N\ell} - v_{N\ell^*}\right) + \frac{1}{2} Y_{Nj}\left(v_{Nm} - v_{Nm^*}\right)\right]$$

where only one half of the forces at locations Li, Lj and Ni, Nj contribute to the energy required to virtually close the area ΔA_M. Half of the forces at locations Li and Lj contribute to the closure of the adjacent area ΔA_K and half of the forces at locations Ni and Nj contribute to the closure of the adjacent area ΔA_O. Additional information with respect to different equations for solid elements are given in the literature [19, 55-60]

3.2.2. Formulae for Plate/Shell Elements. The use of four-noded plate elements to calculate the mixed-mode strain energy release was demonstrated in [56]. Equations for the use of VCCT in conjunction with four- and

nine-noded plate elements were derived by Raju [61]. Two techniques to tie the nodes at the delamination front (row *i* in Figues 13 and 14) were discussed. For nodes of the upper and lower surfaces, which are joined at the crack tip, the first method enforced the compatibility of translational and rotational dregrees-of-freedom for nodes with identical coordinates. In the second technique, only the compatibility of the translational dregrees-of-freedom were enforced. The second technique allowed the nodes to have independent rotations. For the configurations and loads considered, the second technique appeared to provide preferable constraints yielding accurate strain energy release rates [61-63]. Therefore only the equations for this method are mentioned in this paper.

For the four-noded rectangular plate element, as shown in Figure 13, the equations to calculate the strain energy release rate components at the element corner nodes (location *Li*) are

$$G_I = -\frac{1}{2\Delta A} Z_{Li} \left(w_{L\ell} - w_{L\ell^*}\right)$$

$$G_{II} = -\frac{1}{2\Delta A} X_{Li} \left(u_{L\ell} - u_{L\ell^*}\right)$$

$$G_{III} = -\frac{1}{2\Delta A} Y_{Li} \left(v_{L\ell} - v_{L\ell^*}\right)$$

where $\Delta A=\Delta a(b_1+b_2)/2$ is the crack surface closed as shown in Figure 13b [61].

The equations to calculate the strain energy release rate components for a nine-noded plate element as shown in Figure 14 are for the

Mode I components:

$$G_I\big|_L = -\frac{1}{2\Delta A_L}\left[Z_{Li}\left(w_{L\ell} - w_{L\ell^*}\right) + Z_{Lj}\left(w_{Lm} - w_{Lm^*}\right)\right]$$

$$G_I\big|_M = -\frac{1}{2\Delta A_M}\left[Z_{Mi}\left(w_{M\ell} - w_{M\ell^*}\right) + Z_{Mj}\left(w_{Mm} - w_{Mm^*}\right)\right]$$

$$G_I\big|_N = -\frac{1}{2\Delta A_N}\left[Z_{Ni}\left(w_{N\ell} - w_{N\ell^*}\right) + Z_{Nj}\left(w_{Nm} - w_{Nm^*}\right)\right]$$

Mode II components:

$$G_{II}\big|_L = -\frac{1}{2\Delta A_L}\left[X_{Li}\left(u_{L\ell} - u_{L\ell^*}\right) + X_{Lj}\left(u_{Lm} - u_{Lm^*}\right)\right]$$

$$G_{II}\big|_M = -\frac{1}{2\Delta A_M}\left[X_{Mi}\left(u_{M\ell} - u_{M\ell^*}\right) + X_{Mj}\left(u_{Mm} - u_{Mm^*}\right)\right]$$

$$G_{II}\big|_N = -\frac{1}{2\Delta A_N}\left[X_{Ni}\left(u_{N\ell} - u_{N\ell^*}\right) + X_{Nj}\left(u_{Nm} - u_{Nm^*}\right)\right]$$

and Mode III components:

$$G_{III}\big|_L = -\frac{1}{2\Delta A_L}\left[Y_{Li}\left(v_{L\ell} - v_{L\ell^*}\right) + Y_{Lj}\left(v_{Lm} - v_{Lm^*}\right)\right]$$

$$G_{III}\big|_M = -\frac{1}{2\Delta A_M}\left[Y_{Mi}\left(v_{M\ell} - v_{M\ell^*}\right) + Y_{Mj}\left(v_{Mm} - v_{Mm^*}\right)\right]$$

$$G_{III}\big|_N = -\frac{1}{2\Delta A_N}\left[Y_{Ni}\left(v_{N\ell} - v_{N\ell^*}\right) + Y_{Nj}\left(v_{Nm} - v_{Nm^*}\right)\right]$$

as given in [61, 62]. Here indices *L, M, N* denote the column location, as shown in Figure 14b and

$$\Delta A_L = -\frac{1}{6}\Delta a\ \left(b_2 + b_3\right),\ \ \Delta A_M = -\frac{2}{3}\Delta a\ \ b_2 \text{ and } \Delta A_N = -\frac{1}{6}\Delta a\ \left(b_1 + b_2\right)$$

are the equivalent crack surfaces apportioned to corner- and midside-crack front nodes, respectively. The equivalent crack surfaces are obtained by assuming that the strain energy release rate components are constant across the width of an element [61].

For eight noded plate elements the *Mm*-terms are equal to zero and the equations at column *M* are reduced to

$$G_I\big|_M = -\frac{1}{2\Delta A_M}\left[Z_{Mi}\left(w_{M\ell} - w_{M\ell^*}\right)\right]$$

$$G_{II}\big|_M = -\frac{1}{2\Delta A_M}\left[X_{Mi}\left(u_{M\ell} - u_{M\ell^*}\right)\right]$$

$$G_{III}\big|_M = -\frac{1}{2\Delta A_M}\left[Y_{Mi}\left(v_{M\ell} - v_{M\ell^*}\right)\right]$$

with the equations for columns *L* and *N* unaltered.

Built-up structures are traditionally modeled and analyzed using plate or shell finite elements to keep the modeling and computational effort affordable. Computed mixed mode strain energy release rate components, however, depend on many variables such as element order and shear deformation assumptions, kinematic constraints in the neighborhood of the delamination front, and continuity of material properties and section stiffness in the vicinity of the debond when delaminations or debonds are modeled with plate or shell finite elements [61, 62]. For example, in reference [62] mesh refinement studies showed that computed G_I, G_{II}, and G_{III} did not converge when the structure above and below the plane of delamination was modeled with plate elements with different section properties (thickness or layup). A comparison of computed mixed mode strain energy release rates obtained from plate models with values computed from three-dimensional models showed differences in results near the free edges of the structure where the stress state is three-dimensional [64]. These problems may be avoided by using three-dimensional models. Furthermore, three-dimensional analyses are required when matrix cracks and multiple delaminations need to be modeled at different ply interfaces. Since many layers of brick elements through the thickness are often necessary to model the individual plies, the size of finite element models required for accurate analyses may become prohibitively large. For future detailed modeling, the shell/3D modeling technique offers great

potential for saving modeling and computational effort because only a relatively small section in the vicinity of the delamination front needs to modeled with solid elements [65].

3.3. Formulae for Geometrically Nonlinear Analysis. For geometric nonlinear analysis where large deformations may occur, both forces and displacements obtained in the global coordinate system need to be transformed into a local coordinate system (x', z') which originates at the crack tip as shown in Figure 15. The local crack tip system defines the tangential (x', or mode II) and normal (z', or mode I) coordinate directions at the crack tip in the deformed configuration as shown in Figure 15b for the two-dimensional case. The vector through nodes i and k in the deformed configuration defines the local x' direction as shown in Figure 15a. The local z' direction, which defines mode I, is perpendicular to the local x' direction which defines mode II. Forces at node row i and displacements at node row ℓ need to be transformed to the local x'-z' system at the tip as shown in Figure 15b. The equations to calculate the mixed-mode energy release rate components remain the same as before, with forces and displacements now expressed in the local system. For the two-dimensional eight-noded quadrilateral element with quadratic shape functions this yields

$$G_I = -\frac{1}{2\Delta a}\left[Z'_i\left(w'_\ell - w'_{\ell^*}\right) + Z'_j\left(w'_m - w'_{m^*}\right)\right]$$

$$G_{II} = -\frac{1}{2\Delta a}\left[X'_i\left(u'_\ell - u'_{\ell^*}\right) + X'_j\left(u'_m - u'_{m^*}\right)\right]$$

where X'_i, Z'_i and X'_j, Z'_j are the forces at the crack tip (nodal point i) and in front of the crack (nodal point j) in the local crack tip system. The relative sliding and opening behind the crack tip are calculated at nodal points ℓ and ℓ^* from the transformed displacements at the upper crack face u'_ℓ and w'_ℓ and the displacements u'_{ℓ^*} and w'_{ℓ^*} at the lower crack face. Additionally to the relative displacements at nodal points ℓ and ℓ^*, the relative displacements at nodal points m and m^* are required, which are calculated from displacements at the upper crack face u'_m and w'_m and the displacements u'_{m^*} and w'_{m^*} at the lower crack face. Three-dimensional analysis additionally requires the definition of the tangential (y', or mode III) coordinate direction which will be discussed in section 3.5.

3.4. Corrections for Elements with Different Lengths or Widths at the Crack Tip.

3.4.1. Correcting for Elements with Different Lengths at the Crack Tip. All equations in previous paragraphs have been derived under the assumption that the element lengths Δa for the element in front of the crack tip and behind are identical. Once automatic mesh generators are used to create complex models, the ideal case of identical element length can no longer be assumed and corrections are required. In their original paper Rybicki and Kanninen [17] use the $1/\sqrt{r}$ singularity of the stress field at the crack tip to derive the corrected equations. A sketch of a crack tip modeled with two-dimensional finite elements of unequal length is shown in Figure 16. The forces X_i, Z_i at the crack tip (nodal point i) calculated for an element length Δa_2 are known from the finite element analysis.

Required for the virtual crack closure technique, however, are the forces $\tilde{X}_i$, $\tilde{Z}_i$ matching the relative displacements at node ℓ behind the crack tip, which have been calculated for an element length Δa_1.

The stress tip field at the crack tip can be expressed as [46]

$$\sigma(r) = b\ \sigma_\infty\ \frac{1}{\sqrt{r}} = \frac{dX}{dA} = \frac{dX}{b\ dr}$$

where b is the element width or thickness and σ_∞ is the undisturbed far field stress and $\sigma(r)$ is the stress in front of the crack, which is a function of the distance r from the crack tip. The forces at the crack tip for element length Δa_1 and Δa_2. are obtained through integration

$$\tilde{X}_i = \int_0^{\Delta a_1} \frac{dr}{r^{1/2}} = 2\ b\ \sigma_\infty\ \Delta a_1^{1/2}$$

$$X_i = 2\ b\ \sigma_\infty\ \Delta a_2^{1/2}$$

A relationship between the forces can be derived which only depends on the length of the elements in front and behind the crack tip

$$\tilde{X}_i = \left(\frac{\Delta a_1}{\Delta a_2}\right)^{1/2} X_i$$

The calculation of the crack opening force $\tilde{Z}_i$ is done accordingly. With the relationship of the forces established, the required forces $\tilde{X}_i$, $\tilde{Z}_i$ may be substituted with the forces X_i, Z_i obtained from finite element analysis, yielding the corrected equations for the energy release rate components

$$G_I = -\frac{1}{2\Delta a_1}\ Z_i\ \left(w_\ell - w_{\ell^*}\right) \left(\frac{\Delta a_1}{\Delta a_2}\right)^{1/2}$$

$$G_{II} = -\frac{1}{2\Delta a_1}\ X_i\ \left(u_\ell - u_{\ell^*}\right) \left(\frac{\Delta a_1}{\Delta a_2}\right)^{1/2}$$

A different approach for correcting the equations, which does not depend on the assumption of the $1/\sqrt{r}$ singularity of the stress field at the crack tip, is depicted in Figure 17 for the two-dimensional case. The different element lengths are accounted for by correcting the displacements behind the crack tip (at node ℓ), which were computed for a length Δa_1, to match the forces X_i, Z_i at the crack tip (nodal point i), which were computed for an element length Δa_2. The displacements are adjusted by taking into account the shape functions of the elements or approximated by simple linear interpolation. For elements with linear shape functions, where the displacement vary linearly along the element edge, both methods are identical. The displacement at locations $\tilde{\ell}$ and $\tilde{\ell}^*$ are calculated

using linear interpolation for $\Delta a_1 > \Delta a_2$ as shown in Figure 17a and linear extrapolation is used for $\Delta a_1 < \Delta a_2$ as shown in Figure 17b yielding

$$u_{\tilde{\ell}} = u_{\ell} \frac{\Delta a_2}{\Delta a_1} \quad \text{and} \quad u_{\tilde{\ell}^*} = u_{\ell^*} \frac{\Delta a_2}{\Delta a_1}$$

The calculation of the crack opening displacement w is done accordingly. With the relationship of the displacements established, the required displacements at locations $\tilde{\ell}$ and $\tilde{\ell}^*$ may be substituted with the displacements ℓ and ℓ^* obtained directly from finite element analysis, yielding the corrected equations for the energy release rate components

$$G_I = -\frac{1}{2\Delta a_2} Z_i \left(w_{\ell} - w_{\ell^*}\right) \frac{\Delta a_2}{\Delta a_1}$$

$$G_{II} = -\frac{1}{2\Delta a_2} X_i \left(u_{\ell} - u_{\ell^*}\right) \frac{\Delta a_2}{\Delta a_1}$$

The method first described imposes an analytical relationship based on the $1/\sqrt{r}$ singularity of the stress field at the crack tip. However, the second method is less restrictive because the results only depend on the finite element discretisation at the crack tip.

3.4.2. Correcting for Elements with Different Widths Along the Delamination Front. For the derivation of the equations in the previous paragraphs it had been assumed that the front is straight and that element widths b remain constant along the front. Meshing of arbitrarily shaped delamination front contours will however cause element length Δa and width b to vary along the front. Therefore, a two-dimensional representation of a crack or delamination in a plate/shell or a three-dimensional solid finite element models also requires a correction accounting for differences in element widths b along the front. For components modeled with four-noded plate/shell type elements or eight-noded solid brick elements the correction is straight forward as shown in Figure 18. A variation of only the element length, Δa, yields equations equivalent to the two-dimensional case discussed earlier

$$G_I = -\frac{1}{2\Delta a_2\ b} Z_{Li} \left(w_{L\ell} - w_{L\ell^*}\right) \frac{\Delta a_2}{\Delta a_1}$$

$$G_{II} = -\frac{1}{2\Delta a_2\ b} X_{Li} \left(u_{L\ell} - u_{L\ell^*}\right) \frac{\Delta a_2}{\Delta a_1}$$

$$G_{III} = -\frac{1}{2\Delta a_2\ b} Y_{Li} \left(v_{L\ell} - v_{L\ell^*}\right) \frac{\Delta a_2}{\Delta a_1}$$

The additional variation of the element width b requires the separate calculation of the contributing element surfaces $\Delta A_1 = 1/2 \cdot \Delta a_2 \cdot b_1$ and $\Delta A_2 = 1/2 \cdot \Delta a_2 \cdot b_2$ yielding the corrected equations for the energy release rate components

$$G_I = -\frac{1}{2} \frac{1}{\Delta A_1 + \Delta A_2} Z_{Li} \left(w_{L\ell} - w_{L\ell^*}\right) \frac{\Delta a_2}{\Delta a_1}$$

$$G_{II} = -\frac{1}{2}\frac{1}{\Delta A_1 + \Delta A_2} X_{Li} \left(u_{L\ell} - u_{L\ell^*}\right) \frac{\Delta a_2}{\Delta a_1}$$

$$G_{III} = -\frac{1}{2}\frac{1}{\Delta A_1 + \Delta A_2} Y_{Li} \left(v_{L\ell} - v_{L\ell^*}\right) \frac{\Delta a_2}{\Delta a_1}$$

A simple equivalent expression for twenty-noded solid brick elements based on the equations presented in section 3.2.1 is not available. The set of equations given in section 3.2.2 for the higher order plate elements [61] may be used since the change of element width is already accounted for in the expressions for the mixed-mode strain energy release rates. The variation in element length, Δa, may be compensated as described in the section above.

3.5. Procedures for Arbitrarily Shaped Delamination Front Contours. The equations presentend in the previous paragraphs were derived with the assumption that the delamination front is straight. For a straight front as shown in Figures 10-14 and 18 the definition of the modes is intuitive and constant for the entire front: Mode I is caused by the out of plane crack opening, mode II by the shear perpendicular to the straight delamination/crack front and mode III by the shear component tangential to the front. For an arbitrarily shaped front the mode definition constantly changes along the contour as shown in Figure 19. A local crack tip coordinate system therefore needs to be defined at each nodal point along the front [66]. The vector through nodes *i* and *k* in the deformed configuration defines the local x^* direction as shown for one sample node in Figure 19. The secant through adjacent nodes defines the *y'* direction and mode III. The local plane of delamination is defined by x^* and *y'*. The local *z'* direction, which defines mode I, is perpendicular to the plane of delamination. Finally, the local *x'* direction which defines mode II, is perpendicular to the *y'* and z' plane. Forces at node row *i* and displacements at node row ℓ need to be transformed to the local *x'*-*y'*-z' system at the tip. The transformed forces and displacements are used in the previously derived equations to calculate the mixed mode energy release rates.

For the procedure described above it is assumed that the mesh remains normal to the delamination front. Modern pre-processing software allows the modeling of almost any complex configuration, these programs, however, were not developed to guarantee the normality of the mesh and the delamination front. The effect of a lack of normality at the crack front on the computed energy release rates was studied in [67]. It was shown that the standard formulations for VCCT were not able to extract accurate values from models that did not have normality at the crack front when compared to reference solutions. It was also found that an increased variation from the normal condition yielded a greater discrepancy. The formulation of an extraction method for VCCT that yields accurate energy release rates for models that lack normality is given in [67].

3.6. Suggested Solutions for Delaminations with Sharp Corners. Delaminations with sharp corners – as shown in Figure 20a – pose a problem when computing mixed mode energy release rates as the separation into in-plane shear (mode II) and tearing (mode III) is not defined. Ideally sharp corners generally do not exist so that modeling a rounded corner, as shown in Figure 20b, appears to be an acceptable alternative. The mode separation is well defined at the rounded corner and the procedure described in the previous paragraph may be applied to define the appropriate local crack tip coordinate system.

The method suggested has been applied successfully to a specimen with an embedded, square delamination as shown in Figure 21. The method results in an increase of nodes and elements and the model may become large. A recently suggested modified approach uses stair stepped instead of smoothed fronts and thus avoids an increase in model size [68].

4. Dealing with the Problems at a Bi-Material Interface. Previous investigations have shown that care must be exercised in interpreting the values for G_I, G_{II} and G_{III} obtained using the virtual crack closure technique for interfacial delaminations between two orthotropic solids [69-72]. Mathematical solutions of the near crack tip field indicate that stresses start to oscillate in the immediate vicinity of the tip when crack growth occurs at interfaces between materials with dissimilar properties as shown in Figure 22a. The consequence is that the mixed mode ratio is undefined when the virtual crack closure length Δa goes to zero. For crack growth and delamination propagation in composite materials, this phenomenon has to be considered as the delamination is rarely located at an interface between two plies of identical orientation. One way to circumvent this problem is the introduction of an artificial thin resin rich layer which is assumed to exist between the plies [69, 73]. Delamination propagation in this case occurs in a homogenious material and the above mentioned problem does not exist. Although this technique circumvents the issue, it requires larger models with significant refinement in the thin resin layer. Several other papers have addressed the issue of the stress oscillation near the crack tip in the past [74-83].

It was shown in the literature [70] that finite values for the virtual crack closure length, e.g. $\Delta a/a > 0.05$ (Δa*:* virtual crack closure length, *a:* crack length), result in nearly constant mixed mode ratios. In addition it was verified in [71, 72] that evaluating the energy release rates via nodal forces and displacements in the finite element procedure, yields similar results to the analytical evaluation of the crack closure integral based on the near tip fields. For larger values of Δa the energy release rate components were found to be nearly constant, whereas for very small Δa they are functions of element length as sketched in Figure 22b. The total energy release $G_T=G_I+G_{II}+G_{III}$, however, converges to a constant value as shown in [62]. The $\Delta a/a$ values where the oscillation begins is connected with the value of γ found in the expression for the crack tip singularity which is given by $r^{-1/2+i\gamma}$. It was also shown that evaluating energy release rates by using larger values of $\Delta a/a$, where the energy release rate components become stationary yields similar results to values obtained by an analysis performed assuming a resin rich region mentioned above [69]. However, the energy release rates evaluated with a larger Δa are insensitive to material inhomogeneities that exist. This is a prerequisite for an energy release rate that is to be used as fracture criterion in a real situation.

For the virtual crack closure technique, the energy release rates are defined as the virtual crack closure integral over a finite crack closure length. This crack closure length corresponds to the lengths of the elements adjacent to the crack front. This element length, Δa, must be chosen small enough to assure a converged FE solution but large enough to avoid oscillating results. The approach used must be consistent when the definition of the energy release rates used for fracture predictions as well as that employed for material characterisation. This does not imply that the material tests must be evaluated by FE-models, but it should be established that the data reduction scheme is in agreement with the definition of a finite crack closure length. Consequently, it had been suggested to use element

lengths at the crack tip in such a manner that the computed results are insensitive to the variation of the element length Δa at the crack tip as sketched in Figure 22b.

Upper and lower bounds may be assumed for practical applications as shown in Figure 22c. The element size (length and height) should not be less than 1/10 of a ply thickness, h, which corresponds to the diameter of two carbon tows in the carbon/epoxy material modeled as shown in Figure 22c. For smaller element sizes the assumption of modeling each ply as an orthotropic continuum is no longer valid. The ply thickness was suggested as a practical upper limit for element length and height because larger elements would require smearing of the different layer properties over one element as shown in Figure 22c [84]. Smeared or homogenized properties would result in altered properties at the interface where the energy release rates are calculated. Variations in mode mixety between these upper and lower bounds are typically very small and should prove acceptable for practical applications.

In a previous investigation, mixed mode energy release rates were computed for an ENF specimen with multidirectional layup, where the delaminated interface was located between a +30˚ and –30˚ ply [85]. A study indicated that computed energy release rates, G_{II} and G_{III}, do not exhibit a significant variation with mesh refinement as shown in Table 1.

Table 1: Dependence of mixed-mode ratio in bimaterial interface on element size at the crack tip

Element length Δa in mm	Relative element size $\Delta a/h$	Relative crack closure length $\Delta a/a$	Mode ratio G_{II}/G_T	Mode ratio G_{III}/G_T
0.0625	0.492	0.001969	0.92048	0.079509
0.03125	0.246	0.000984	0.92045	0.079548
0.015625	0.123	0.000492	0.92020	0.079792
0.078125	0.0615	0.000246	0.91574	0.084262
0.00390625	0.0307	0.000123	0.91562	0.084377

Layup [±30/-30/30/-30/30/30/-30/30/-30/-30/30/$_{\uparrow}$-30/30/30/-30/30/-30/-30/30/-30/30/±30], C12K/R6376 tape, delamination length a=31.75 mm, ply thickness h=0.127 mm

In another study the influence of the mesh size at the delamination tip was investigated for a Single Leg Bending (SLB) specimen with multidirectional layup, where the delaminated interface was located between a +30˚ and –30˚ ply [86]. The three-dimensional model of the SLB specimen is shown in Figure 23. Along the length of the model, a refined mesh of length, c, was used in the vicinity of the delamination front. The influence of mesh size on computed mixed mode strain energy release rates was studied by keeping the length of the refined zone, c, constant, and increasing the number of elements, n, in this zone as shown in the detail of Figure 23. The corresponding values of relative element size, $\Delta a/h$, and relative crack closure length, $\Delta a/a$, are given in Table 2. The influence of mesh

refinement on the mode I strain energy release rate distribution across the width is moderate and only very long elements (n=3, $\Delta a=c/n$=1 mm) need to be avoided as shown in Figure 24. This is confirmed by the mode II and mode III distributions as shown in Figures 25 and 26 where the mode II strain energy release rate is fairly constant across almost the entire width of the specimen and peaks near the edges accompanied by local mode III contribution. The distribution of the mixed mode ratio G_I/G_{II} is shown in Figure 27. For the range studied (n=3 up to 48), there is only a small dependence of computed mixed mode ratio on element size Δa.

Table 2: Mesh size at the crack tip for SLB specimen with multidirectional layup.

length c of refined section in mm	Number of elements n	Element length Δa in mm	Relative element size $\Delta a/h$	Relative crack closure length $\Delta a/a$
3.0	3	1.0	7.874	0.029
3.0	6	0.5	3.937	0.0145
3.0	12	0.25	1.9685	0.0073
3.0	24	0.125	0.984	0.00365
3.0	48	0.0625	0.492	0.00183

Layup [±30/0/-30/0/30/0_4/30/0/-30/0/-30/30/$_\uparrow$-30/30/30/0/30/0/-30/0_4/-30/0/30/0/±30], C12K/R6376 tape
delamination length a=34.3 mm, ply thickness h=0.127 mm

The results from the above studies of the multidirectional ENF and SLB specimens confirm the suggestion made earlier for lower bounds ($\Delta a/h$ >0.1) and upper bounds ($\Delta a/h$ <1.0) of element lengths to be used.

5. Application of the Virtual Crack Closure Technique to Engineering Problems. Selected engineering problems where the virtual crack closure technique is applied to fracture of composite structures are referenced in this section. Two examples from recent studies showing the application of VCCT to two-dimensional and three-dimensional finite element analyses are discussed in more detail.

5.1. Applying the Virtual Crack Closure Technique with Two-Dimensional Finite-Element Analysis. Two-dimensional finite element models where the crack or delamination is simulated as a line have been used extensively in the past. In general two-dimensional models are preferred by industry due to the fact that modeling time, as well as computational time, remains affordable, especially if many different configurations have to be analyzed during the initial design phase. However, the geometry, boundary conditions, and other properties across the entire width are are inherently constant in a two-dimensional finite element model. Additionally, a two-dimensional plane-stress model in the x-y plane imposes the out of plane stresses to be zero ($\sigma_{zz}=\tau_{xz}=\tau_{yz}=0$) and allows the displacement to be the free parameter. A plane-strain model in the x-y plane, on the other hand,

imposes the out of plane strains to be zero ($\varepsilon_{zz} = \gamma_{xz} = \gamma_{yz} = 0$), which excessively constrains the plies. The effect of two-dimensional modeling assumptions is most marked for 45° plies because of their high in-plane Poisson's ratio, while it is small for 0° and 90°. The influence of two-dimensional finite element modeling assumptions on computed energy release rates was studied in detail in [87]. Based on the results of this investigation it is recommended to use results from plane stress and plane strain models as upper and lower bounds. Two-dimensional models may also be used to qualitatively evaluate the variation of energy release rates and mixed mode ratios with delamination length. For more accurate predictions, however, a three-dimensional analysis is required.

Two-dimensional finite element models have been used to study the behavior of specimens used and suggested for fracture toughness testing in [88-95] and three-point bending specimen [96]. Iosipescu specimens were studied in [97, 98]. The behavior of edge delaminations was investigated in [4, 99] and the failure of composite hat stringer pull-of specimens was examined in [100, 101]. The failure of a lap joints was investigated in [102, 103] and the durability of bonded joints in [104]. The virtual crack closure technique was also used to investigate the facesheet delaminating from the sandwich core [105-108] as well as delamination buckling [109, 110]. Delamination initiation from ply drops in general was studied in [111] while the initiation specific to rotorcraft flexbeams was investigated in [112, 113].

To illustrate the application of VCCT to structural delamination, an example is taken from the study of skin/stringer debond failure as shown in Figure 28 [114]. The specimens consisted of a tapered laminate, representing the stringer, bonded onto a skin as shown in Figure 28a. An IM7/8552 graphite/epoxy system was used for both the skin and flange. The skin was made of prepreg tape and had a nominal ply thickness of 0.142 mm and a [45/-45/0/-45/45/90/90/-45/45/0/45/-45] lay-up. The flange was made of a plain-weave fabric of 0.208 mm nominal ply thickness. The flange lay-up was $[45/0/45/0/45/0/45/0/45]_f$, where the subscript "f" denotes fabric, "0" represents a 0°-90° fabric ply and "45" represents a 0°-90° fabric ply rotated by 45º. Quasi-static tension tests were performed in a servohydraulic load frame where the specimens were mounted in hydraulic grips with a gage length of 101.6 mm as shown in Figure 28b. The value of the damage onset load, P was averaged from four tests and determined to be 17.8 kN with a coefficient of variation of 8.9%. The tests were terminated when the flange debonded from the skin. Micrographic investigations showed that at corners 2 and 3, a delamination formed at the top 45°/-45° skin ply interface. The initial crack was modeled at the location suggested by the microscopic investigation as shown in the detail in Figure 28b. Finite element solutions were obtained using the commercial ABAQUS®/Standard finite element software. Eight-noded quadrilateral plane-stress (CPS8R) elements with quadratic shape functions and a reduced (2x2) integration scheme were utilized for the geometric nonlinear analyses. For this investigation, the delamination growing between the skin top 45º and –45º plies was extended by releasing multi-point constraints at the crack tip and in front of the crack tip. During a series of nonlinear finite element analyses, strain energy release rates were computed at each tip location for the loads applied in the experiments. A critical energy release rate, G_c, needs to be determined to predict delamination onset. This critical G is generally identified based on the shape of the total energy release rate versus delamination length curve, which is determined through analysis as shown in Figure 29. The G_T versus x curve reached a maximum (as marked in Figure 29) at some virtual delamination length and then decreased. The delamination was extended to a total simulated length of

2.2 mm to ascertain that the peak value had been captured. The total energy release rates and the corresponding mixed mode ratios G_{II}/G_T are plotted in Figures 29 and 30. The maximum total energy release rate, G_T, as marked in the graph, was chosen as the critical value to be used for the fatigue life prediction [114]. This peak in G_T also corresponded to the maximum mode I percentage, i.e., minimum value of G_{II}/G_T in Figure 30. Similar investigations of skin/flange debonding are reported in [115-118].

5.2. Applying the Virtual Crack Closure Technique to Analysis with Plate and Shell Elements. In a finite element model made of plate or shell type elements the delamination is represented as a two-dimensional discontinuity by two surfaces with identical nodal point coordinates. Flanagan developed a code based on sublaminate analysis and demonstrated its application to simple fracture toughness specimens, the curved-beam test and edge delamination [119]. The problem of a composite stringer separating from the skin has been investigated using plate and shell models in [61, 120, 121]. Fractures mechnics analyses performed by Glaessgen et.al. focussed on the debonding of stitched composite structures [122-124]. Delamination buckling has been investigated as well using plate/shell models [56, 125-129].

5.3. Applying the Virtual Crack Closure Technique to Analysis with Solid Finite Elements. Three-dimensional finite element models have been used to study the behavior of specimens traditionally used in fracture toughness testing [16, 23, 55, 64, 65, 85, 130-136], three-point bending specimen [137] as well as the behavior of edge delaminations [138-140]. Skin-stiffener debonding was analysed in [54, 87]. Damage in titanium-grahite hybrid lamiantes was investigated in [141] and Ireman et.al. studied the damage propagation in composite structural elements [142]. Three-dimensional models were also used to study the growth of near-surface delaminations in composite laminates under fatigue loading [143-145]. Delamination buckling has been investigated extensively using three-dimensional models [56, 66, 111, 146-156]. A comparison of two-dimensional and three-dimensional analysis for skin/stringer debond failure was performed in [87, 157, 158].

The example chosen is taken from an investigation of delamination buckling and growth as shown in Figure 31a [143, 144, 159]. The specimens were made of T300/914C tape material with a [±5/+45/±5/-45/0/±85/0/-45/-+5/+45/-+5] layup. An embedded circular delamination of 10 mm diameter at interface 2/3 was assumed to simulate an impact damage near the surface as shown in Figure 31b. The specimens were subjected to tension-compression (R=-1) fatigue loading. Stress maxima in the range of 220-240 N/mm^2 had shown to yield stable delamination growth. During the experiment, the out-of-plane (i.e. buckling) deformation was monitored by Moirè technique. Using numerical post-processing procedures, the size and shape of the delaminated sublaminate was determined from this information, yielding the delamination contours, which were used as input to the numerical model. Additional X-ray photographies (as shown in Figure 31b) were used to verify this method. Finite element solutions were obtained using the *NOVA* finite element software. Due to the extensive computation times seen for three-dimensional models, a special layered element with eight nodes, formulated according to a continuum based three dimensional shell theory, was used for the nonlinear simulations [160]. Interpenetration of the layers in the delaminated region was prevented by using a contact processor that utilizes a contactor target concept applying the

penalty method [161]. Figure 31a shows the specimen outline, details of the section modeled and the deformed FE-model. The distributions of the mixed mode energy release rates along the front s_2 (i.e. after 200,000 load cycles) as shown in Figure 31b, are plotted in Figure 32. The global maximum of the total energy release rate G_T is now found perpendicular to the loading direction (s≈0.25 and s≈0.75) with a second maximum occuring in the loading direction. The values for interlaminar shear failure also reach their maximum perpendicular to the load direction (s≈0.22 and s≈0.72) and a second maximum for s=0 and s=0.5. This also holds for the G_I distribution where again the maximum is reached perpendicular to the loading direction, in loading direction however it ceases to zero. Details of the entire investigation are discussed in [162].

6. Concluding Remarks. The increased interest in using a fracture mechanics based approach to assess the damage tolerance of composite structures in the design phase and during certification has renewed the interest in the virtual crack closure technique. Efforts are underway to incorporate these approaches in the *Composites Material MIL-17 Handbook*, which has been the motivation for the overview presented.

The approach used in the virtual crack closure technique was discussed. Equations for the use of the technique in conjunction with two-dimensional elements, three-elements solids as well as plate/shell elements were given and insight into the application to engineering problems was provided. The paper, however, is not a comprehensive literature survey, but more a summary and review of issues relevant to the successful application of the virtual crack closure technique. Nevertheless, an effort was made to pay proper tribute to the relevant contributions made during a quarter century since the original publication.

Acknowledgements. The author gratefully acknowledges Dr. Fritz Buchholz of the University of Paderborn for his generous help in providing old manuscripts and insight into the history of the Virtual Crack Closure Technique. The author would also like to thank Dr. Manfred König of the University of Stuttgart and Jeffery Schaff of United Technologies Research Center for many discussions and their valuable input. Thanks are due to Dr. Ed Glaessgen of NASA Langley Research Center and Dr. Vasyl Harik of ICASE for the thorough review of this report.

Appendix A.

Implementation of the Virtual Crack Closure Technique. Currently, the large commercial finite element codes do not offer the choice for calculating the mixed mode energy release rates using the virtual crack closure technique (VCCT) as described in the main text. Therefore, the energy release rate components G_I , G_{II} and G_{III} need to be computed by user written subroutines. These subroutines may either interface directly with the finite element code during its execution, provided this option has been made available for this particular software, or operate as an entirely separate post-processing step. In both cases the strategy is similar and attention has to be given to the modeling of the discontinuity as shown in Figure A1 and the calculation of the mixed mode energy release rate as outlined in the flowchart of Figure A2.

As mentioned in section 3.1, the crack of length, a, in a two-dimensional finite element model is represented as a one-dimensional discontinuity by a line of nodes as shown in Figures 5 and 33. Nodes at the top surface and the

bottom surface have identical coordinates, however, are not connected with each other as shown in Figure 33a. The crack tip is represented by either a single node (Figure 33a) or two nodes with identical coordinates coupled through multi-point constraints (Figure 33b). The undamaged section or the section where the crack is closed and the structure is still intact is modeled using single nodes (Figure 33a) or two nodes with identical coordinates coupled through multi-point constraints (Figure 33b). It is generally up to the user to decide how to model the crack tip and the intact region. However, the use of multi-point constraints may be preferred if a crack propagation analysis is to be performed. The use of multi-point constraints may also be preferable if the finite element code used provides *"forces at constraints"* as a standard output. This feature would render obsolete the step where element forces at nodes have to be retrieved and summed to obtain forces at the crack tip. The same logic applies to a finite element model made of plate/shell type elements or three-dimensional solid elements, where the delamination of length, a, is represented as a two-dimensional discontinuity by two surfaces.

The application of the virtual crack closure technique based on results from finite element analysis requires access to the element forces at nodes, the nodal point displacements and the nodal point coordinates. The flow chart, depicted in Figure 34 as an example, shows an independent post-processing procedure where input data for the VCCT was extracted directly from an ABAQUS® binary result file. The strategy to use VCCT, however, is the same if data is retrived from a data file in ASCII format or if a user written subroutine interfaces directly with the finite element software during execution:

1. Establish interface with finite element sortware if required.

2. Provide input interface to read variable problem specific external data such as crack length, Young's modulus, etc., and control parameters such as element type, etc., which is generally not hard coded into the subroutine.

3. Create output file to store echo print of control parameters, input data, and retrieved data as well as intermediate and final results.

4. Read element forces, or forces at constraints, nodal point coordinates, and nodal displacements from binary result file, or output file in ASCII format or data bank if data is stored externally. Alternatively retrieve required data from specific common blocks or arrays of the finite element software if a user interface is provided.

5. Store the data retrieved in step 4 in external files, data base, or internal common blocks and arrays for further access during the calculation.

6. Calculate area virtually closed, ΔA, using nodal point coordinates.

7. Calculate local coordinate system x', y' and z' at crack tip for geometrically nonlinear analysis and arbitrarily shaped delamination front as discussed in sections 3.3, 3.5, and 3.6.

8.

a. Obtain the forces at the crack tip and in front of the crack tip from the forces at element nodes by summing the forces at common nodes from elements belonging either to the

upper or the lower surface. This step may be skipped if forces at contraints are available directly from the finite element software.

b. Obtain relative displacements between the surfaces from the nodal point displacements.

c. Transform forces and displacements to local crack tip coordinate system.

9. Calculate mixed mode strain energy release rates using the equations given for the individual element type and correct for different element lengths and widths if necessary.

10. Repeat steps 6 through 9 for all nodes along the delamination front and write results to output file.

REFERENCES

[1] A. C. GARG, *Delamination - A Damage Mode in Composite Structures*, Eng. Fracture Mech., Vol. 29, pp. 557-584, 1988.

[2] V. V. BOLOTIN, *Delaminations in composite structures: its origin, buckling, growth and stability*, Composites Part B: Engineering, Vol. 27B, pp. 129-145, 1996.

[3] N. J. PAGANO AND G. A. SCHOEPPNER, *Delamination of Polymer Matrix Composites: Problems and Assessment*, in Comprehensive Composite Materials, Vol. 2, A. Kelly and C. Zweben, Eds.: Elsevier Science Ltd., 2000, pp. 433-528.

[4] T. K. O'BRIEN, *Characterization of Delamination Onset and Growth in a Composite Laminate*, in Damage in Composite Materials, ASTM STP 775, 1982, pp. 140-167.

[5] T. K. O'BRIEN, *Interlaminar fracture toughness: The long and winding road to standardization*, Composites Part B, Vol. 29, pp. 57-62, 1998.

[6] R. H. MARTIN, *Incorporating interlaminar fracture mechanics into design*, in International Conference on Designing Cost-Effective Composites: IMechE Conference Transactions, London, U.K., 1998, pp. 83-92.

[7] T. K. O'BRIEN AND R. H. MARTIN, *Round Robin Testing for Mode I Interlaminar Fracture Toughness of Composite Materials*, J. of Composite Technology and Research., pp. 269-281, 1993.

[8] T. K. O'BRIEN, *Composite Interlaminar Shear Fracture Toughness, G_{IIc}: Shear Measurement or Sheer Myth ?*, in Composite Materials: Fatigue and Fracture, Seventh Volume, ASTM STP 1330, 1998, pp. 3-18.

[9] J. R. REEDER AND J. H. CREWS, *Mixed Mode Bending Method for Delamination Testing*, AIAA J., Vol. 28, pp. 1270--1276, 1990.

[10] J. R. REEDER AND J. H. CREWS, *Redesign of the Mixed-Mode Bending Delamination Test to Reduce Nonlinear Effects*, Journal Composite Tech. Res., Vol. 14, pp. 12-19, 1992.

[11] J. R. REEDER, *A Bilinear Failure Criterion for Mixed-Mode Delamination*, in Composite Materials: Testing and Design (Eleventh Volume), ASTM STP 1206, 1993, pp. 303-322.

[12] P. HANSEN AND R. MARTIN, *DCB, 4ENF and MMB Delamination Characterisation of S2/8552 and IM7/8552*, Materials Engineering Research Laboratory Ltd. (MERL), Hertford, UK, N68171-98-M-5177, 1999.

[13] S. M. LEE, *Failure Mechanics of Edge Delamination of Composites*, J. Composite Mat., Vol. 24, pp. 1200-1212, 1990.

[14] R. H. MARTIN, *Evaluation of the Split Cantilever Beam for Mode III Delamination Testing*, in Composite Materials: Fatigue and Fracture (Third Volume), ASTM STP 1110, 1991, pp. 243--266.

[15] P. ROBINSON AND D. Q. SONG, *Development of an improved mode III delamination test for composites*, Composites Science and Technology, Vol. 52, pp. 217-233, 1994.

[16] J. LI, S. M. LEE, E. W. LEE, AND T. K. O'BRIEN, *Evaluation of the Edge Crack Torsion ECT Test for Mode III Interlaminar Fracture Toughness of Laminated Composites*, Journal of Composites Technology and Research, Vol. 19, pp. 174-183, 1997.

[17] E. F. RYBICKI AND M. F. KANNINEN, *A Finite Element Calculation of Stress Intensity Factors by a Modified Crack Closure Integral*, Eng. Fracture Mech., Vol. 9, pp. 931-938, 1977.

[18] I. S. RAJU, *Calculation Of Strain-Energy Release Rates With Higher Order And Singular Finite Elements*, Eng. Fracture Mech., Vol. 28, pp. 251-274, 1987.

[19] F. G. BUCHHOLZ, H. GREBNER, K. H. DREYER, AND H. KROME, *2D- and 3D- Applications of the Improved and Generalized Modified Crack Closure Integral Method*, in Computational Mechanics '88, S. N. Atluri and G. Yagawa, Eds., 1988.

[20] A. INGRAFFEA AND P. WAWRZYNEK, *FRANC2D: A Case Study in Transfer of Software Technology*, in Research Transformed into Practice: Implementations of NSF Research, J. Colville and A. Amde, Eds.: ASCE Press, New York, 1995, pp. 233-344.

[21] R. SINGH, B. J. CARTER, P. A. WAWRZYNEK, AND A. R. INGRAFFEA, *Universal crack closure integral for SIF estimation*, Engineering Fracture Mechanics, Vol. 60, pp. 133-146, 1998.

[22] J. ST. DOLTSINIS, H. KNAPP, P. STREINER, AND H. WÜSTENBERG, *PERMAS-FM, Fracture Mechanics*, INTES GmbH, Stuttgart, User Manual, Publication No. 226, Rev. C, 1985.

[23] R. KRÜGER, M. KÖNIG, AND T. SCHNEIDER, *Computation of Local Energy Release Rates Along Straight and Curved Delamination Fronts of Unidirectionally Laminated DCB- and ENF- Specimens*, in Proceedings of the 34th AIAA/ASME/ASCE/AHS/ASC SSDM Conference, La Jolla, CA: American Institute of Aeronautics and Astronautics, Washington, 1993, pp. 1332-1342.

[24] T. K. HELLEN, *On the Method of Virtual Crack Extension*, Int. J. Num. Meth. Eng., Vol. 9, pp. 187-207, 1975.

[25] D. M. PARKS, *A stiffness derivative finite element technique for determination of crack tip stress intensity factors*, Int. J. Fracture, Vol. 10, pp. 487-502, 1974.

[26] D. M. PARKS, *The Virtual Crack Extension Method For Nonlinear Material Behaviour*, Comput. Methods Appl. Mech. Eng., Vol. 12, pp. 353-364, 1977.

[27] D. M. PARKS, *Virtual Crack Extension: A General Finite Element Technique for J-Integral Evaluation*, in Numerical Methods in Fracture Mechanics, A. R. Luxmoore and D. R. J. Owen, Eds., 1978, pp. 464-479.

[28] H. G. DELORENZI, *On the energy release rate and the J-integral for 3-D crack configurations*, Int. J. Fracture, Vol. 19, pp. 183-193, 1982.

[29] H. G. DELORENZI AND C. D. SHIH, *3-D Elastic-plastic investigation of fracture parameters in side-grooved compact specimen*, Int. J. Fracture, Vol. 21, pp. 195-220, 1983.

[30] H. G. DELORENZI, *Energy Release Rate Calculations by the Finite Element Method*, Eng. Fracture Mech., Vol. 21, pp. 129-143, 1985.

[31] S. C. LIN AND J. F. ABEL, *Variational aproach for a new direct-integration form of the virtual crack extension method*, International Journal of Fracture, Vol. 38, pp. 217-235, 1988.

[32] P. W. CLAYDON, *Maximum Energy Release Rate Distribution From a Generalized 3D Virtual Crack Extension Method*, Engineering Fracture Mechanics, Vol. 42, pp. 961-969, 1992.

[33] C. G. HWANG, P. A. WAWRZYNEK, A. K. TAYEBI, AND A. R. INGRAFFEA, *On the virtual crack extension method for calculation of the rates of energy release rate*, Engineering Fracture Mechanics, Vol. 59, pp. 521-542, 1998.

[34] H. ISHIKAWA, *A Finite Element Analysis of Stress Intensity Factors for Combined Tensile and Shear Loading by Only a Virtual Crack Extension*, Int. J. Fracture, Vol. 16, pp. R243-R246, 1980.

[35] G. T. SHA, *On the Virtual Crack Extension Technique for Stress Intensity Factors and Energy Release Rate Calculations for Mixed Fracture Mode*, Int. J. Fracture, Vol. 25, pp. R 33-R 42, 1984.

[36] K. N. SHIVAKUMAR AND I. S. RAJU, *An Equivalent Domain Integral Method for Three-Dimensional Mixed-Mode Fracture Problems*, Engineering Fracture Mechanics, Vol. 42, pp. 935-959, 1992.

[37] I. S. RAJU AND K. N. SHIVAKUMAR, *An Equivalent Domain Integral Method in the Two-Dimensional Analysis Mixed-Mode Crack Problems*, Engineering Fracture Mechanics, Vol. 37, pp. 707-725, 1990.

[38] L. BANKS-SILLS, *Application of the finite element method to linear elastic fracture mechanics*, Applied Mechanics Reviews, Vol. 44, pp. 447-461, 1991.

[39] W. T. CHOW AND S. N. ATLURI, *Stress intensity factors as the fracture parameters for delamination crack growth in composite laminates*, Composites, Part B, Vol. 28B, pp. 375-384, 1997.

[40] M. GOSZ AND B. MORAN, *An interaction energy integral method for computation of mixed-mode stress intensity factors along non-planar crack fronts in three dimensions*, Engineering Fracture Mechanics, Vol. 69, pp. 299-319, 2002.

[41] O. PARK AND B. V. SANKAR, *Crack-tip force method for computing energy release rate in delaminated plates*, Composite Structures, Vol. 55, pp. 429-434, 2002.

[42] E. F. RYBICKI, D. W. SCHMUESER, AND J. FOX, *An Energy Release Rate Approach for Stable Crack Growth in the Free-Edge Delamination Problem*, Journal of Composite Materials, Vol. 11, pp. 470-487, 1977.

[43] J. SCHÖN AND B. ANDERSSON, *Calculation of Mode-Separated Energy Release Rates During Delamination Growth*, in Proceedings of the American Society for Composites - 13th Technical Conference on Composite Materials, 1998.

[44] N. K. MUKHOPADHYAY, A. KAKODKAR, AND S. K. MAITI, *Further considerations in modified crack closure integral based computation of stress intensity factor in BEM*, Eng. Fracture Mech., Vol. 59, pp. 269-279, 1998.

[45] G. R. IRWIN, *Fracture I*, in Handbuch der Physik VI, Flügge, Ed., 1958, pp. 558-590.

[46] D. BROEK, *Elementary Engineering Fracture Mechanics*, 4th revised ed: Kluwer Academic Publishers, 1991.

[47] F. G. BUCHHOLZ, *Improved Formulae for the FE-Calculation of the Strain Energy Release Rate by the Modified Crack Closure Integral Method*, in Proceedings of the 4th World Congress on Finite Elements, Interlaken, 1984, pp. 650-659.

[48] F. G. BUCHHOLZ AND B. MEINERS, *On the Accuracy of the Modified Crack Closure Integral Method in Combination with Higher Order Finite Elements*, in Accuracy Estimates and Adaptive Refinements in Finite Element Computations, Proceedings of the International Conference, Lisbon, vol. I: Technical University of Lisbon, 1984, pp. 131-140.

[49] T. S. RAMAMURTHY, et al., *Modified Crack Closure Integral Method With Quarter Point Elements*, Mechanics Research Communications, Vol. 13, pp. 179-186, 1986.

[50] K. B. NARAYANA, B. DATTAGURU, T. S. RAMAMURTHY, AND K. VIJAYAKUMAR, *Modified Crack Closure Integral Using Six-Noded Isoparametric Quadrilateral Singular Elements*, Eng. Fracture Mech., Vol. 36, pp. 945-955, 1990.

[51] K. B. NARAYANA AND B. DATTAGURU, *Certain aspects related to computation by modified crack closure integral (MCCI)*, Eng. Fracture Mech., Vol. 55, pp. 335-339, 1996.

[52] R. SETHURAMAN AND S. K. MAITI, *Finite Element Based Computation of Strain Energy Release Rate by Modified Crack Closure Integral*, Engineering Fracture Mechanics, Vol. 30, pp. 227-231, 1988.

[53] K. N. SHIVAKUMAR, P. W. TAN, AND J. C. NEWMAN, *A Virtual Crack-Closure Technique for Calculating Stress Intensity Factors for Cracked Three Dimensional Bodies*, Int. J. Fracture, Vol. 36, pp. R43-R50, 1988.

[54] I. S. RAJU, R. SISTLA, AND T. KRISHNAMURTHY, *Fracture Mechanics Analyses for Skin-Stiffener Debonding*, Eng. Fracture Mech., Vol. 54, pp. 371-385, 1996.

[55] I. S. RAJU, K. N. SHIVAKUMAR, AND J. H. CREWS~JR., *Three-Dimensional Elastic Analysis of a Composite Double Cantilever Beam Specimen*, AIAA J., Vol. 26, pp. 1493-1498, 1988.

[56] J. D. WHITCOMB AND K. N. SHIVAKUMAR, *Strain-Energy Release Rate Analysis of Plates with Postbuckled Delaminations*, J. Composite Mat., Vol. 23, pp. 714-734, 1989.

[57] F. G. BUCHHOLZ, *Finite Element Analysis of a 3D Mixed-Mode fracture Problem by Virtual Crack Closure Intergral Method*, in Proceedings of the Indo-German Workshop, Indian Institute of Science, A. V. K. Murthy and F. G. Buchholz, Eds.: Interline Publications, Bangalore, 1994, pp. 7-12.

[58] K. B. NARAYANA, et al., *Modified Crack Closure Integral (MCCI) for 3-d Problems Using 20-Noded Brick Elements*, Fatigue Fract. Engng. Mater. Struct., Vol. 17, pp. 145-157, 1994.

[59] R. SINGH, S. K. PATEL, AND B. DATTAGURU, *Decomposed crack closure integrals for estimation of SIF variations*, Engineering Fracture Mechanics, Vol. 63, pp. 165-178, 1999.

[60] G. D. ROECK AND M. M. A. WAHAB, *Strain Energy Release Rate Formulae for 3D Finite Element*, Eng. Fracture Mech., Vol. 50, pp. 569-580, 1995.

[61] J. T. WANG AND I. S. RAJU, *Strain energy release rate formulae for skin-stiffener debond modeled with plate elements*, Engineering Fracture Mechanics, Vol. 54, pp. 211-228, 1996.

[62] E. H. GLAESSGEN, W. T. RIDDELL, AND I. S. RAJU, *Effect of Shear Deformation and Continuity on Delamination Modeling with Plate Elements*, in The 39rd AIAA/ASME/ASCE/AHS/ASC Structures, Structural Dynamics and Materials Conference, 1998.

[63] E. H. GLAESSGEN, W. T. RIDDELL, AND I. S. RAJU, *Nodal Constraint, Shear Deformation and Continuity Effects Related to the Modeling of Debonding of Laminates, Using Plate Elements*, CMES, Vol. 3, pp. 103-116, 2002.

[64] M. KÖNIG, R. KRÜGER, AND S. RINDERKNECHT, *Finite Element Analysis of Delamination Growth in a Multidirectional Composite ENF Specimen*, in Composite Materials: Theory and Practice, ASTM STP 1383, P. Grant and C. Q. Rousseau, Eds.: American Society for Testing and Materials, 2000, pp. 345-365.

[65] R. KRUEGER AND T. K. O'BRIEN, *A Shell/3D Modeling Technique for the Analysis of Delaminated Composite Laminates*, Composites Part A: Applied Science and Manufacturing, Vol. 32, pp. 25-44, 2001.

[66] J. D. WHITCOMB, *Mechanics of Instability-Related Delamination Growth*, in Composite Materials: Testing and Design (Ninth Volume), S. P. Garbo, Ed., 1990, pp. 215-230.

[67] S. A. SMITH AND I. S. RAJU, *Evaluation of Stress-Intensity Factors Using General Finite-Element Models*, in Fatigue and Fracture Mechanics (Twenty-Ninth Volume) ASTM STP 1332, T. L. Pantonin and S. D. Sheppard, Eds.: American Society for Testing and Materials, 1999, pp. 176-200.

[68] C. H. FERRIE AND C. Q. ROUSSEAU, *A Method of Applying VCCT to Corner Crack Nodes*, presented at Proceedings of the American Society for Composites - 16th Annual Technical Conference on Composite Materials, Blacksburg, Va., USA, 2001.

[69] I. S. RAJU, J. H. CREWS, AND M. A. AMINPOUR, *Convergence of Strain Energy Release Rate Components for Edge-Delaminated Composite Laminates*, Eng. Fracture Mech., Vol. 30, pp. 383-396, 1988.

[70] C. HWU AND J. HU, *Stress Intensity Factors and Energy Release Rates of Delaminations in Composite Laminates*, Eng. Fracture Mech., Vol. 42, pp. 977-988, 1992.

[71] C. T. SUN AND C. J. JIH, *On Strain Energy Release Rates for Interfacial Cracks in Bi-Material Media*, Eng. Fracture Mech., Vol. 28, pp. 13-20, 1987.

[72] C. T. SUN AND M. G. MANOHARAN, *Strain Energy Release Rates of an Interfacial Crack Between Two Orthotropic Solids*, J. Composite Materials, Vol. 23, pp. 460-478, 1989.

[73] B. DATTAGURU, K. S. VENKATESHA, T. S. RAMAMURTHY, AND F. G. BUCHHOLZ, *Finite Element Estimates of Strain Energy Release Rate Components at the Tip of an Interface Crack Under Mode I Loading*, Enineering Fracture Mechanics, Vol. 49, pp. 451-463, 1994.

[74] J. L. BEUTH AND S. H. NARAYAN, *Separation of Crack Extension Modes in Composite Delamination Problems*, in Composite Materials: Fatigue and Fracture (Sixth Volume), ASTM STP 1285, E. A. Armanios, Ed.: American Society for Testing and Materials, 1997, pp. 324-342.

[75] H. HUANG AND G. A. KARDOMATEAS, *Mixed-mode stress intensity factors for cracks located at or parallel to the interface in bimaterial half planes*, Int. J. of Solids and Structures, Vol. 38, pp. 3719-3734, 2001.

[76] W. QIAN AND C. T. SUN, *Calculation of stress intensity factors for interlaminar cracks in composite laminates*, Composites Science and Technology, Vol. 57, pp. 637-650, 1997.

[77] W. QIAN AND C. T. SUN, *Methods for calculating stress intensity factors for interfacial cracks between two orthotropic solids*, Int. J. of Solids and Structures, Vol. 35, pp. 3317-3330, 1998.

[78] V. BONIFACE AND K. R. Y. SIMHA, *Re-examination of crack opening model of interface fracture*, Eng. Fracture Mech., Vol. 64, pp. 677-691, 1999.

[79] C. T. SUN AND W. QIAN, *The use of finite extension strain energy release rates in fracture of interfacial cracks*, Int. J. of Solids and Structures, Vol. 34, pp. 2595-2609, 1997.

[80] K. S. VENKATESHA, B. DATTAGURU, AND T. S. RAMAMURTHY, *Finite Element Analysis of an Interface Crack with Large Crack-Tip Contact Zones*, Engineering Fracture Mechanics, Vol. 54, pp. 847-860, 1996.

[81] K. S. VENKATESHA, B. DATTAGURU, AND T. S. RAMAMURTHY, *Generalized Modified Crack Closure Intergral (GMCCI) and its Application to Interface Crack Problems*, Computers & Structures, Vol. 60, pp. 665-676, 1996.

[82] K. S. VENKATESHA, T. S. RAMAMURTHY, AND B. DATTAGURU, *A study of the behaviour of subinterface cracks in bimaterial plates*, Eng. Fracture Mech., Vol. 59, pp. 241-252, 1998.

[83] Z. ZOU, S. R. REID, P. D. SODEN, AND S. LI, *Mode separation of energy release rate for delamination in composite laminates using sublaminates*, Int. J. of Solids and Structures, Vol. 38, pp. 2597-2613, 2001.

[84] T. K. O'BRIEN, *Personal Communication.*, 2001.

[85] R. KRÜGER, *Three Dimensional Finite Element Analysis of Multidirectional Composite DCB, SLB and ENF Specimens*, Institute for Statics and Dynamics of Aerospace Structures, University of Stuttgart ISD-Report No. 94/2, 1994.

[86] R. KRUEGER AND T. K. O'BRIEN, *A Shell/3D Modeling Technique for the Analysis of Delaminated Composite Laminates*, NASA/TM-2000-210287, ARL-TR-2207, June 2000.

[87] R. KRUEGER, I. L. PARIS, T. K. O'BRIEN, AND P. J. MINGUET, *Comparison of 2D Finite Element Modeling Assumptions with Results from 3D Analysis for Composite Skin-Stiffener Debonding*, presented at Eleventh International Conference on Composite Structures, Melbourne, Australia, 19th-21th November, 2001.

[88] R. L. RAMAKUMAR AND J. D. WHITCOMB, *Characterization of Mode I and Mixed-Mode Delamination Growth in T300/5208 Graphite/Epoxy*, in Delamination and Debonding of Materials, ASTM STP 876, W. S. Johnson, Ed., 1985, pp. 315-335.

[89] Y. TANZAWA, N. WATANABE, AND T. ISHIKAWA, *FEM simulation of a modified DCB test for 3-D orthogonal interlocked fabric composites*, Composites Science and Technology, Vol. 61, pp. 1097-1107, 2001.

[90] K. Y. RHEE, *On the validity of applying the elastic work factor approach to determine G_{Ic} of fiber-reinforced laminated composites*, Composite Structures, Vol. 37, pp. 57-63, 1997.

[91] R. RIKARDS, et al., *Investigation of mixed mode I/II interlaminar fracture toughness of laminated composites by using a CTS type specimen*, Engineering Fracture Mechanics, Vol. 61, pp. 325-342, 1998.

[92] R. RIKARDS, et al., *Interlaminar Fracture Toughness of GFRP Influenced by Fiber Surface Treatment*, J. Composite Materials, Vol. 32, pp. 1528-1559, 1998.

[93] S. JOSE, R. R. KUMAR, M. K. JANAB, AND G. V. RAOB, *Intralaminar fracture toughness of a cross-ply laminate and its constituent sub-laminates*, Composites Science and Technology, Vol. 61, 2001.

[94] A. PIERACCI, B. D. DAVIDSON, AND V. SUNDARARAMAN, *Nonlinear Analyses of Homogeneous, Symmetrically Delaminated Single Leg Bending Specimens*, Journal Composite Tech. Res., Vol. 20, pp. 170-178, 1998.

[95] C. SCHUECKER AND B. D. DAVIDSON, *Effect of Friction on the Perceived Mode II Delamination Toughness from Three- and Four-Point Bend End-Notched Flexure Tests*, in Composite Materials: Theory and Practice, ASTM STP 1383, P. Grant and C. Q. Rousseau, Eds.: American Society for Testing and Materials, 2000, pp. 334-344.

[96] H. WANG, S. DING, F. G. BUCHHOLZ, AND R. RIKARDS, *Delamination analysis for 2D- and 3D-models of a cross-ply laminated three-point bending specimen*, in Localized Damage III, M. H. Aliabadi, A. Carpinteri, S. Kalisky, and D. J. Cartwright, Eds.: Computational Mechanics Publications, 1994, pp. 251-258.

[97] A. BANSAL AND M. KUMOSA, *Analysis of double edge-cracked iosipescu specimens under biaxial loads*, Eng. Fracture Mech., Vol. 59, pp. 89-100, 1998.

[98] F. G. BUCHHOLZ, M. BÜRGER, M. KUMOSA, AND H. EGGERS, *Mixed-Mode Fracture Analysis of Orthotropic Laminates by Local and Global Energy Methods*, in Numerical Methods in Fracture Mechanics, A. R. Luxmoore and D. R. J. Owen, Eds.: Pineridge Press, 1990, pp. 391-402.

[99] J. D. WHITCOMB AND I. S. RAJU, *Analysis of Interlaminar Stresses in Thick Composite Laminates With and Without Edge Delamination*, in Delamination and Debonding of Materials, ASTM STP 876, W. S. Johnson, Ed., 1985, pp. 69-94.

[100] J. LI, T. K. O'BRIEN, AND C. Q. ROUSSEAU, *Test and Analysis of Composite Hat Stringer Pull-off Test Specimens*, Journal of the American Helicopter Society, pp. 350-357, 1997.

[101] J. LI, *Flange delamination prediction in composite structures with ply waviness*, AIAA J., Vol. 38, pp. 893-897, 2000.

[102] M. M. A. WAHAB, *On the use of fracture mechanics in designing a single lap adhesive joint*, J. Adhes. Sci. Technol., Vol. 14, pp. 851-865, 2000.

[103] M. QIN AND Y. DZENIS, *Nonlinear Numerical and Experimental Analysis of Single Lap Adhesive Composie Joinmts with Delaminated Adherends*, in Proceedings of the Thirteenth International Conference on Composite Materials (ICCM13), Y. Zhang, Ed. Beijing, 2001.

[104] W. S. JOHNSON, L. M. BUTKUS, AND R. V. VALENTIN, *Applications of Fracture Mechanics to the Durability of Bonded Composite Joints*, U.S. Department of Transportation, Federal Aviation Administration DOT/FAA/AR-97/56, 1998.

[105] S. GOSWAMIA AND W. BECKER, *The effect of facesheet/core delamination in sandwich structures under transverse loading*, Composite Structures, Vol. 54, pp. 515-521, 2001.

[106] J. G. A. RATCLIFFE, *Interfacial Fracture Toughness Characterisation of Sandwich Structures*, Ph.D. Thesis, The University of Liverpool, 2001.

[107] W. J. CANTWELL, R. SCUDAMORE, J. RATCLIFFE, AND P. DAVIES, *Interfacial fracture in sandwich laminates*, Composites Science and Technology, Vol. 59, pp. 2079-2085, 1999.

[108] E. H. GLAESSGEN, D. W. SLEIGHT, T. KRISHNAMURTHY, AND I. S. RAJU, *Analyses for Debonding of Stitched Composite Sandwich Structures Using Improved Constitutive Models*, in The 42nd AIAA/ASME/ASCE/AHS/ASC Structures, Structural Dynamics, and Materials Conference, 2001.

[109] J. D. WHITCOMB, *Strain-Energy Release Rate Analysis of Cyclic Delamination Growth in Compressively Loaded Laminates*, in Effect of Defects in Composite Materials, ASTM STP 836, 1984, pp. 175-193.

[110] S.-F. HWANG AND C.-P. MAO, *Failure of delaminated interply hybrid composite plates under compression*, Composites Science and Technology, Vol. 61, pp. 1513-1527, 2001.

[111] K. L. SINGH, B. DATTAGURU, T. S. RAMAMURTHY, AND P. D. MANGALGIRI, *3D Fracture Analysis of Delaminations in Laminated Composites*, in Modeling and Simulation Based Engineering, vol. II, S. N. Atluri and P. E. O'Donoghue, Eds.: Tech Science Press, 1999, pp. 1592-1597.

[112] G. B. MURRI, T. K. O'BRIEN, AND C. Q. ROUSSEAU, *Fatigue Life Methodology for Tapered Composite Flexbeam Laminates*, Journal of the American Helicopter Society, Vol. 43, pp. 146-155, 1998.

[113] G. B. MURRI, J. R. SCHAFF, AND A. L. DOBYNS, *Fatigue and Damage Tolerance Analysis of a Hybrid Composite Tapered Flexbeam*, in Proceedings of the American Helicopter Society 57th Annual Forum. Washington, DC, May 9-11, 2001.

[114] R. KRUEGER, I. L. PARIS, T. K. O'BRIEN, AND P. J. MINGUET, *Fatigue Life Methodology for Bonded Composite Skin/Stringer Configurations*, Journal of Composites Technology and Research, Vol. 24, 2002.

[115] P. J. MINGUET AND T. K. O'BRIEN, *Analysis of Composite Skin/Stringer Bond Failures Using a Strain Energy Release Rate Approach*, in The Tenth International Conference on Composite Materials, vol. I, A. Poursartip and K. Street, Eds., 1995, pp. 245--252.

[116] P. J. MINGUET, *Analysis of the Strength of the Interface Between Frame and Skin in a Bonded Composite Fuselage Panel*, in The 38rd AIAA/ASME/ASCE/AHS/ASC Structures, Structural Dynamics and Materials Conference, 1997, pp. 2783--2790.

[117] R. KRUEGER, M. K. CVITKOVICH, T. K. O'BRIEN, AND P. J. MINGUET, *Testing and Analysis of Composite Skin/Stringer Debonding Under Multi-Axial Loading*, J. Composite Materials, Vol. 34, pp. 1263-1300, 2000.

[118] D. M. HOYT, S. H. WARD, AND P. J. MINGUET, *Strength and Fatigue Life Modeling of Bonded Joints in Composite Structure*, J. of Composite Technology and Research, Vol. 24, 2002.

[119] G. FLANAGAN, *A General Sublaminate Analysis Method for Determining Strain Energy Release Rates in Composites*, in The 35rd AIAA/ASME/ASCE/AHS/ASC Structures, Structural Dynamics and Materials Conference, 1994, pp. 381-389.

[120] J. W. H. YAP, et al., *An Automated Finite Element Modelling Tool for Analysis of Skin-to-Stiffener Debonds in Composite Aerospace Structures*, in Proceedings of the Thirteenth International Conference on Composite Materials (ICCM13), Y. Zhang, Ed. Beijing, 2001.

[121] R. R. KUMAR AND G. V. RAO, *Some Studies on Interlaminar and Intralaminar Fracture Toughness of Multilayered Composite Structures*, in Proceedings of the Thirteenth International Conference on Composite Materials (ICCM13), Y. Zhang, Ed. Beijing, 2001.

[122] E. H. GLAESSGEN, I. S. RAJU, AND C. C. POE, *Fracture Mechanics Analysis of Stitched Stiffener-Skin Debonding*, in The 39rd AIAA/ASME/ASCE/AHS/ASC Structures, Structural Dynamics and Materials Conference, Long Beach, California, AIAA 98-2022, April 20-23, 1998.

[123] E. H. GLAESSGEN, I. S. RAJU, AND C. C. POE, *Delamination and Stitch Failure in Stitched Composite Joints*, in Proceedings of the 40th AIAA/ASME/ASCE/AHS/ASC Structures, Structural Dynamics and Materials Conference, 1999.

[124] E. H. GLAESSGEN, I. S. RAJU, AND C. C. POE, *Debonding of Stitched Composite Joints: Testing and Analysis*, in Society for Experimental Mechanics Spring Conference and Exposition. Cincinnati, Ohio, June 7-9, 1999.

[125] S. RINDERKNECHT AND B. KRÖPLIN, *A Finite Element Model for the Delamination in Composite Plates*, Mechanics of Composite Materials and Structures, Vol. 2, pp. 19-47, 1995.

[126] S. RINDERKNECHT AND B. KROPLIN, *Computational method for the analysis of delamination growth in composite plates*, Computers and Structures, Vol. 64, pp. 359-374, 1997.

[127] J. KLUG, X. X. WU, AND C. T. SUN, *Efficient modeling of postbuckling delamination growth in composite laminates using plate elements*, AIAA Journal, Vol. 34, pp. 178-184, 1996.

[128] S. ZHENG AND C. T. SUN, *Delamination interaction in laminated structures*, Eng. Fracture Mech., Vol. 59, pp. 225-240, 1998.

[129] J. R. REEDER, K. SONG, P. B. CHUNCHU, AND D. R. AMBUR, *Postbuckling and Growth of Delaminations in Composite Plates Subjected to Axial Compression*, presented at 43rd AIAA/ASME/ASCE/AHS/ASC Structures, Structural Dynamics, and Materials Conference, Denver, Colorado, USA, 2002.

[130] J. H. CREWS, K. N. SHIVAKUMAR, AND I. S. RAJU, *Strain Energy Release Rate Distribution for Double Cantilever Beam Specimens*, AIAA J., Vol. 29, pp. 1686-1691, 1991.

[131] B. D. DAVIDSON, R. KRÜGER, AND M. KÖNIG, *Three Dimensional Analysis of Center Delaminated Unidirectional and Multidirectional Single Leg Bending Specimens*, Composites Science and Technology, Vol. 54, pp. 385-394, 1995.

[132] B. D. DAVIDSON, R. KRÜGER, AND M. KÖNIG, *Three Dimensional Analysis and Resulting Design Recommendations for Unidirectional and Multidirectional End-Notched Flexure Tests*, J. Composite Materials, Vol. 29, pp. 2108-2133, 1995.

[133] B. D. DAVIDSON, R. KRÜGER, AND M. KÖNIG, *Effect of Stacking Sequence on Energy Release Rate Distributions in Multidirectional DCB and ENF specimens*, Eng. Fracture Mech., Vol. 55, pp. 557-569, 1996.

[134] K. SHIVAKUMAR, S. GHANTAE, AND M. SHARPE, *Split Angle-Ply Beam Specimen for Measurement of Fracture Toughness with Mode III Stress State*, in Proceedings of the Thirteenth International Conference on Composite Materials (ICCM13), Y. Zhang, Ed. Beijing, 2001.

[135] H. SUEMASU, *An experimental method to measure the mode-III interlaminar fracture toughness of composite laminates*, Composites Science and Technology, Vol. 59, pp. 1015-1021, 1999.

[136] G. DHONDT, A. CHERGUI, AND F.-G. BUCHHOLZ, *Computational fracture analysis of different specimens regarding 3D and mode coupling effects*, Eng. Fracture Mech., Vol. 68, pp. 383-401, 2001.

[137] H. WANG, F. G. BUCHHOLZ, AND R. RIKARDS, *Delamination Analysis of an Angle-Ply Laminated Three-Point Bending Specimen*, in Computational Mechanics '95: Theory and Application, vol. II, S. N. Atluri, G. Yagawa, and T. A. Cruse, Eds.: Springer Verlag Heidelberg, 1995, pp. 2323-2328.

[138] S. A. SALPEKAR AND T. K. O'BRIEN, *Combined Effect of Matrix Cracking and Free Edge on Delamination*, in Composite Materials: Fatigue and Fracture, Third Volume, ASTM STP 1110, 1991, pp. 287-311.

[139] K. KACZMAREK, M. R. WISNOM, AND M. I. JONES, *Edge delamination in curved $(0_4/\pm45_6)_s$ glass-fibre/epoxy beams loaded in bending*, Composites Science and Technology, Vol. 58, pp. 155-161, 1998.

[140] J. LINDEMANN AND W. BECKER, *The tendency for free-edge delamination in laminates and its minimization*, Composites Science and Technology, Vol. 62, pp. 233-242, 2002.

[141] D. A. BURIANEK AND S. M. SPEARING, *Interacting Damage Modes in Titanium-Graphite Hybrid Laminates*, in Proceedings of the Thirteenth International Conference on Composite Materials (ICCM13), Y. Zhang, Ed. Beijing, 2001.

[142] T. IREMAN, et al., *Damage propagation in composite structural elements-coupon experiments and analyses*, Composite Structures, Vol. 36, pp. 209-220, 1996.

[143] R. KRÜGER AND M. KÖNIG, *Prediction of Delamination Growth Under Cyclic Loading*, in Composite Materials: Fatigue and Fracture (Sixth Volume), ASTM STP 1285, E. A. Armanios, Ed.: American Society for Testing and Materials, 1997, pp. 162-178.

[144] R. KRÜGER, M. KÖNIG, AND B. KRÖPLIN, *Delamination Growth in CFRP-Laminates: Development of a predictive tool based on computational fracture mechanics*, in Proceedings of the 38th AIAA/ASME/ASCE/AHS/ASC SSDM Conference, Kissimmee, FL., 1997, pp. 2064-2072.

[145] S. C. PRADHAN AND T. E. TAY, *Three-dimensional finite element modelling of delamination growth in notched composite laminates under compression loading*, Eng. Fracture Mech., Vol. 60, pp. 157-171, 1998.

[146] J. D. WHITCOMB, *Three-Dimensional Analysis of a Postbuckled Embedded Delamination*, J. Composite Mat., Vol. 23, pp. 862--889, 1989.

[147] J. D. WHITCOMB, *Analysis of a Laminate with a Postbuckled Embedded Delamination, Including Contact Effects*, J. Composite Mat., Vol. 26, pp. 1523--1535, 1992.

[148] K. N. SHIVAKUMAR AND J. D. WHITCOMB, *Buckling of a Sublaminate in a Quasi-Isotropic Laminate*, J. Composite Mat., Vol. 19, pp. 2--18, 1985.

[149] P. GAUDENZI, P. PERUGINI, AND A. RICCIO, *Post-buckling behavior of composite panels in the presence of unstable delaminations*, Composite Structures, Vol. 51, pp. 301-309, 2001.

[150] T. E. TAY, et al., *Mesh design in finite element analysis of post-buckled delamination in composite laminates*, Composite Structures, Vol. 47, pp. 603-611, 1999.

[151] F. SHEN, K. H. LEE, AND T. E. TAY, *Modeling delamination growth in laminated composites*, Composites Science and Technology, Vol. 61, pp. 1239-1251, 2001.

[152] A. RICCIO, P. PERUGINI, AND F. SCARAMUZZINO, *Modelling compression behaviour of delaminated composite panels*, Computers & Structures, Vol. 78, pp. 73-81, 2000.

[153] A. RICCIO, F. SCARAMUZZINO, AND P. PERUGINI, *Embedded delamination growth in composite panels under compressive load*, Composites Part B: Engineering, Vol. 32, pp. 209-218, 2001.

[154] B. PRADHAN AND D. CHAKRABORTY, *Fracture behavior of FRP composite laminates with an embedded elliptical delamination at the interface*, Journal of Reinforced Plastics Composites, Vol. 19, pp. 1004-1023, 2000.

[155] H. SUEMASU AND T. KUMAGAI, *Compressive behavior of multiply delaminated composite laminates. Part 2: Finite element analysis*, AIAA J., Vol. 36, pp. 1286-1290, 1998.

[156] F. LACHAUD, B. LORRAIN, L. MICHEL, AND R. BARRIOL, *Experimental and numerical study of delamination caused by local buckling of thermoplastic and thermoset composites*, Compos. Sci. Technol., Vol. 58, pp. 727-733, 1998.

[157] J. LI AND J. K. SEN, *Analysis of Frame-to-Skin Joint Pull-off Tests and Prediction of the Delamination Failure*, in Proceedings of the 42nd AIAA/ASME/ASCE/AHS/ASC SSDM Conference, Seattle, WA, 2001.

[158] J. LI, *Three-Dimensional Effect in the Prediction of Flange Delamination in Composite Skin-Stringer Pull-off Specimens*, in Proceedings of the American Society for Composites - 15th Annual Technical Conference on Composite Materials: Technomic Publishing, 2000, pp. 983-990.

[159] R. KRÜGER, S. RINDERKNECHT, C. HÄNSEL, AND M. KÖNIG, *Computational Structural Analysis and Testing: An Approach to Understand Delamination Growth*, in Fracture of Composites, vol. 120-121, Key Engineering Materials, E. A. Armanios, Ed.: Trans Tech Publications, 1996, pp. 181-202.

[160] H. PARISCH, *A Continuum-Based Shell Theory for Non-Linear Applications*, Int. J. Num. Meth. Eng., Vol. 38, pp. 1855-1883, 1995.

[161] H. PARISCH, *A Consistent Tangent Stiffness Matrix for Three-Dimensional Non-Linear Contact Analysis*, Int. J. Num. Meth. Eng., Vol. 28, pp. 1803-1812, 1989.

[162] R. KRÜGER, C. HÄNSEL, AND M. KÖNIG, *Experimental-Numerical Investigation of Delamination Buckling and Growth*, Institute for Statics and Dynamics of Aerospace Structures, University of Stuttgart ISD-Report No. 96/3, 1996.

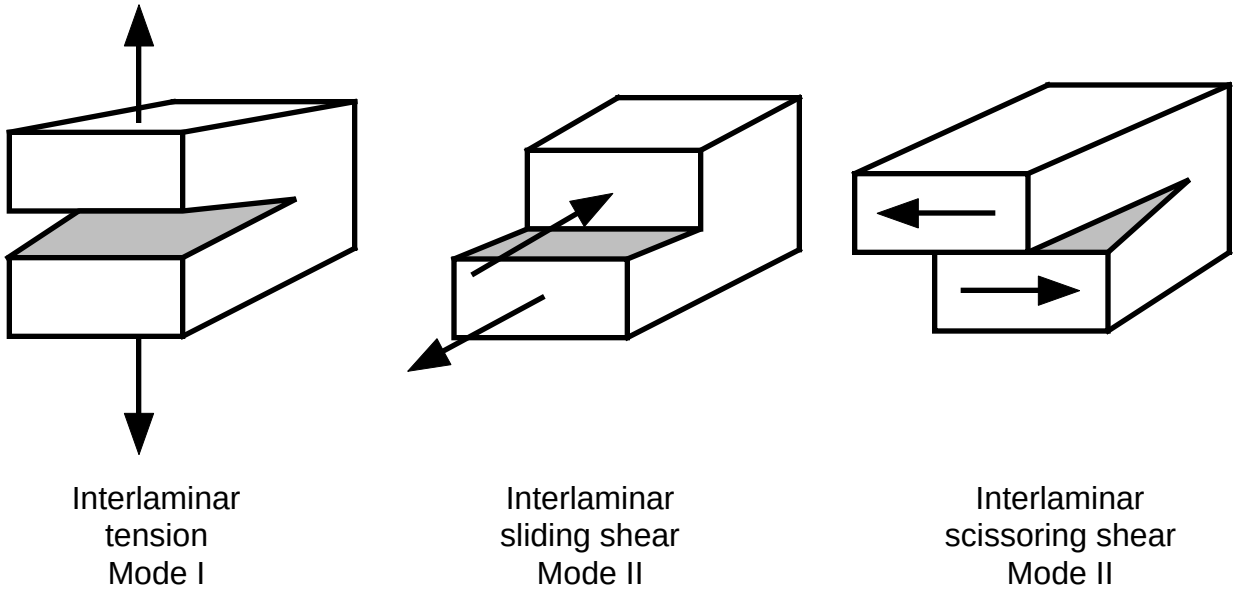

FIGURE 1. *Fracture Modes.*

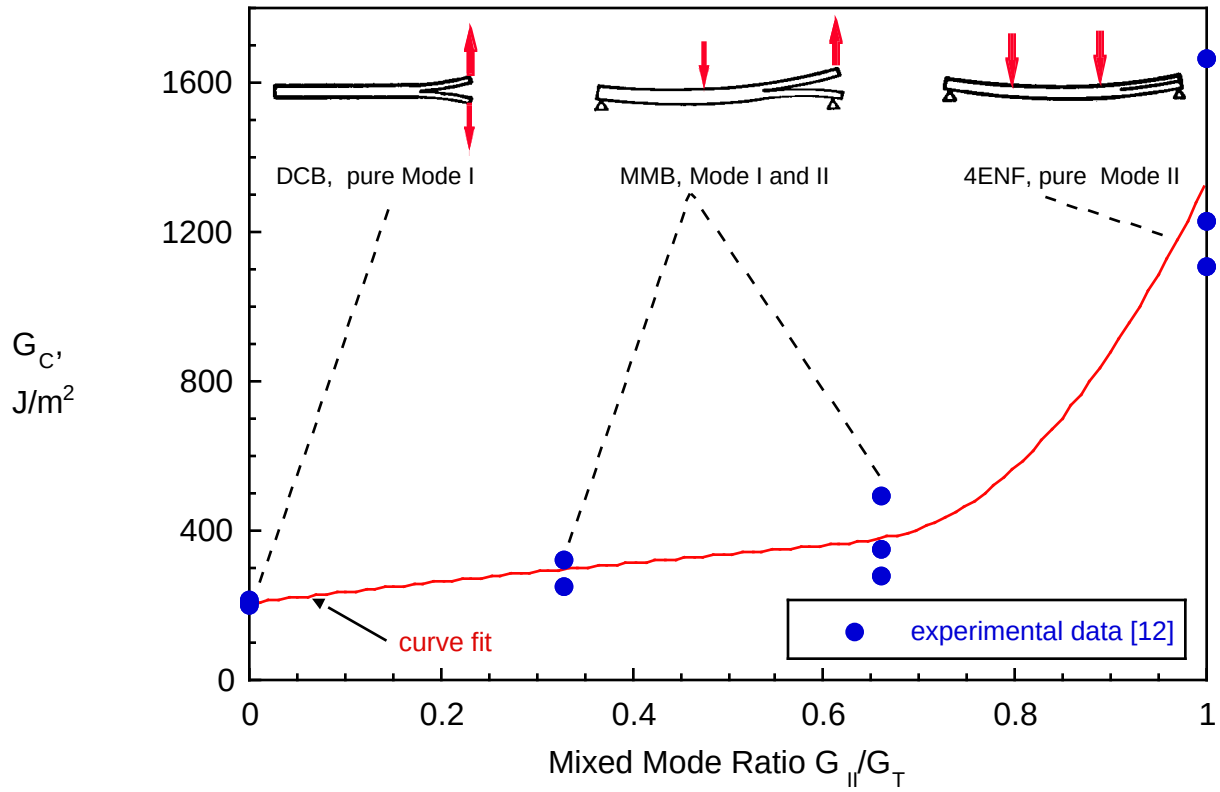

FIGURE 2. *Mixed-mode delamination criterion for IM7/8552.*

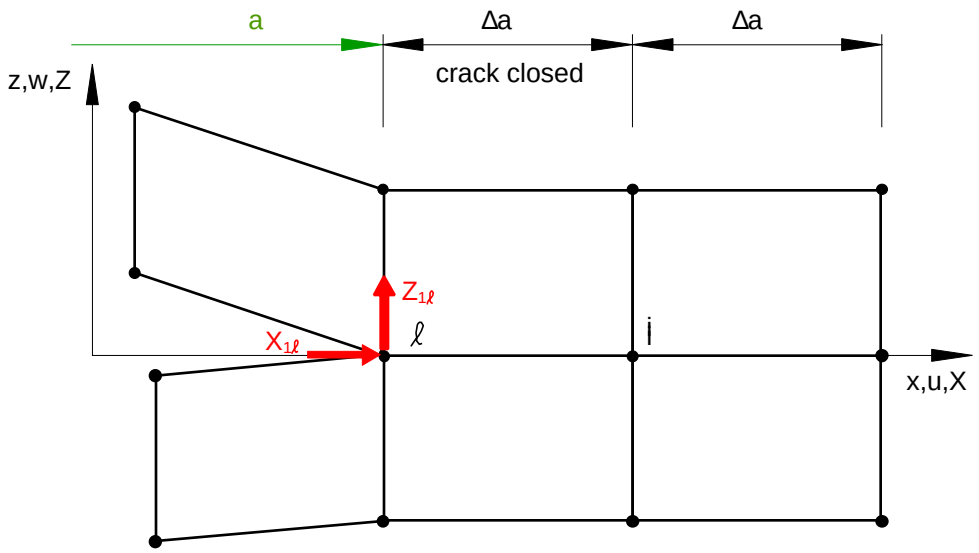

(a). *First Step - Crack closed*

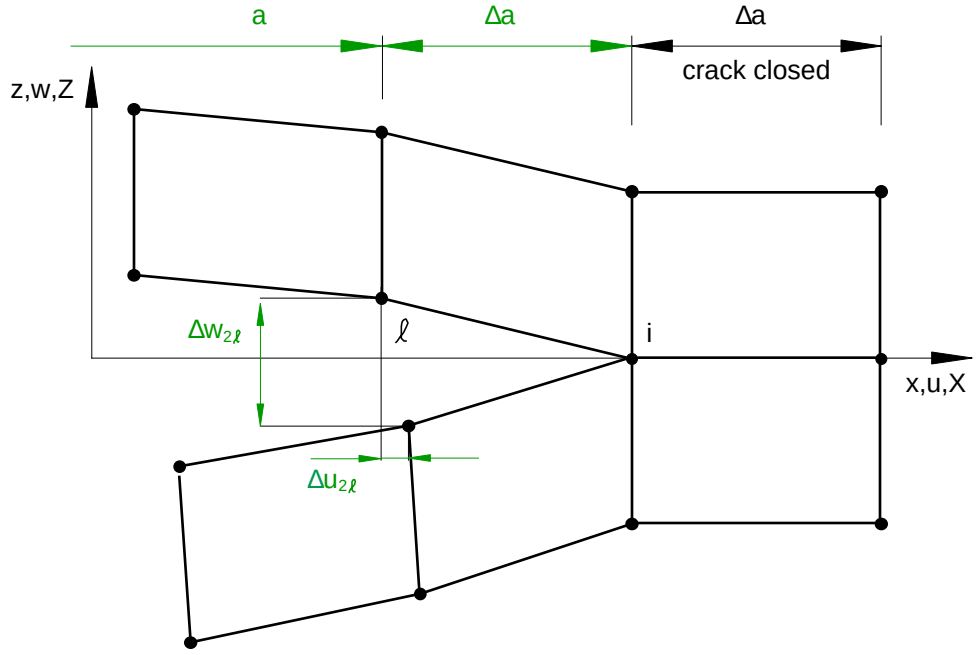

(b). *Second Step - Crack extended*

FIGURE 3. *Crack Closure Method (Two step VCCT).*

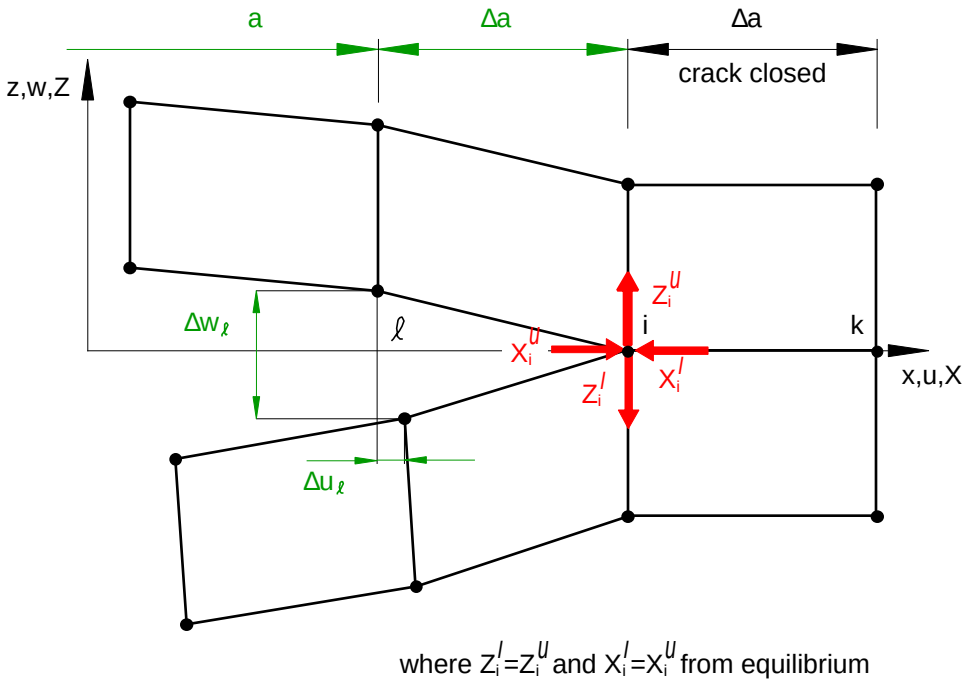

FIGURE 4. *Modified Crack Closure Method (One step VCCT).*

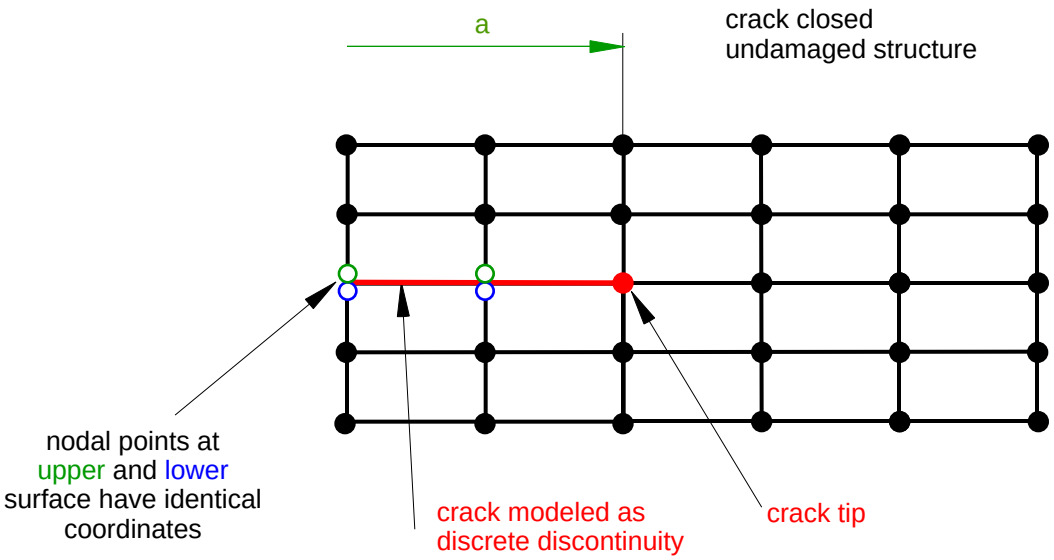

(a). *Initially modeled, undeformed finite element mesh*

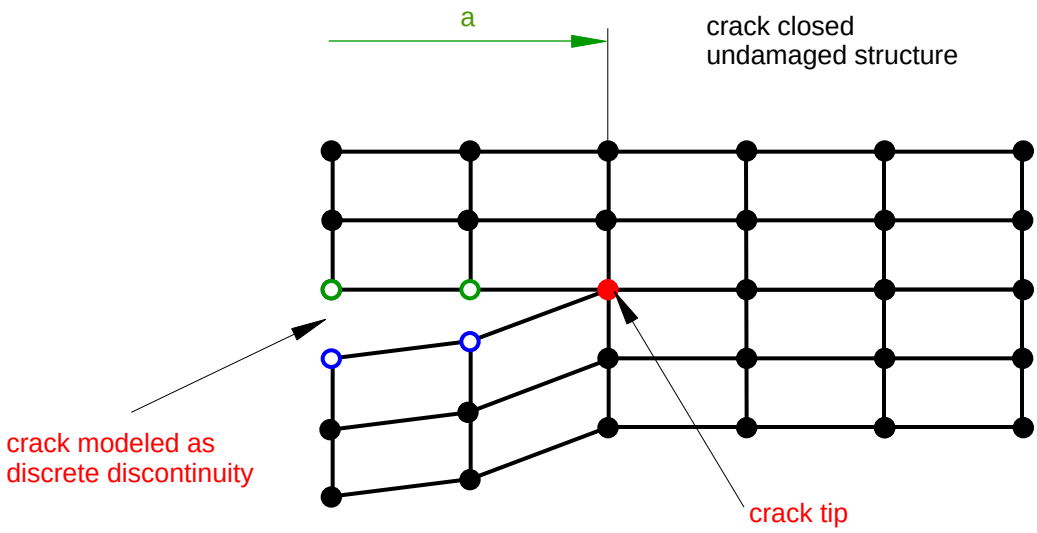

(b). *Deformed finite element mesh*

FIGURE 5. *Crack modeled as one-dimensional discontinuity.*

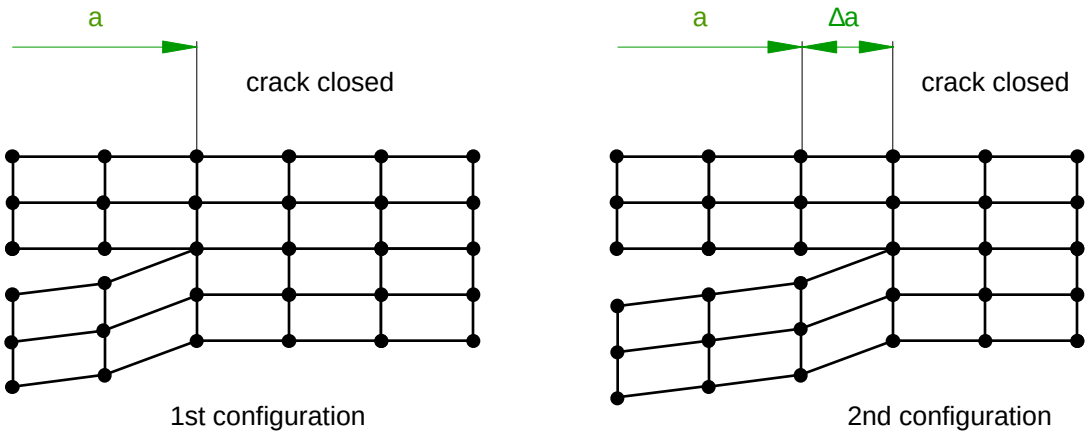

(a). *Node wise crack opening for four-noded element*

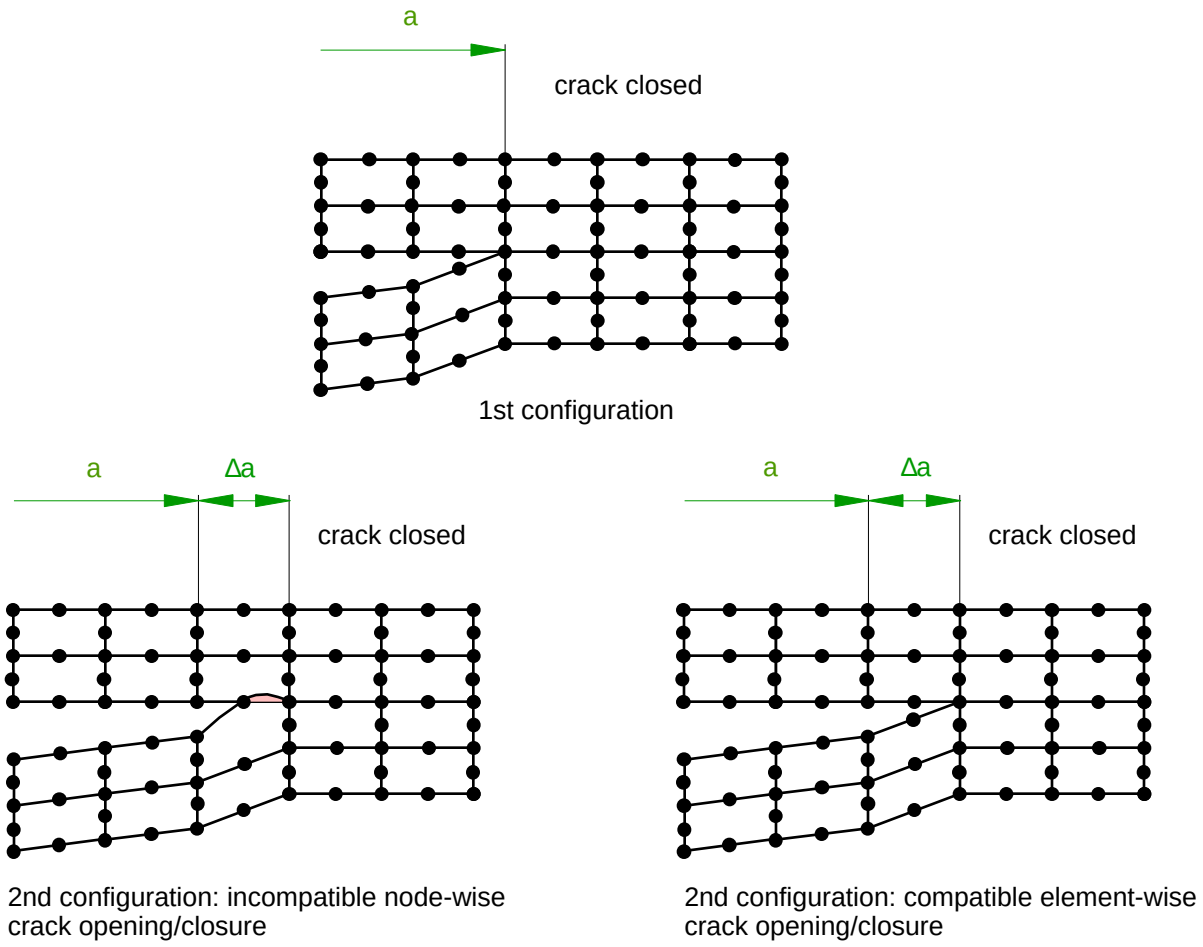

(b). *Crack opening for eight-noded element*

FIGURE 6. *Kinematic compatible crack opening/closure*.

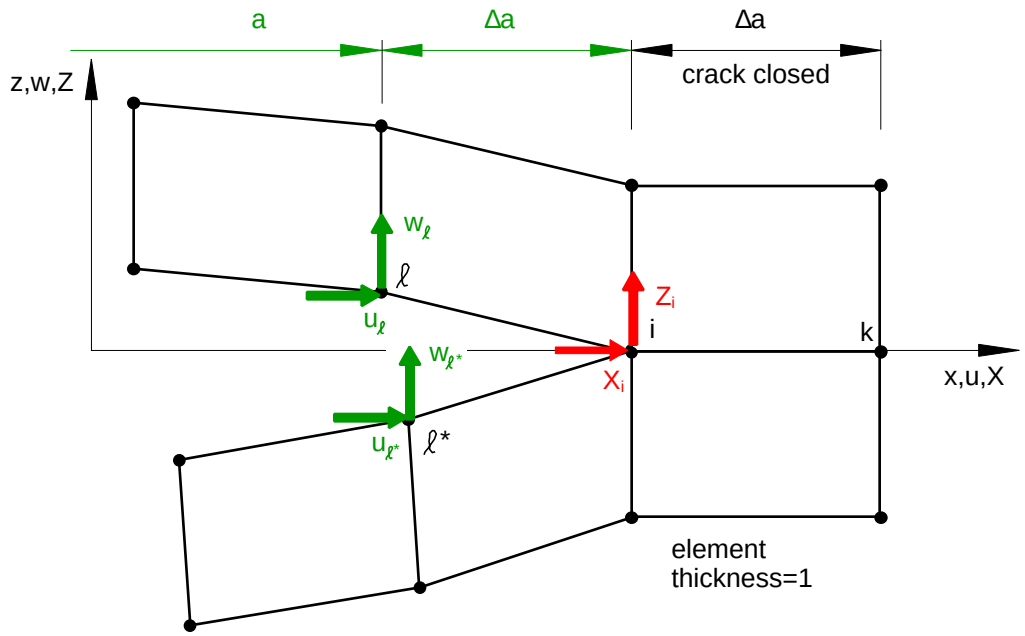

$$G_I = - Z_i (w_\ell - w_{\ell^*}) / (2\Delta a)$$

$$G_{II} = - X_i (u_\ell - u_{\ell^*}) / (2\Delta a)$$

(a). *Virtual Crack Closure Technique for four-noded element.*

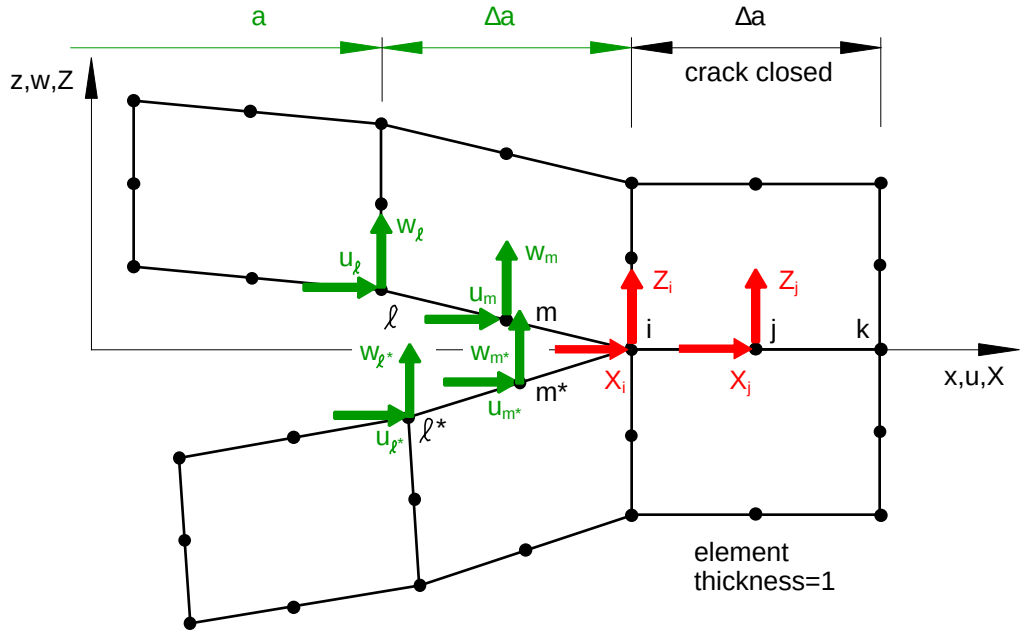

$$G_I = -[Z_i (w_\ell - w_{\ell^*}) + Z'_j (w_m - w_{m^*})] / (2\Delta a)$$

$$G_{II} = -[X_i (u_\ell - u_{\ell^*}) + X'_j (u_m - u_{m^*})] / (2\Delta a)$$

(b). *Virtual Crack Closure Technique for eight-noded element.*

FIGURE 7. *Virtual Crack Closure Technique for two-dimensional solid elements.*

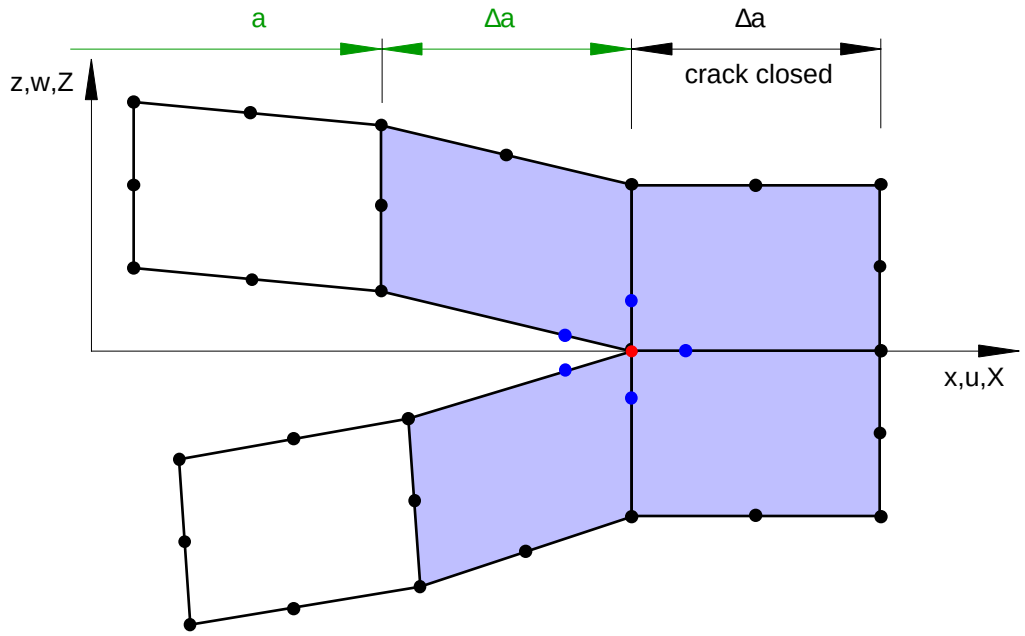

(a). *Quadtrilateral elements with quarter point nodes.*

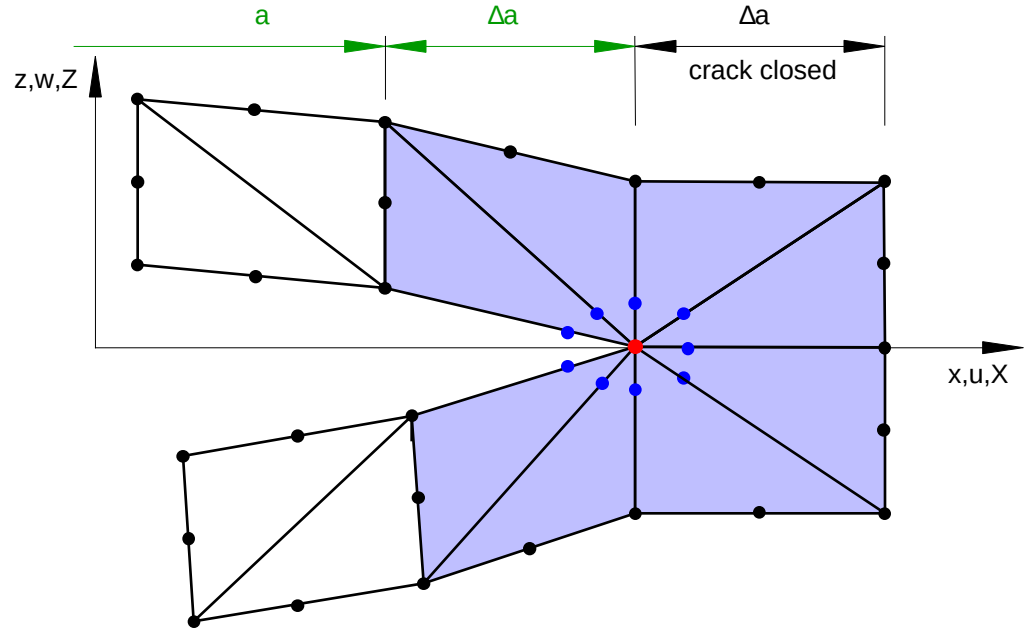

(b). *Collapsed quarter point element.*

FIGURE 8. *Singularity elements with quarter point nodes at crack tip.*

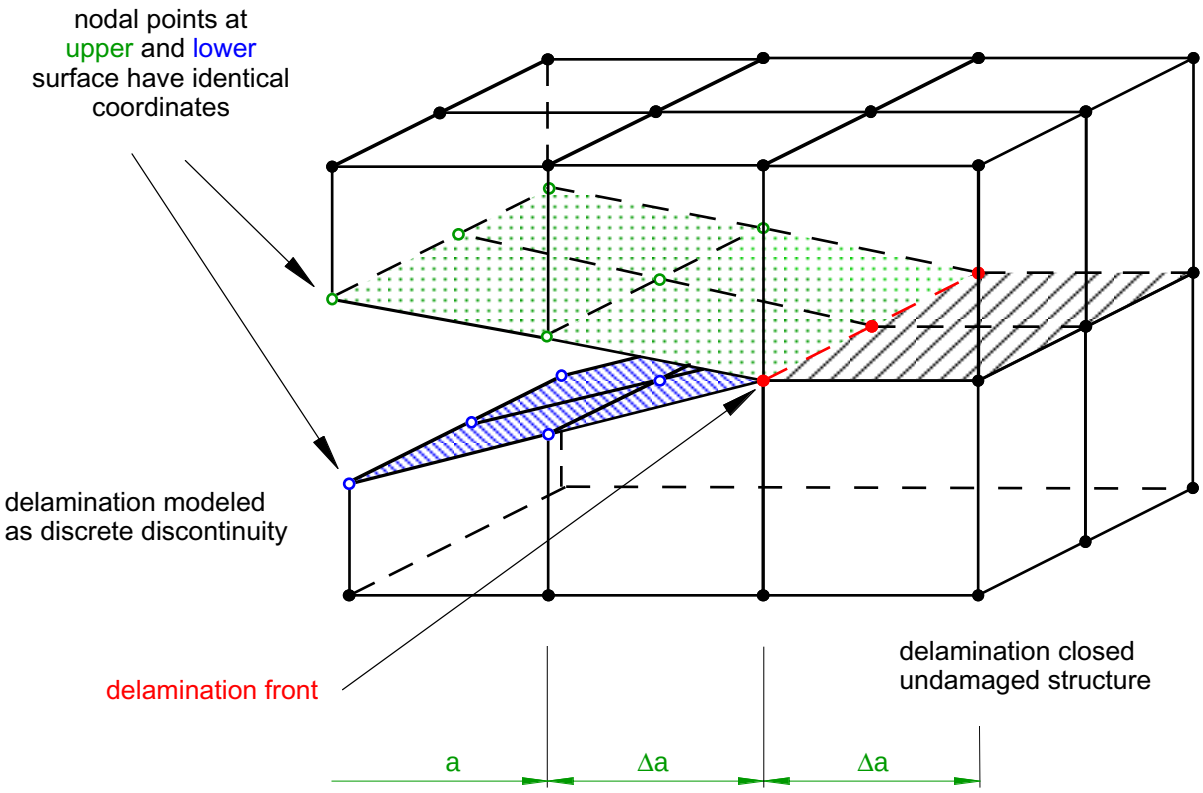

(a). *Delamination modeled with bilinear three-dimensional solid elements*

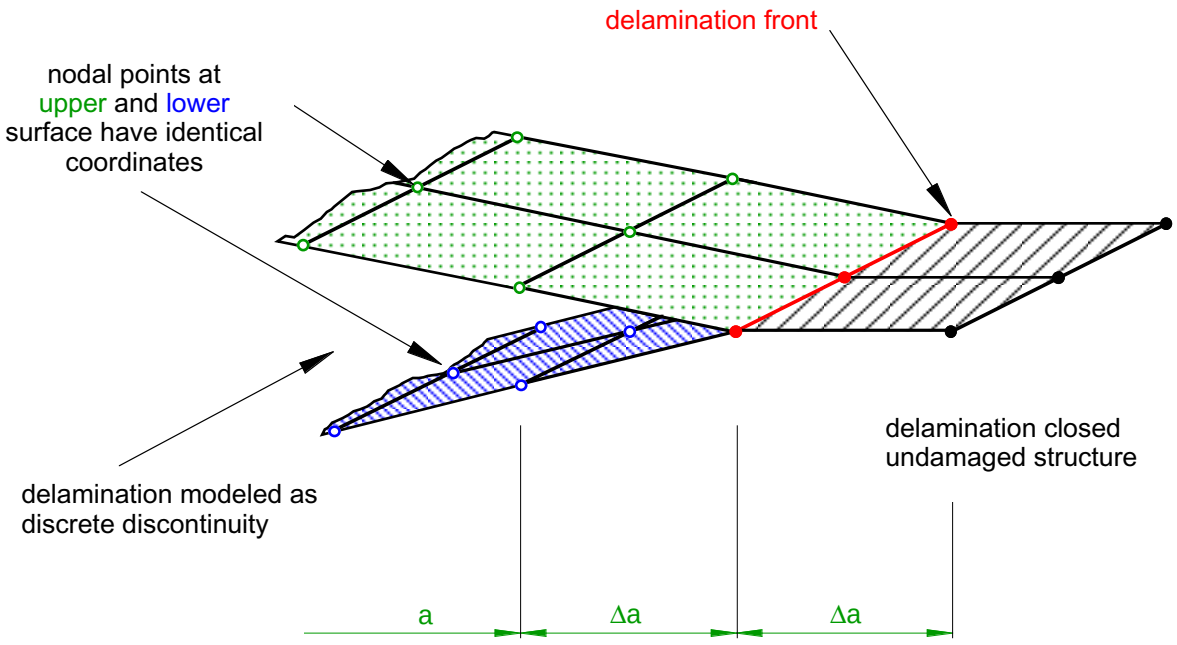

(b). *Delamination modeled with bilinear plate/shell type elements*

FIGURE 9. *Delaminations modeled as two-dimensional discontinuity.*

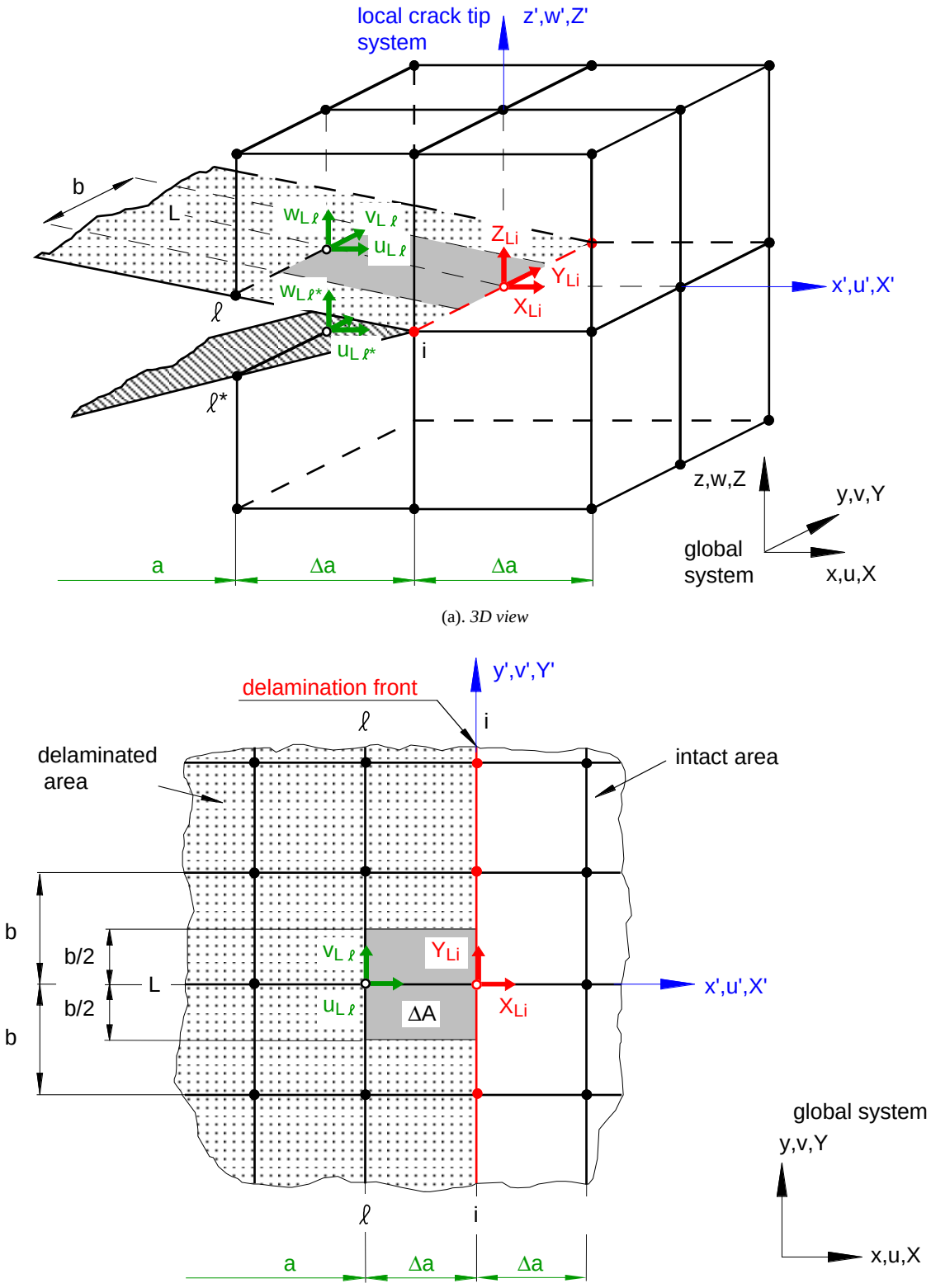

(a). *3D view*

(b). *Top view of upper surface (lower surface terms are omitted for clarity)*

FIGURE 10. *Virtual Crack Closure Technique for four noded plate/shell and eight noded solid elements.*

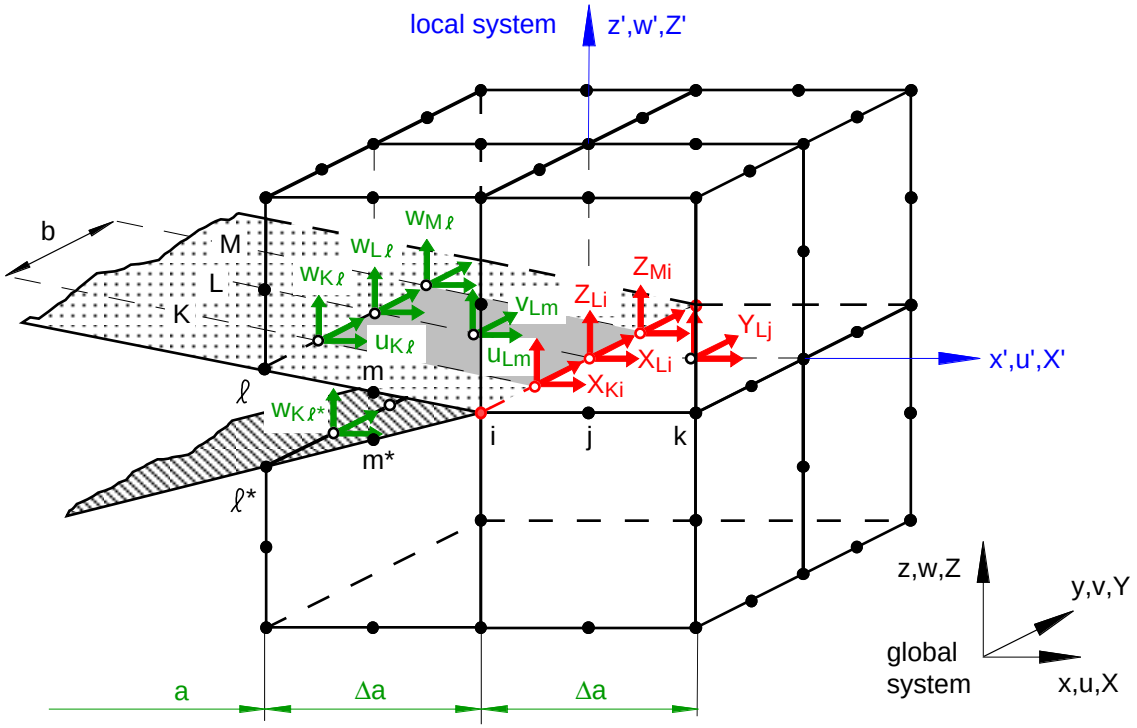

(a). *3D view*

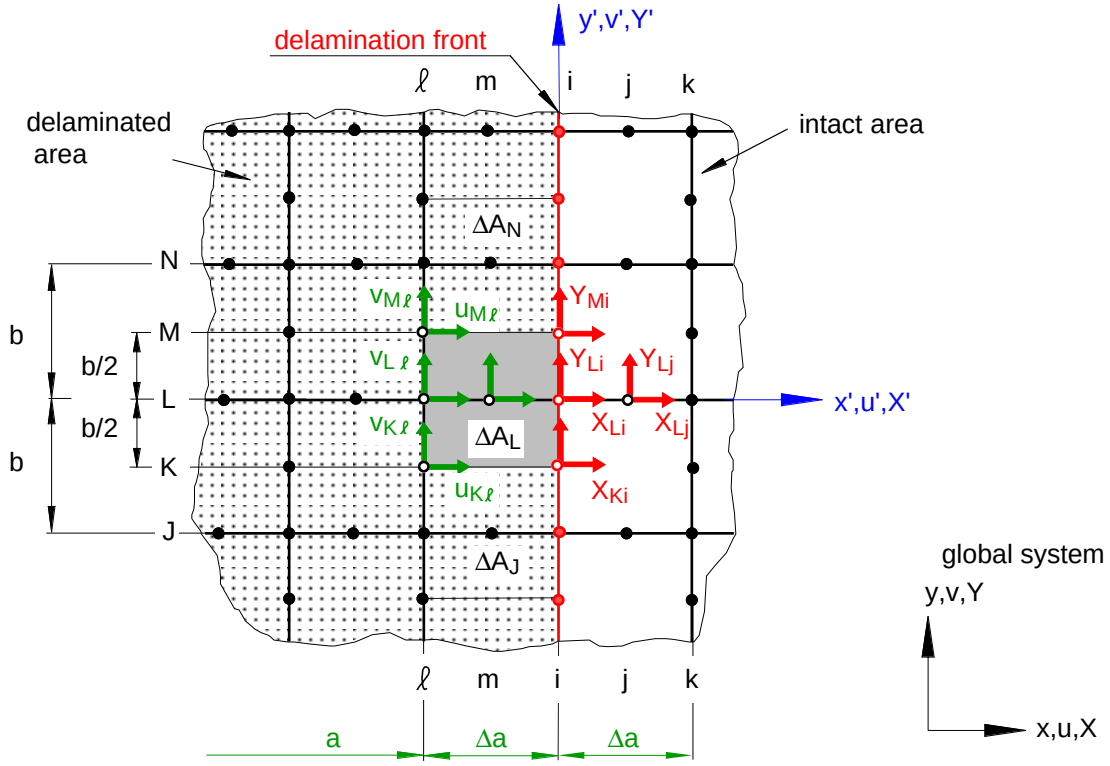

(b). *Top view of upper surface (lower surface terms are omitted for clarity)*

FIGURE 11. *Virtual Crack Closure Technique for corner nodes in eight noded plate/shell and twenty noded solid elements.*

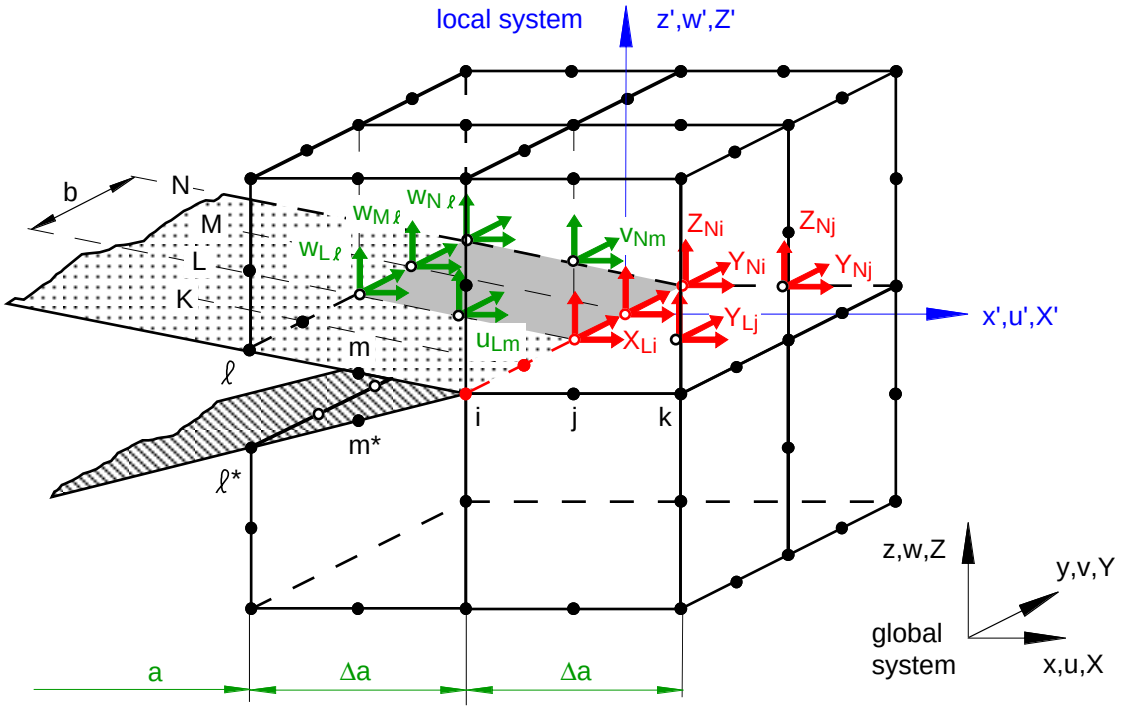

(a). *3D view*

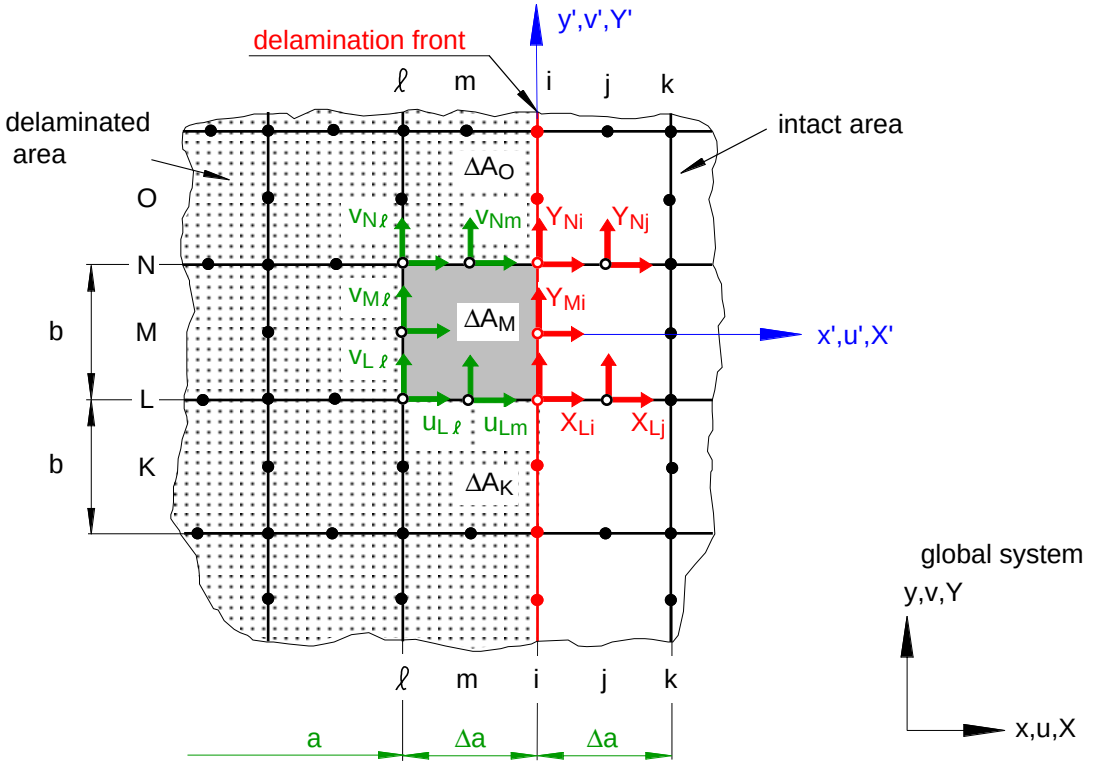

(b). *Top view of upper surface (lower surface terms are omitted for clarity)*

FIGURE 12. *Virtual Crack Closure Technique for midside nodes in eight noded plate/shell and twenty noded solid elements.*

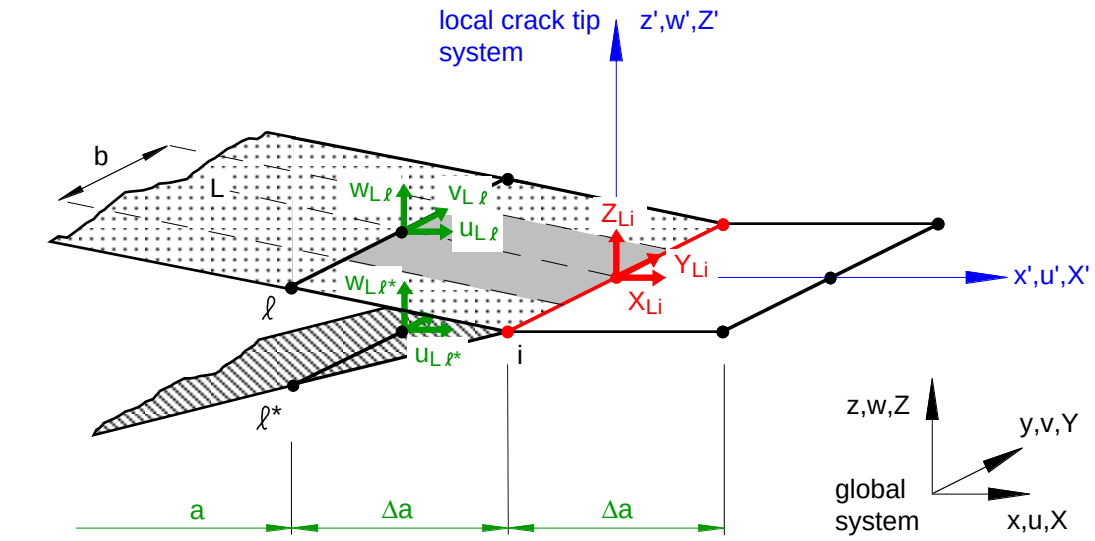

(a). *3D view*

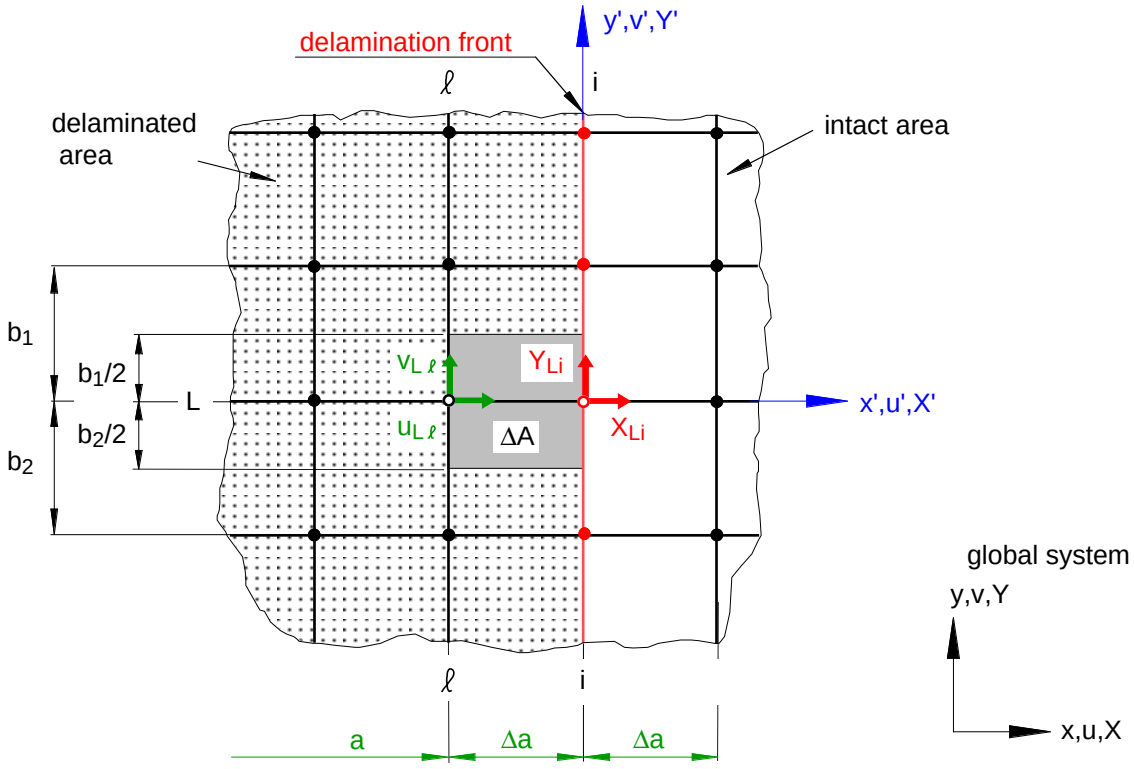

(b). *Top view of upper surface (lower surface terms are omitted for clarity)*

FIGURE 13. *Virtual Crack Closure Technique for four noded plate/shell elements.*

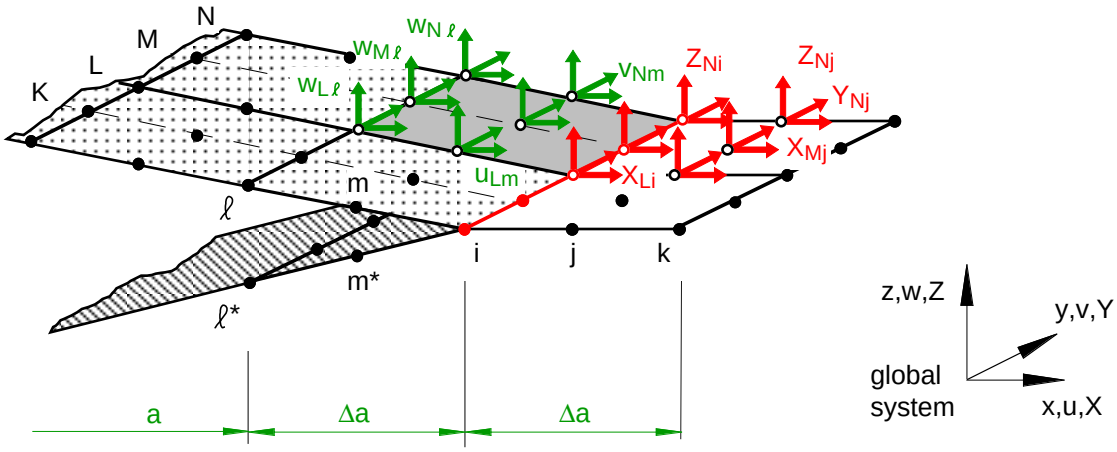

(a). *3D view*

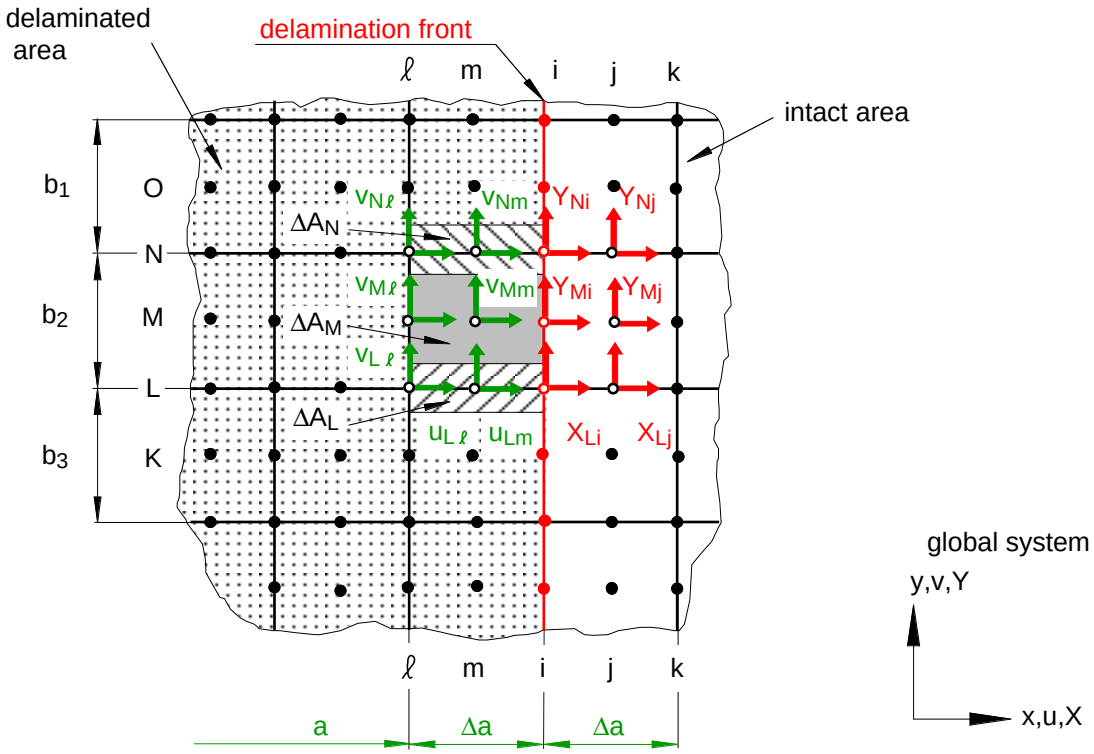

(b). *Top view of upper surface (lower surface terms are omitted for clarity)*

FIGURE 14. *Virtual Crack Closure Technique for nine noded plate/shell elements.*

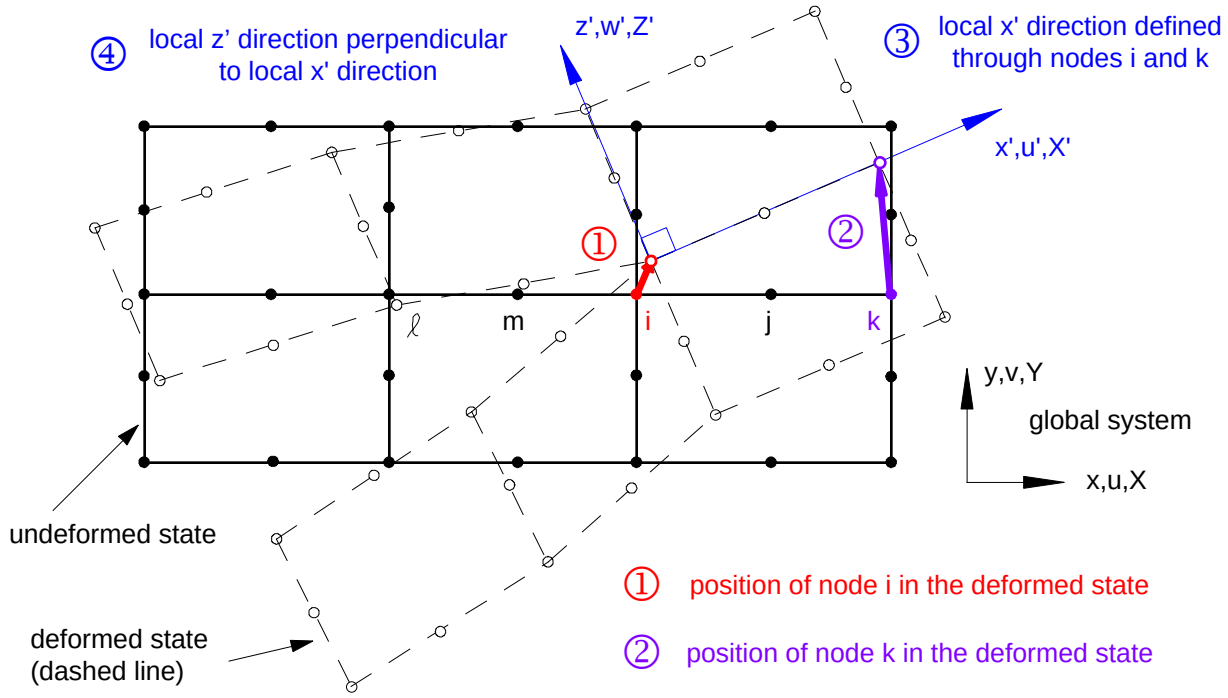

(a). *Definition of local crack tip coordinate system*

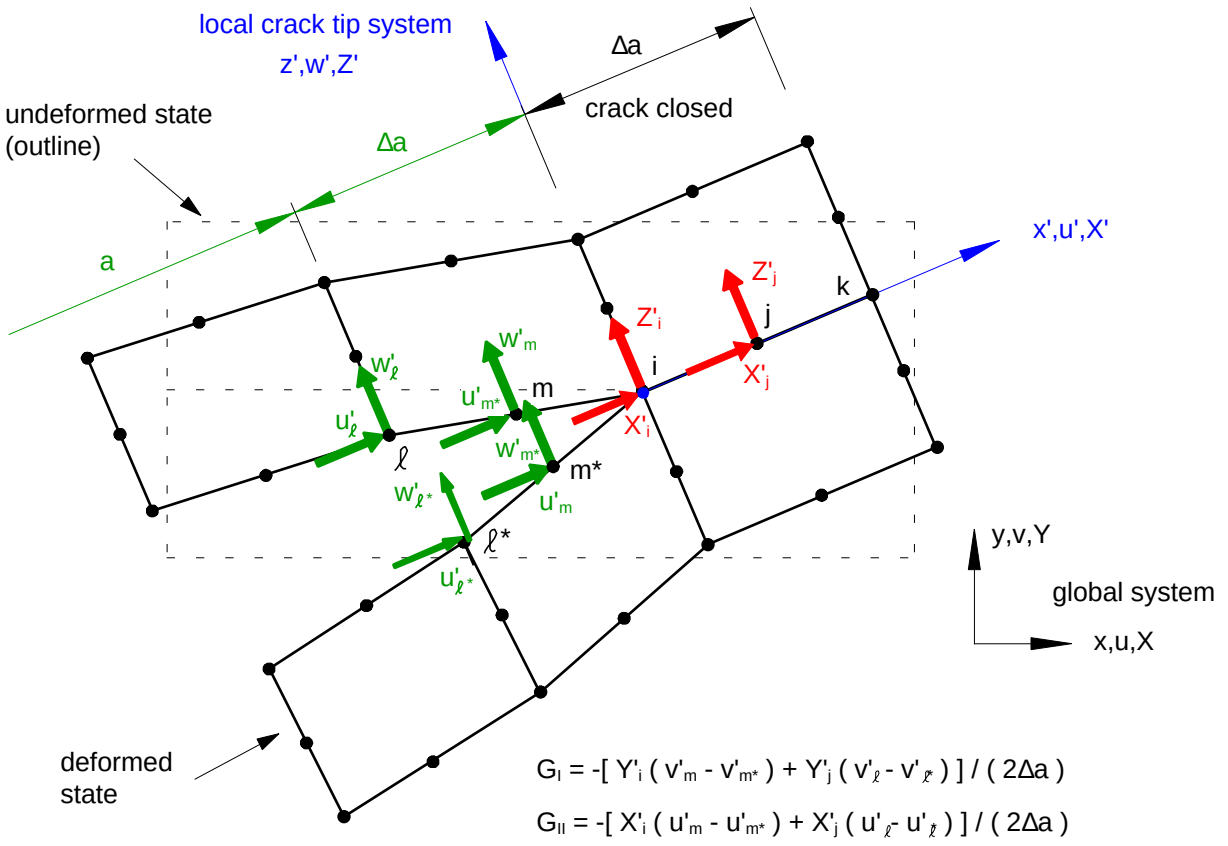

(b). *Forces and displacements in local coordinate system*

FIGURE 15: *Virtual Crack Closure Technique for geometrically nonlinear analysis.*

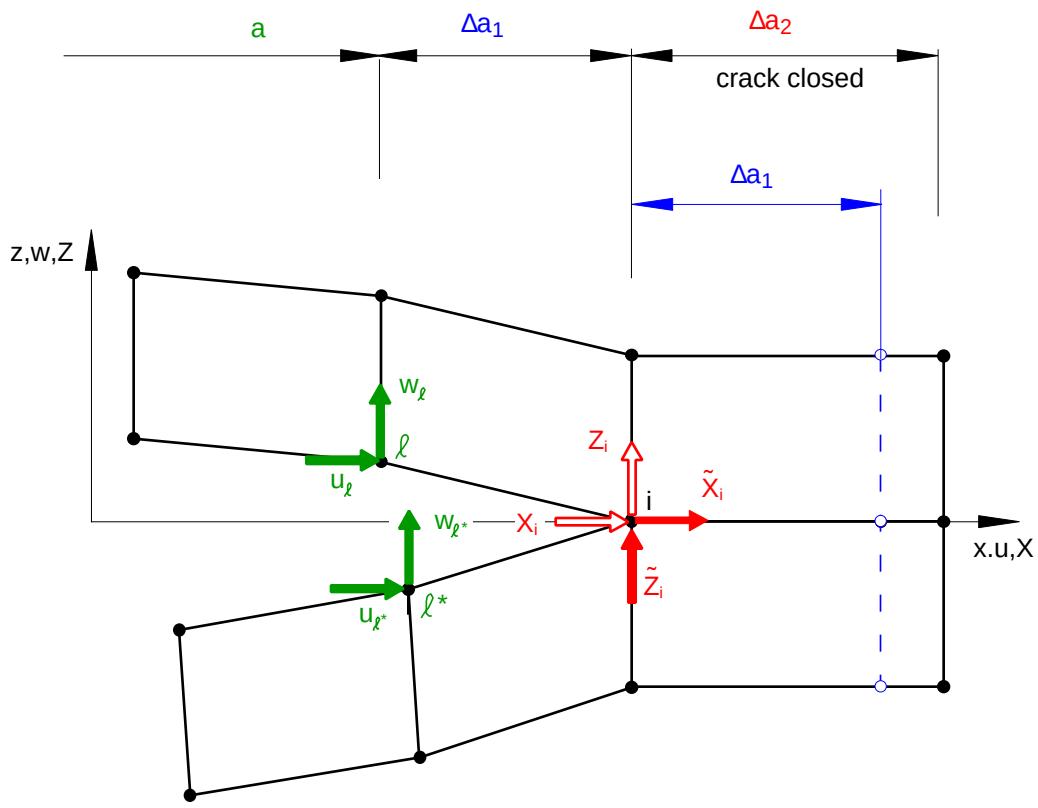

FIGURE 16. *Correction for elements with different lengths in front and behind the crack tip* .

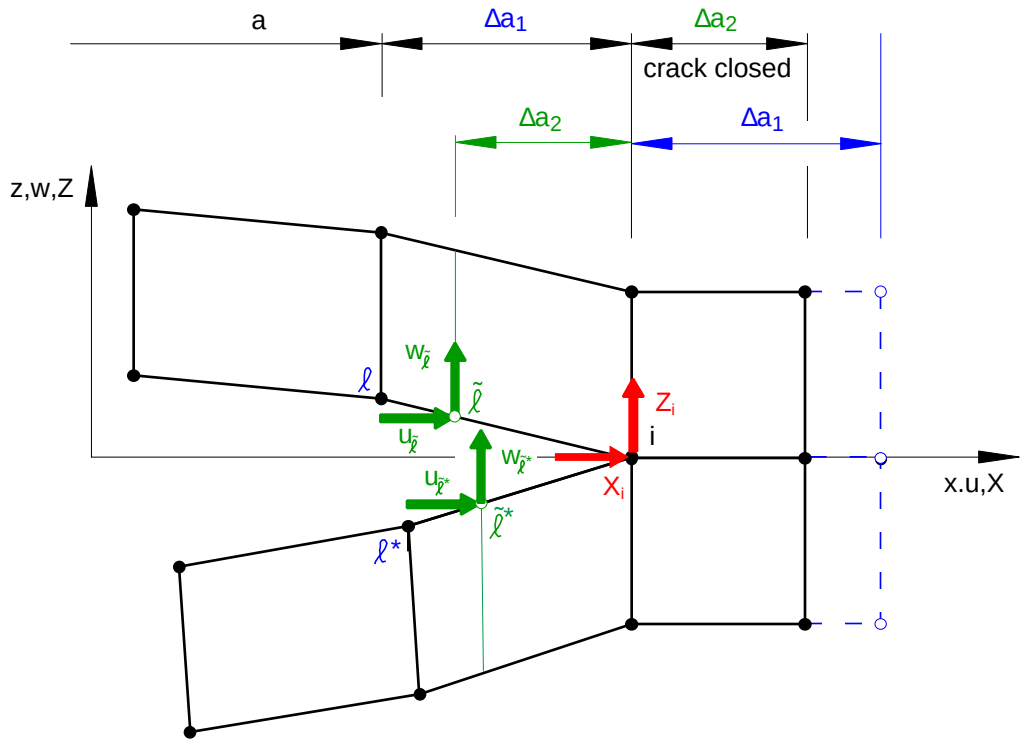

(a) *Shorter elements in front of the crack tip*

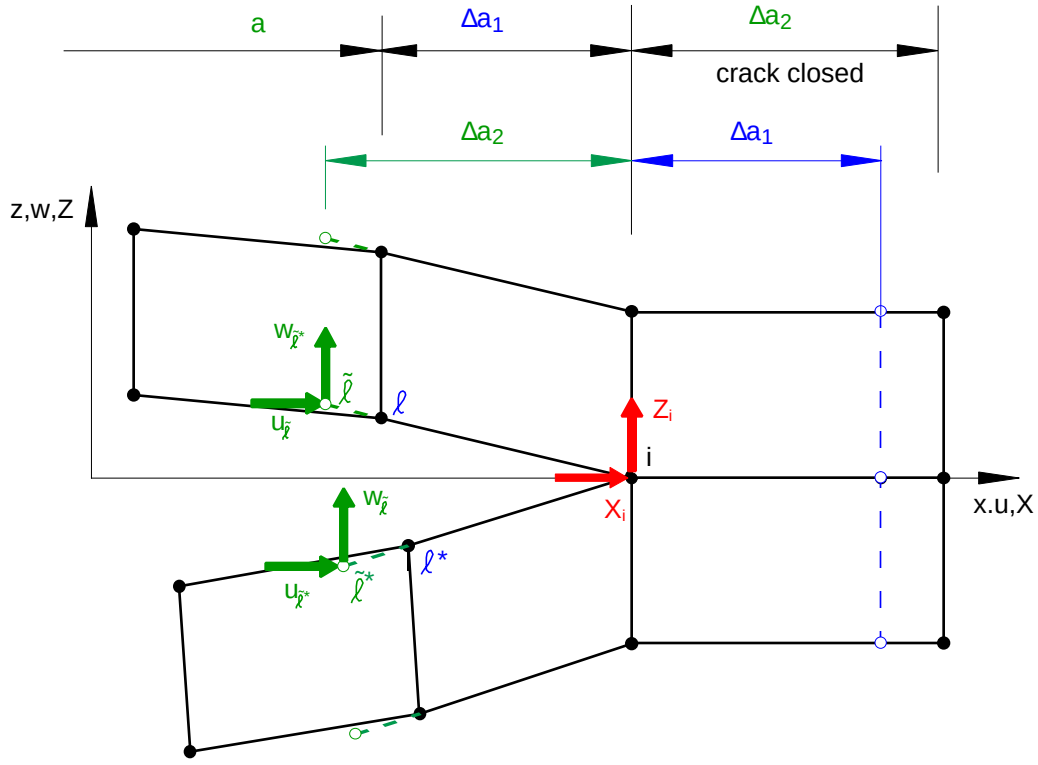

(b) *Longer elements in front of the crack tip* .

FIGURE 17. *Correction for elements with different lengths in front and behind the crack tip* .

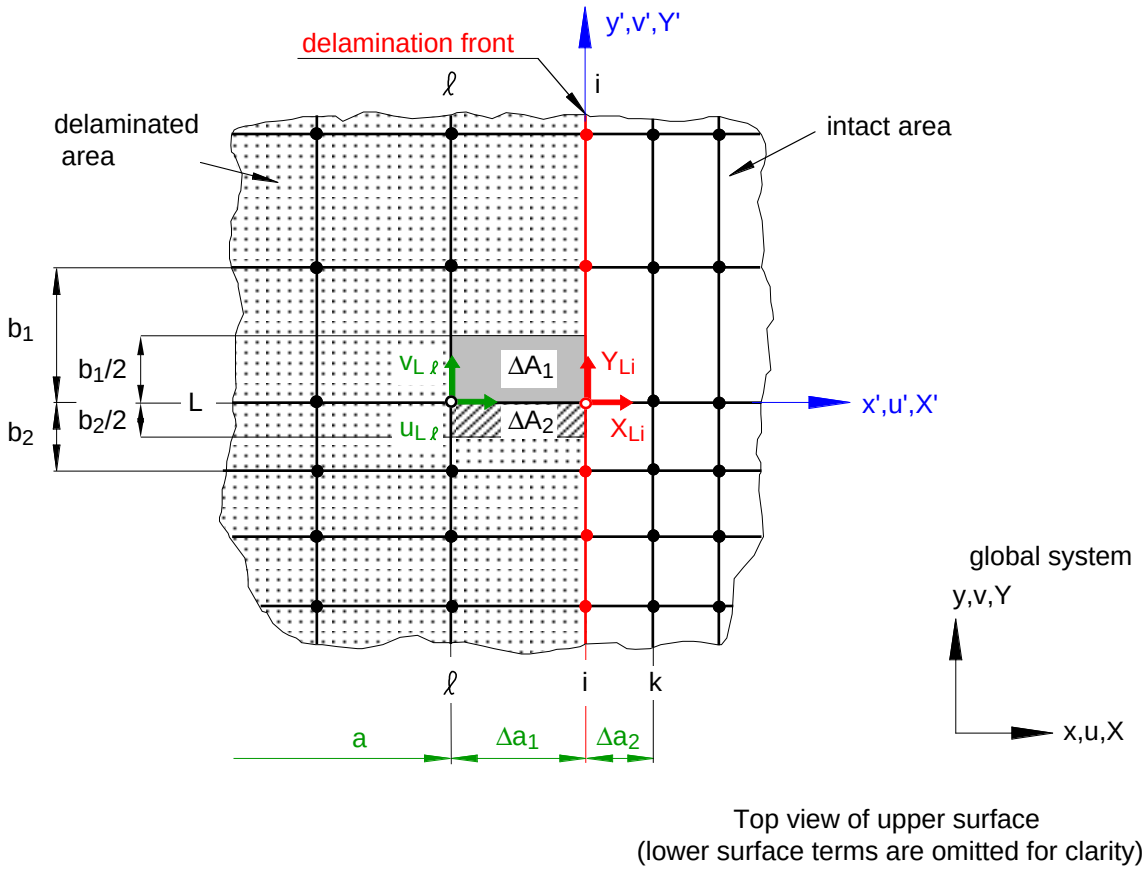

FIGURE 18. *Virtual Crack Closure Technique for eight noded solid elements with different widths.*

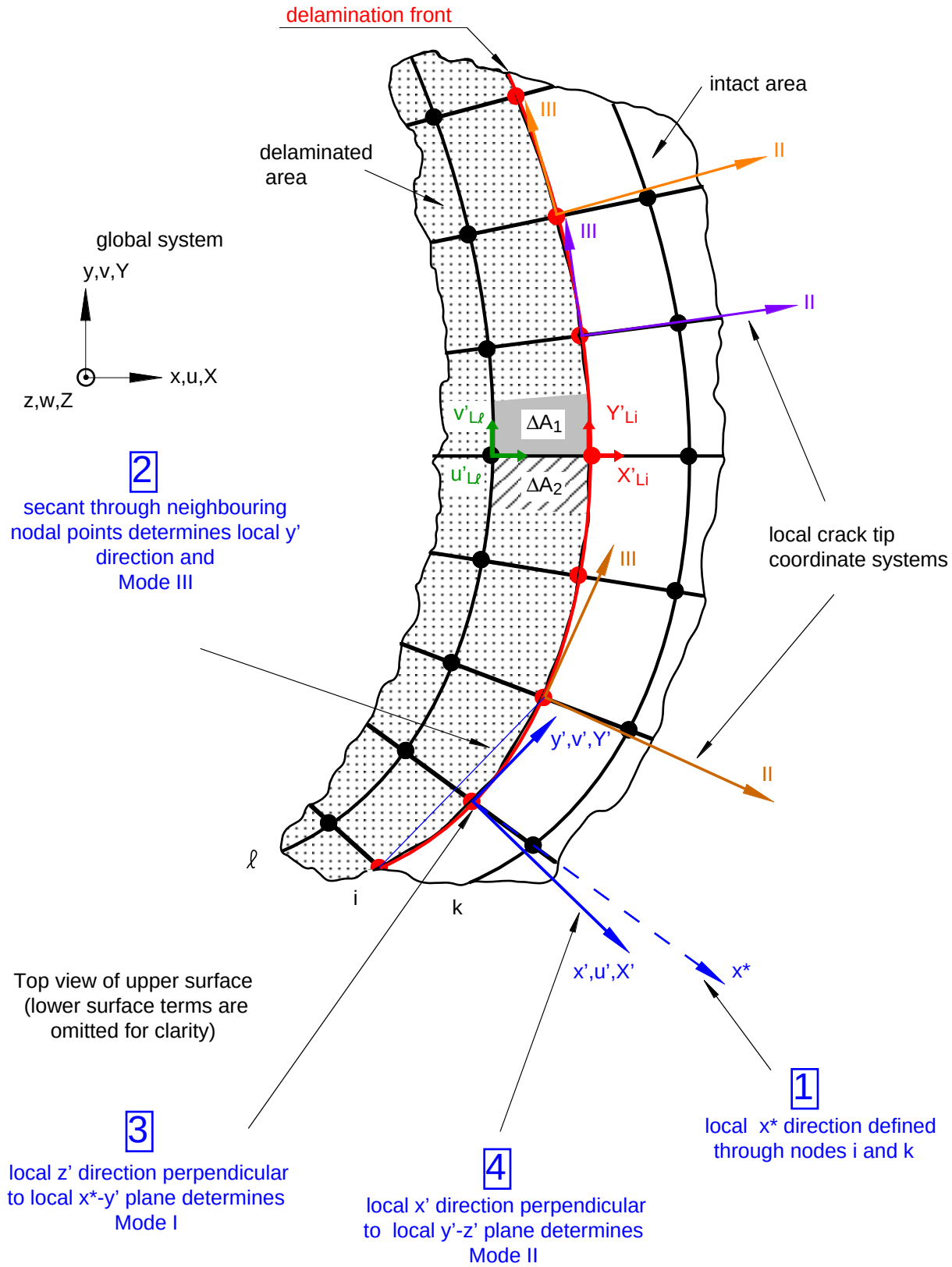

FIGURE 19. *Virtual Crack Closure Technique for arbitrarily shaped front*

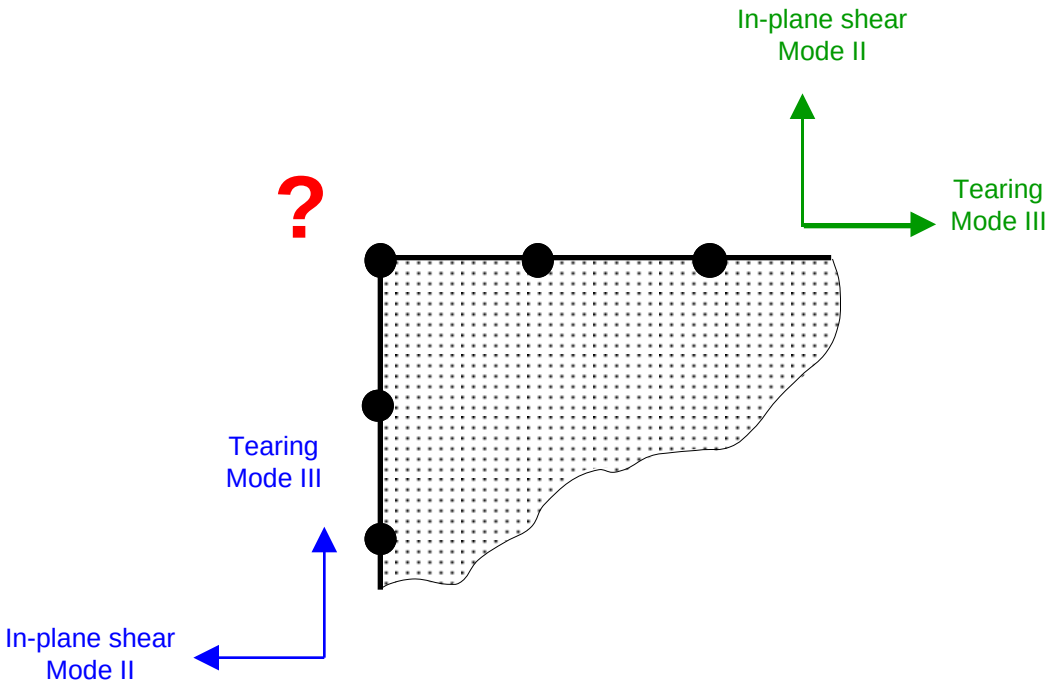

(a). *Undefined mode separation at corner nodal point*

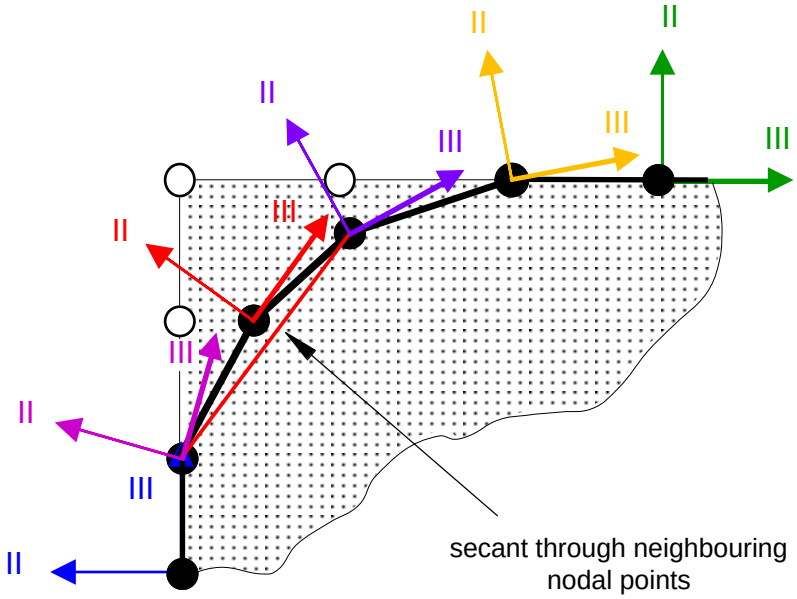

(b). *Well defined mode separation at rounded corner.*

FIGURE 20. *Definition of mode separation at sharp corners.*

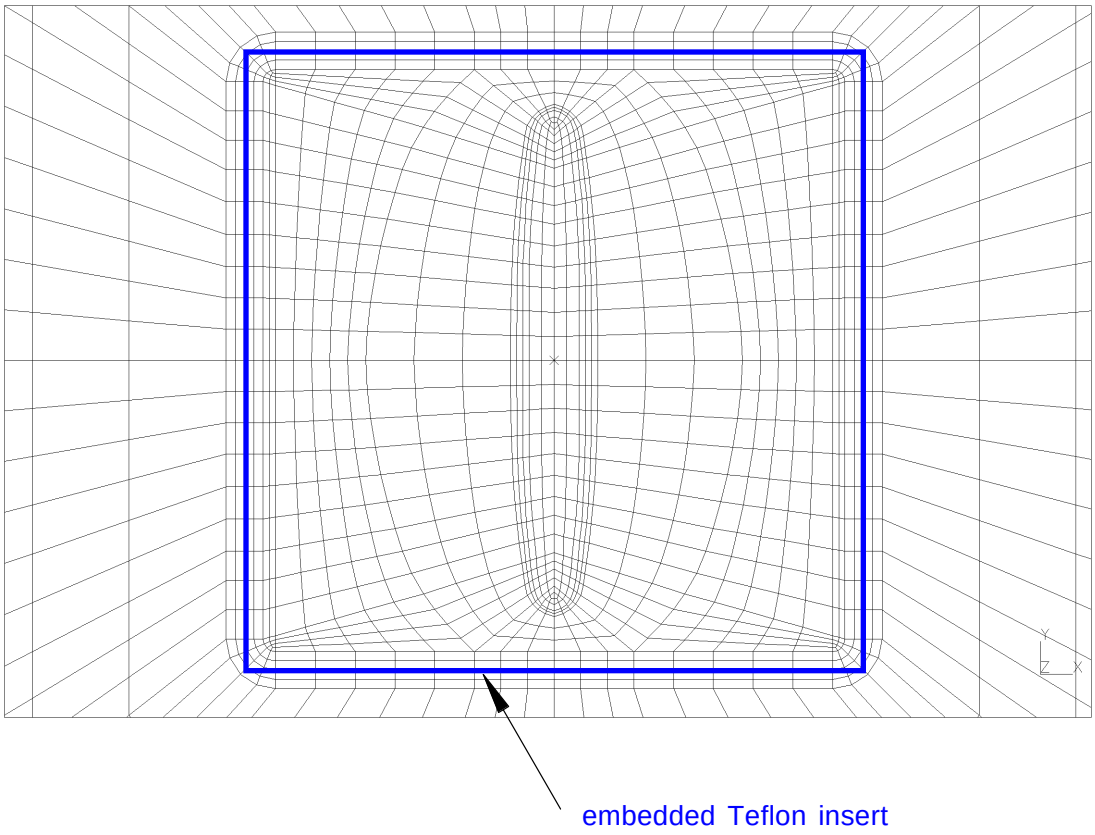

FIGURE 21. *Detail of a finite element mesh with modeled square insert.*

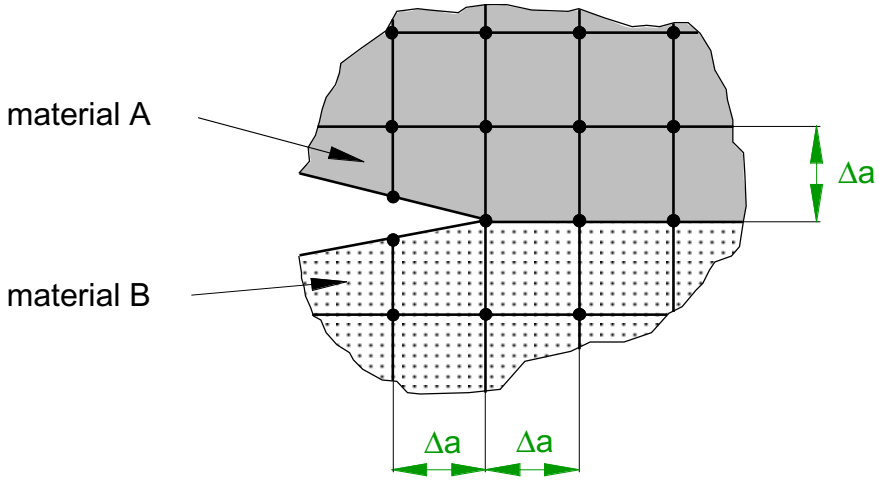

(a). *Bimaterial Interface*

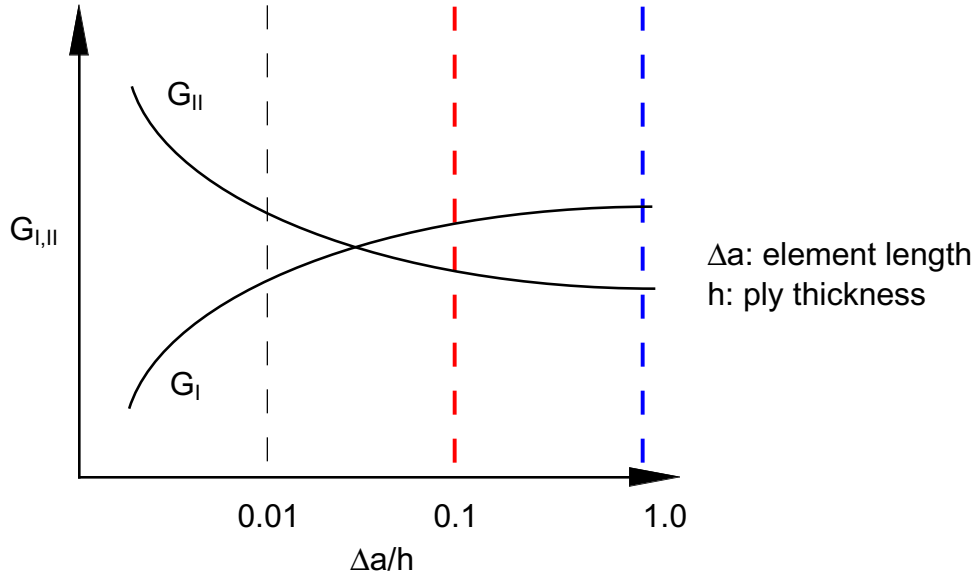

(b). *Dependence of computed energy release rate on element size at crack tip*

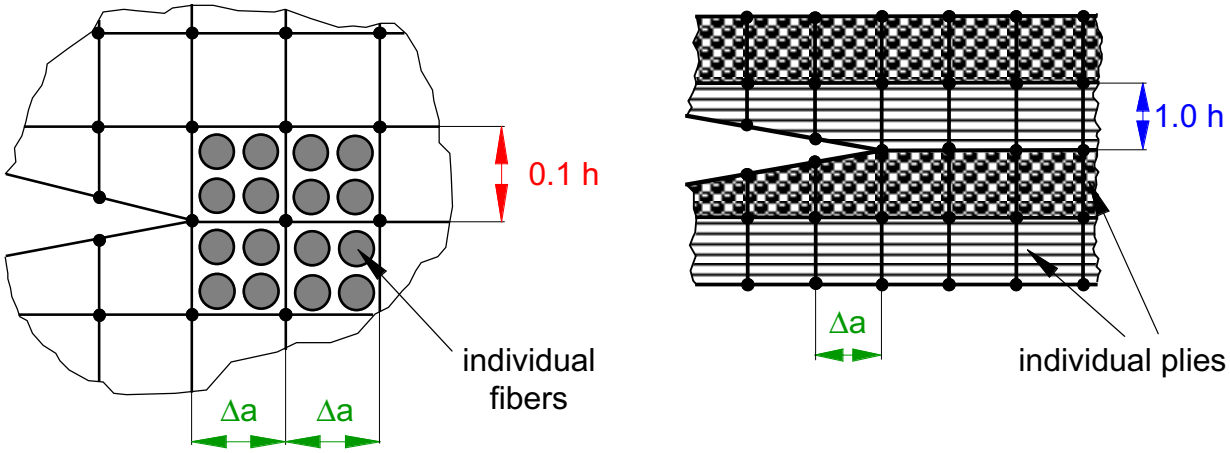

(c). *Upper and lower bounds for element size at crack tip*

FIGURE 22. *Bi-Material Interface.*

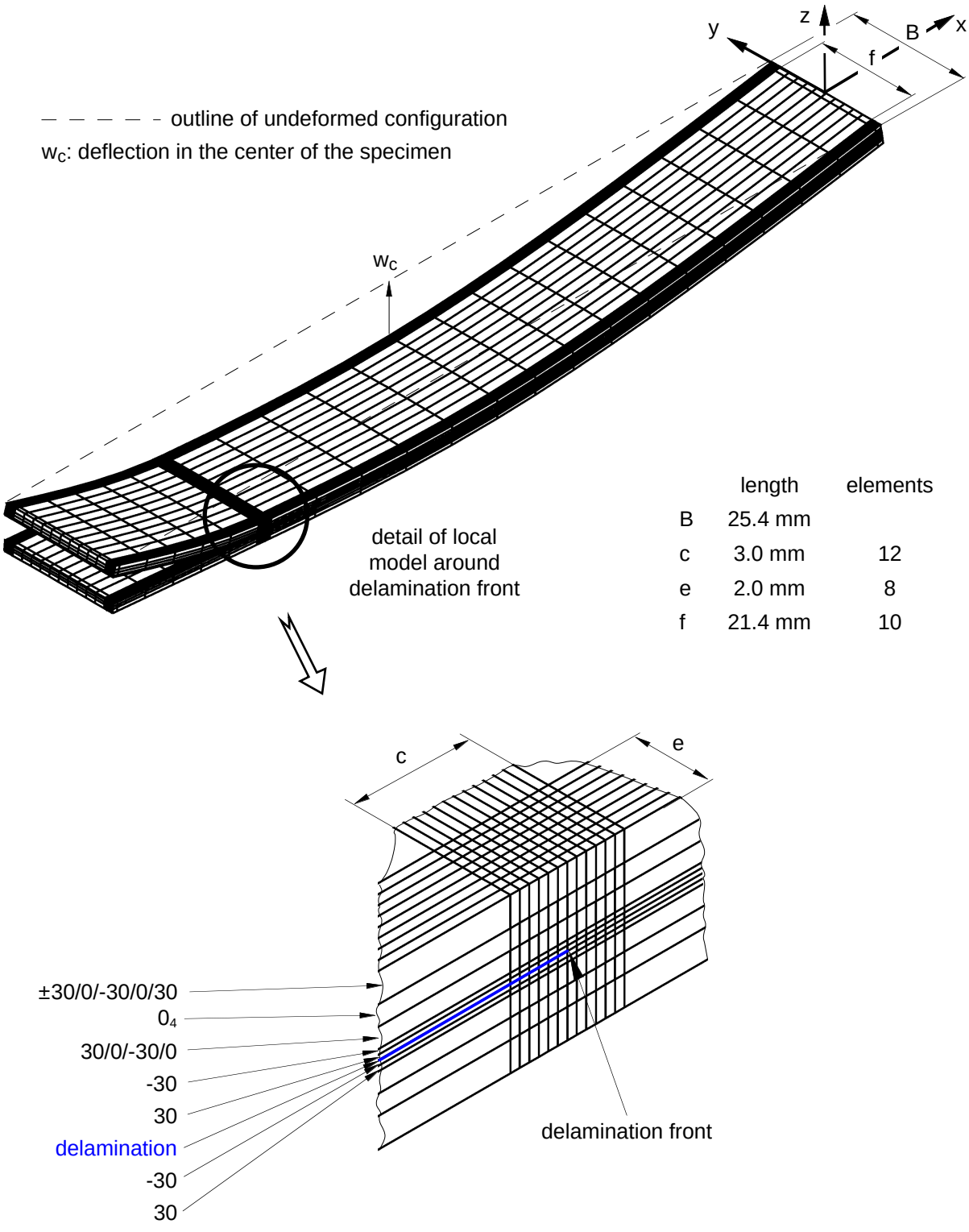

FIGURE 23. *Three-dimensional finite element model of SLB specimen.*

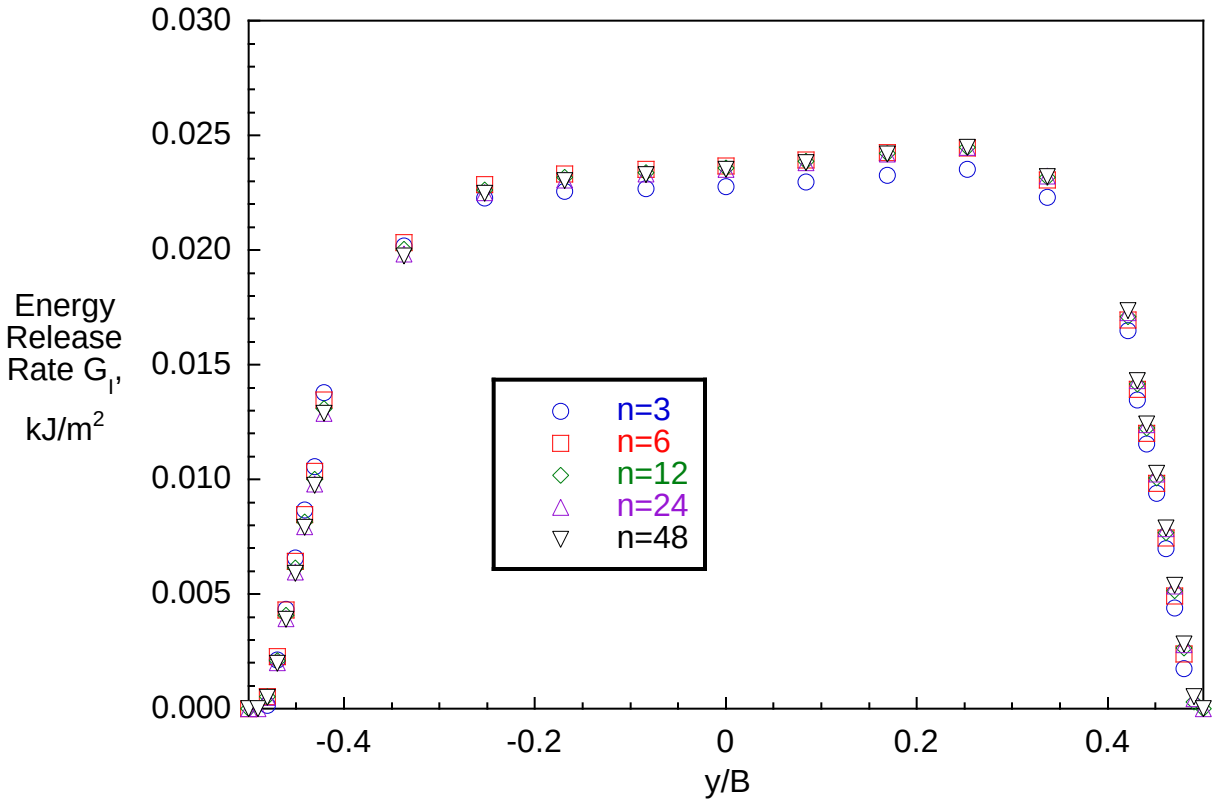

FIGURE 24. *Influence of number of elements in refined section on computed mode I strain energy release rate distribution across the width of a SLB specimen.*

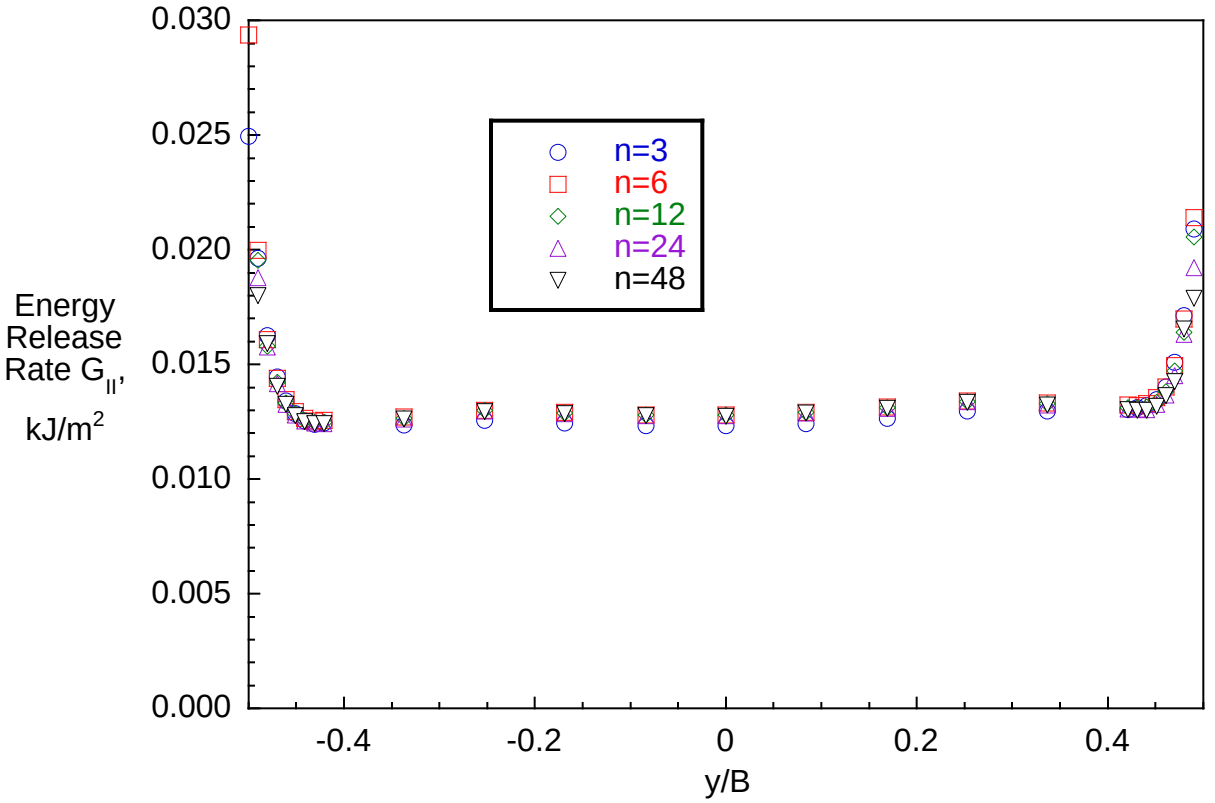

FIGURE 25. *Influence of number of elements in refined section on computed mode II strain energy release rate distribution across the width of a SLB specimen.*

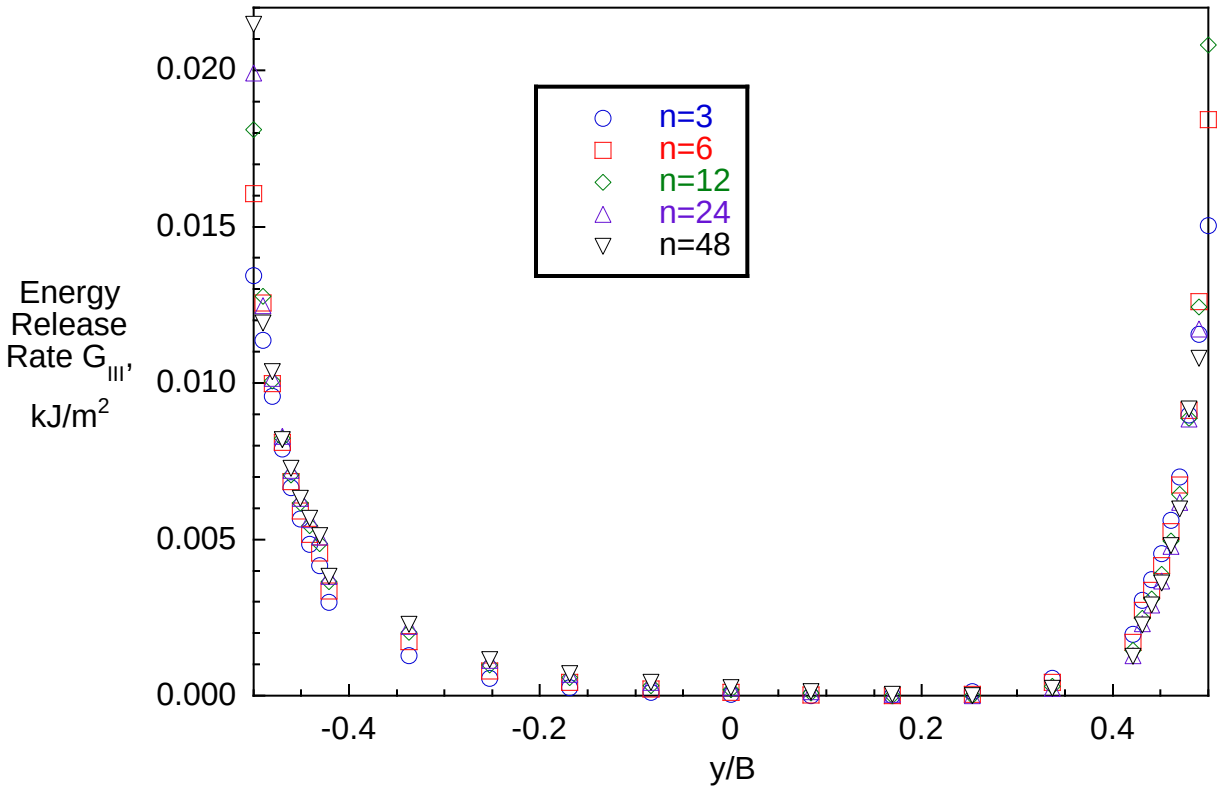

FIGURE 26. *Influence of number of elements in refined section on computed mode III strain energy release rate distribution across the width of a SLB specimen.*

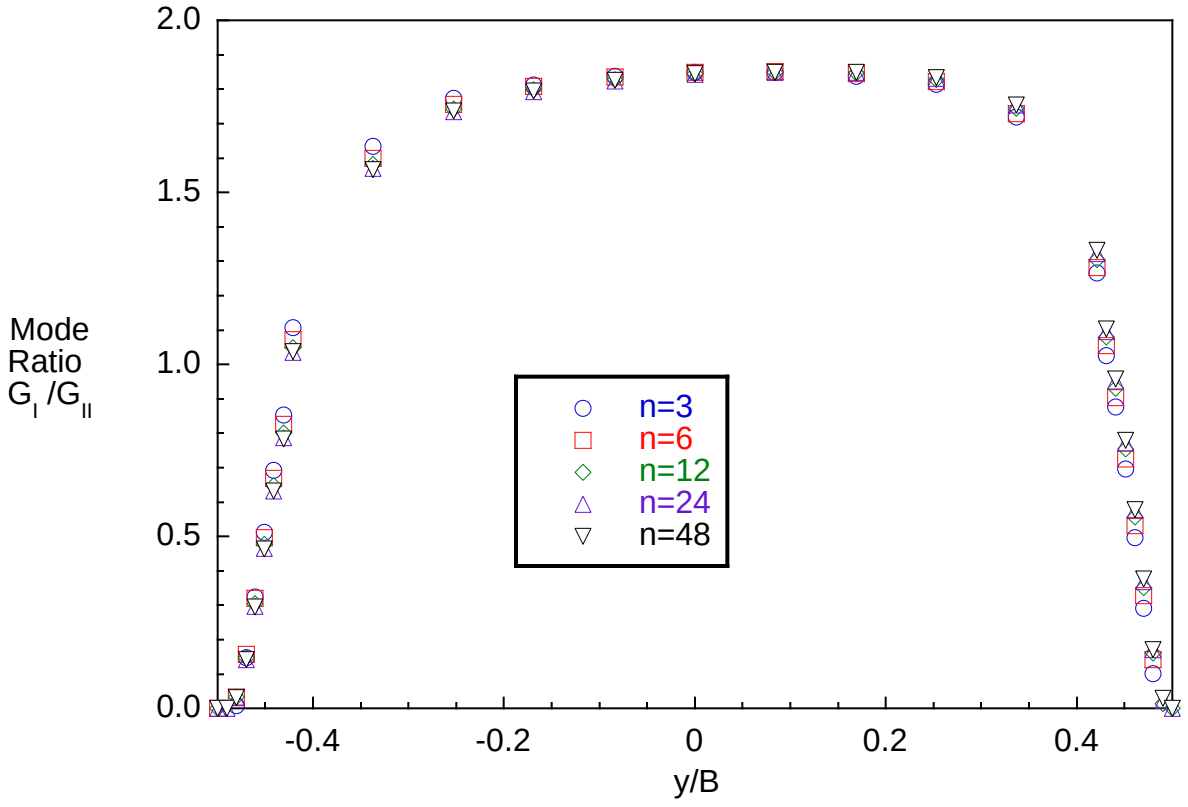

FIGURE 27. Influence of number of elements in refined section on mode ratio distribution across the width of a SLB specimen.

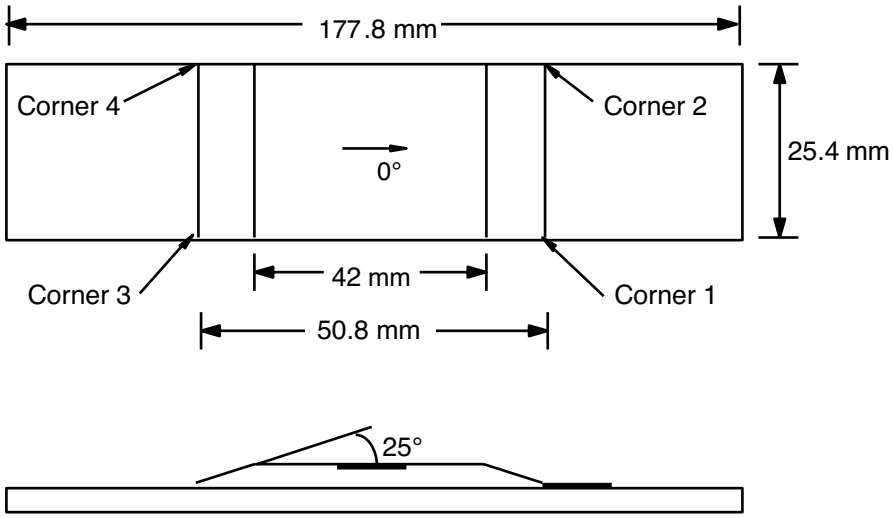

(a) *Specimen configuration*

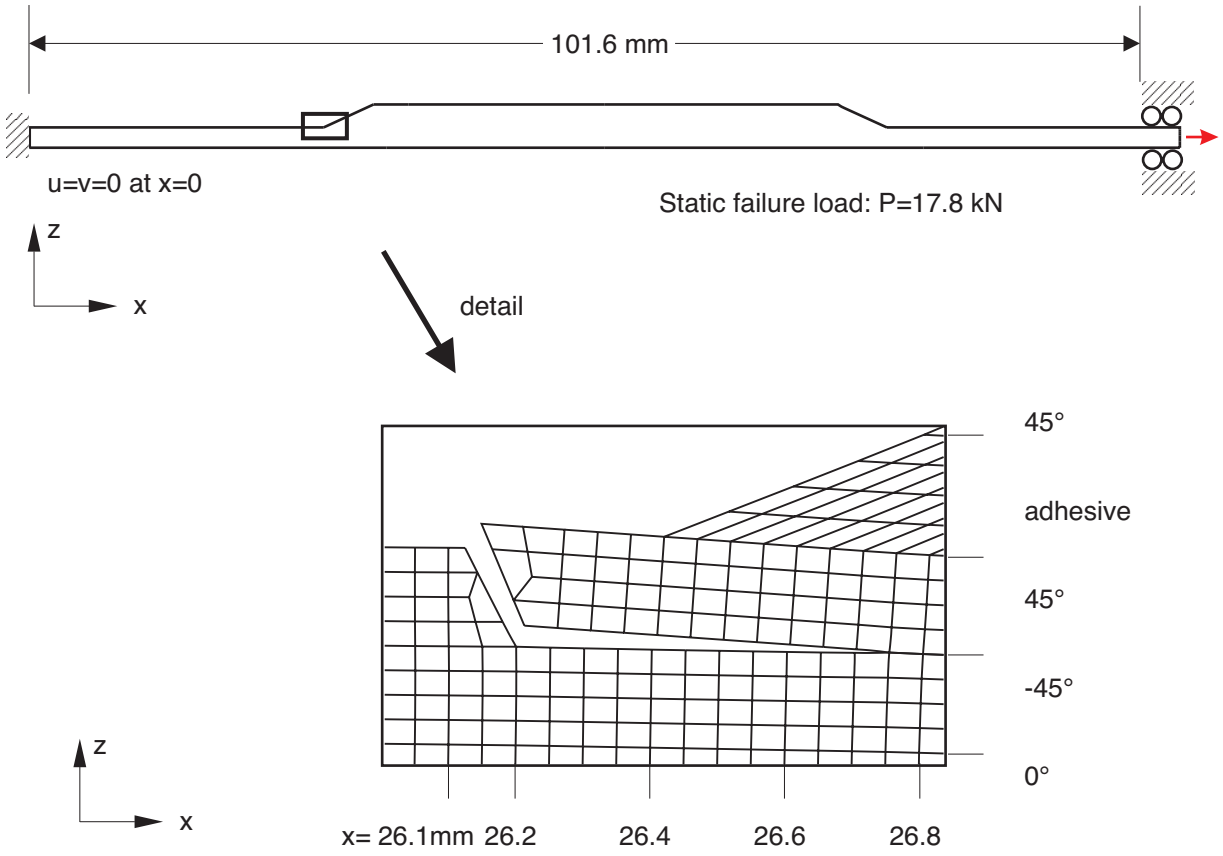

(b). *Finite element model of skin/flange specimen*

FIGURE 28. *Skin/flange debonding specimen*.

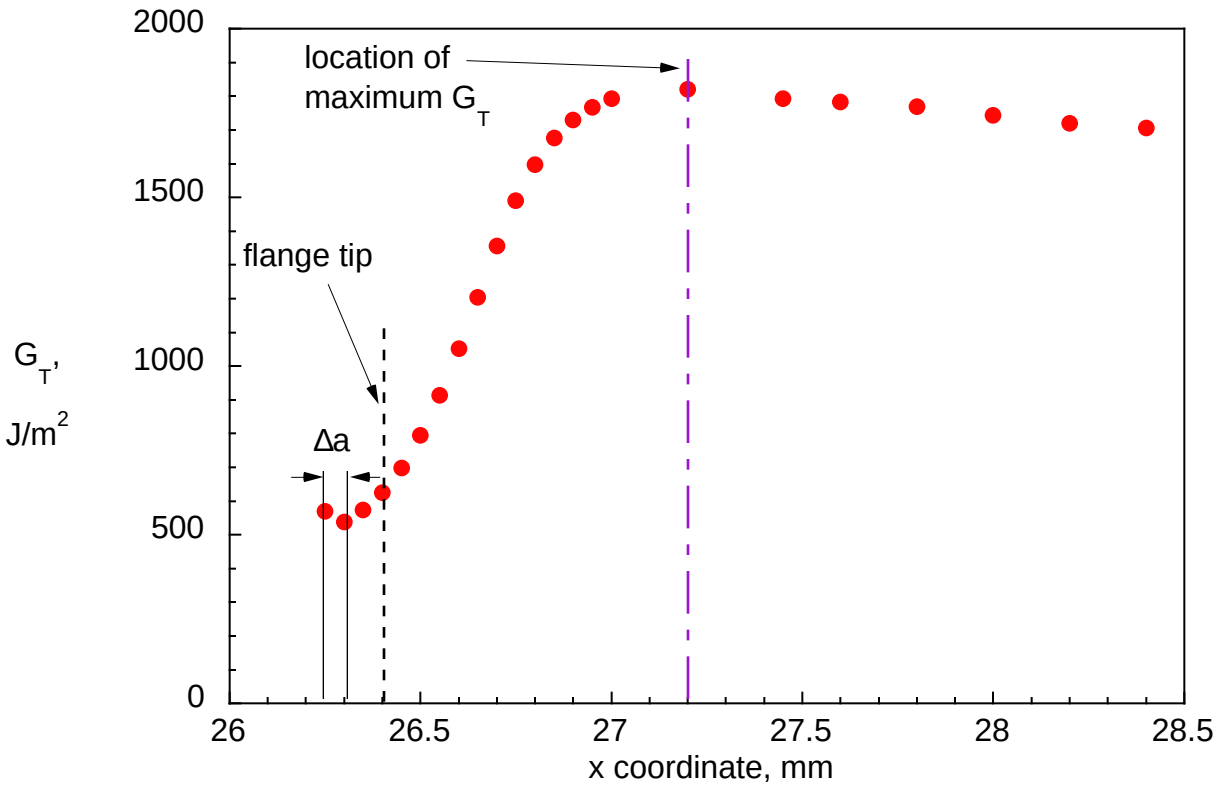

FIGURE 29. *Computed total strain energy release rate for delamination between top 45°/-45° skin plies.*

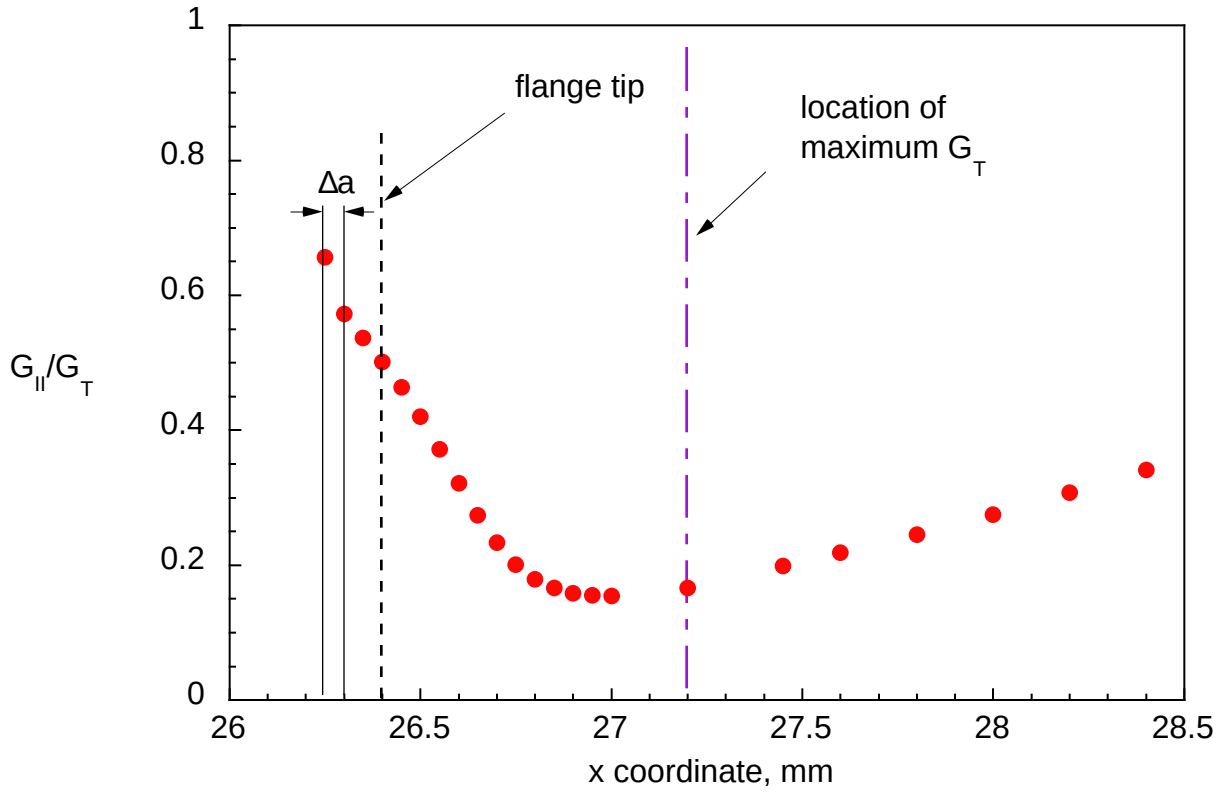

FIGURE 30. *Computed mixed mode ratio for delamination between top 45°/-45° skin plies.*

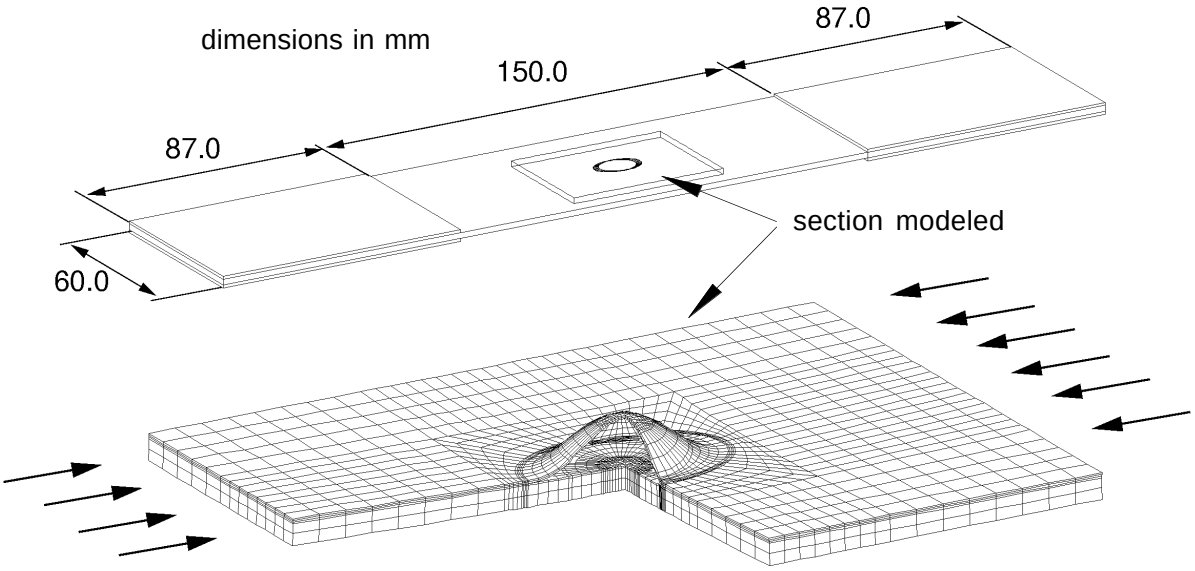

(a). *Delamination buckling specimen and section modeled with three-dimensional solid elements*

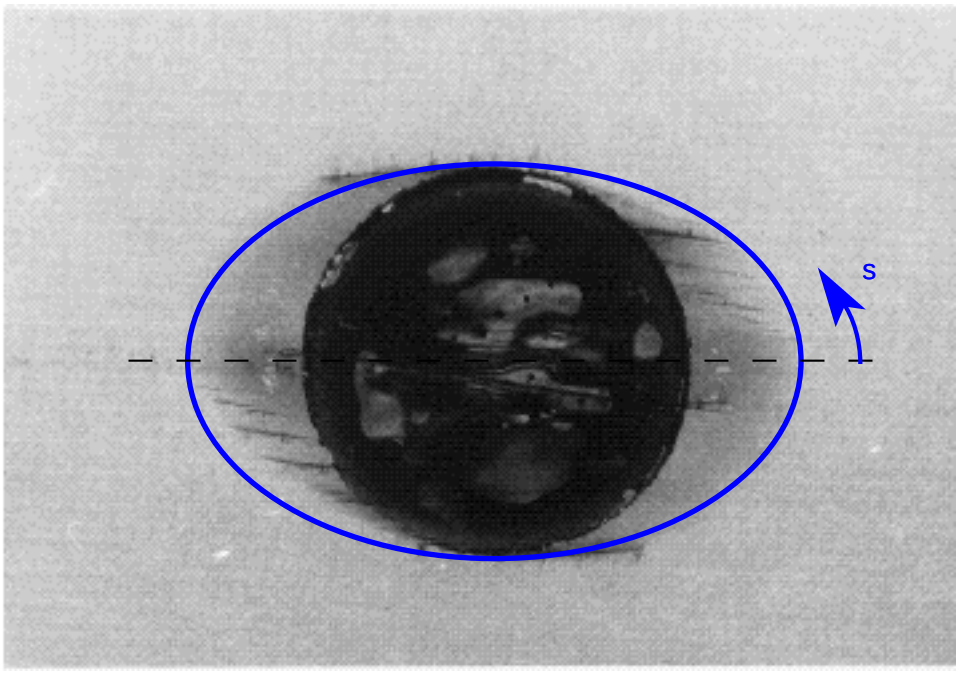

(b). *X-Ray showing the initial circular delamination and detected growth after 200,000 load cycles*

FIGURE 31. *Delamination buckling specimen.*

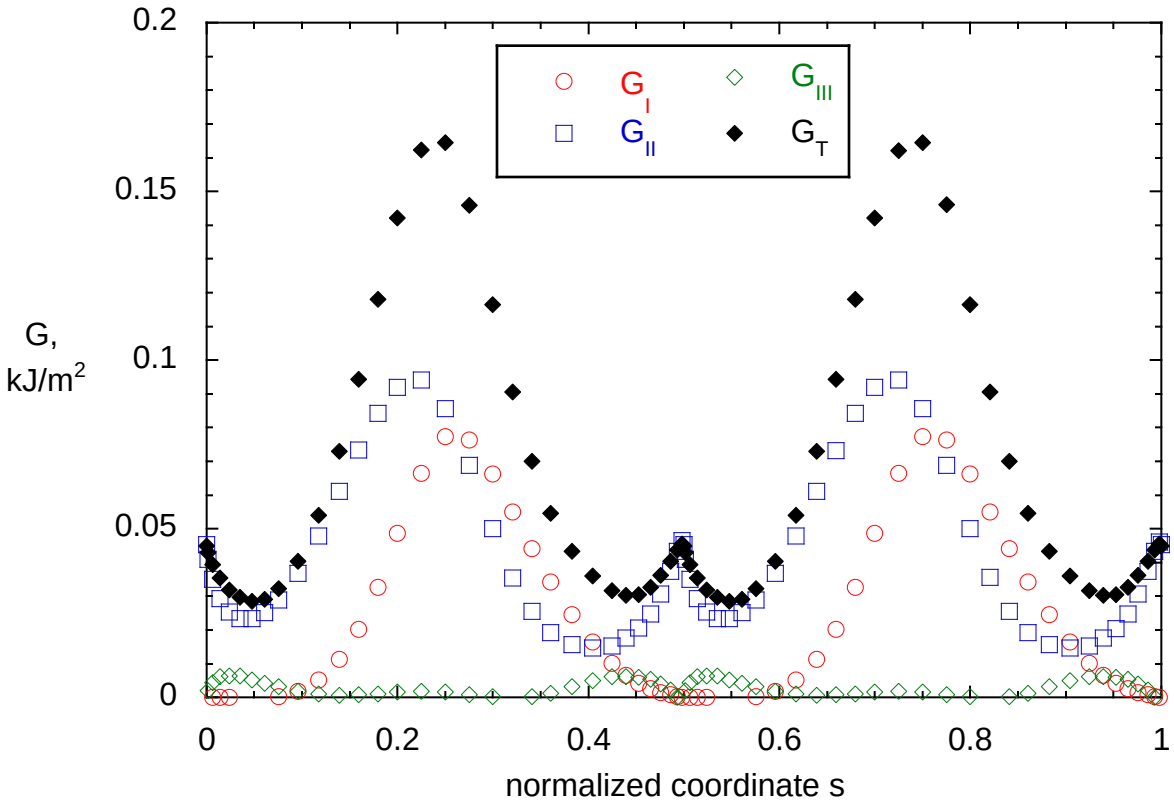

FIGURE 32. *Computed mixed mode strain energy release rate along detected delamination front after 200,000 load cycles.*

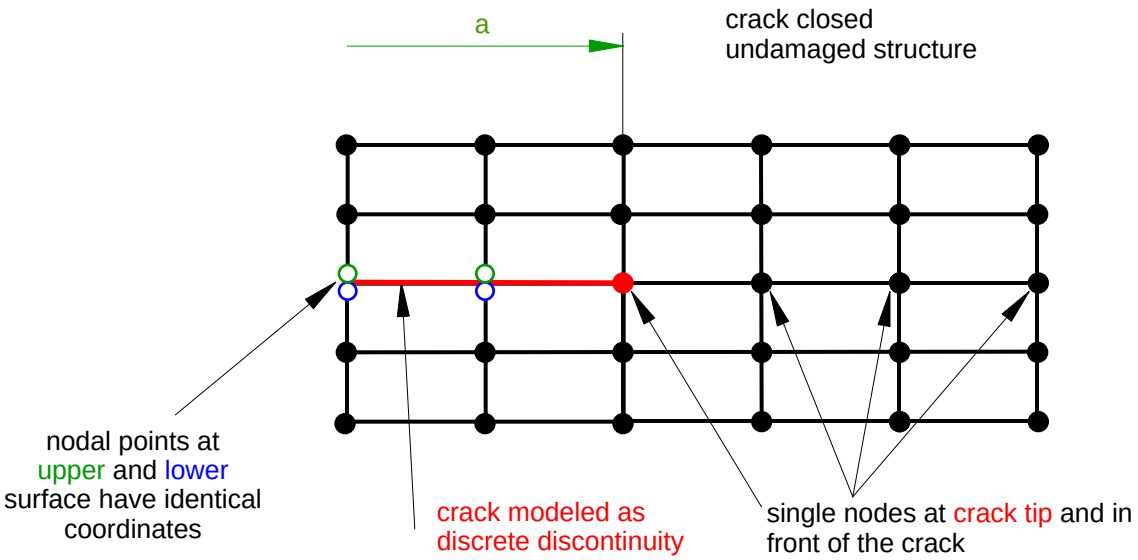

(a). *Intact region in front of the crack modeled with single nodes*

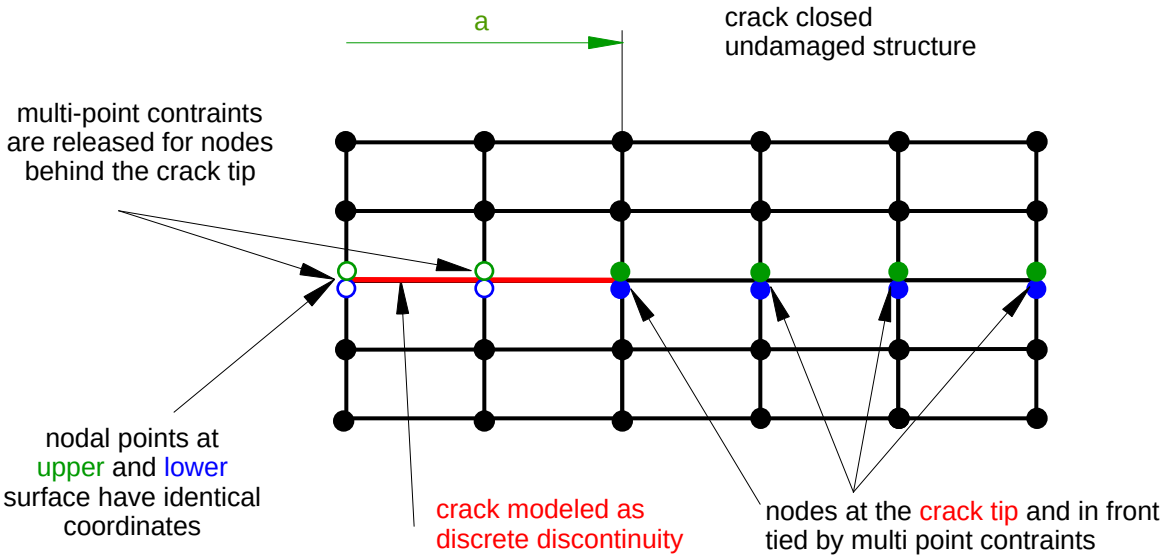

(b). *Intact region in front of the crack modeled with double nodes tied by multi-point contsraints*

FIGURE A1. *Crack modeled as one-dimensional discontinuity*

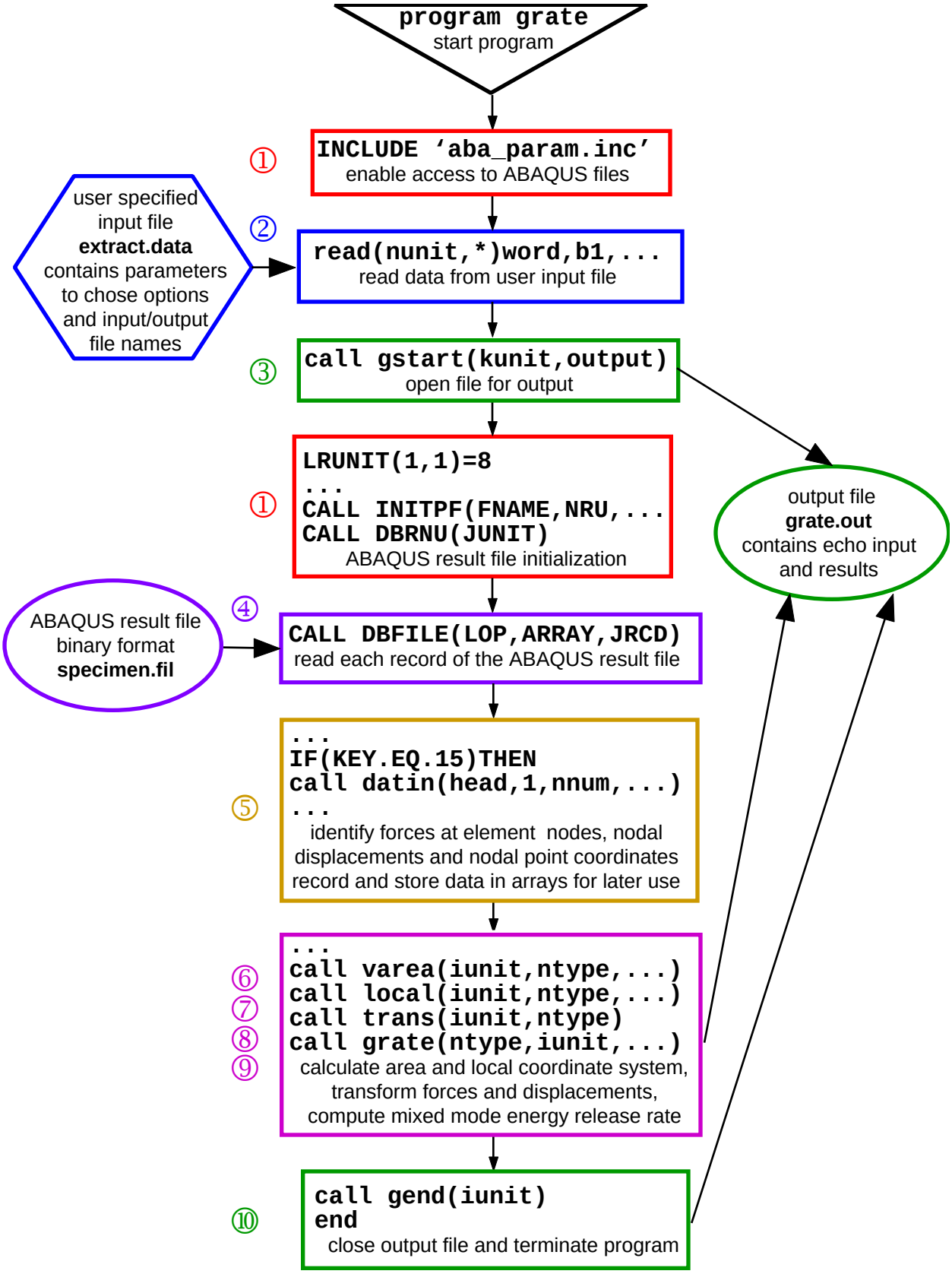

FIGURE A2. *Flow chart of routine extract.f to calculate strain energy release rates.*